PREPARATION AND CHARACTERIZATION OF PROPERTIES OF ELECTRODEPOSITED COPPER OXIDE FILMS

by

LONGCHENG WANG

Presented to the Faculty of the Graduate School of

The University of Texas at Arlington in Partial Fulfillment

of the Requirements

for the Degree of

DOCTOR OF PHILOSOPHY

THE UNIVERSITY OF TEXAS AT ARLINGTON

December 2006

ACKNOWLEDGEMENTS

I would like to express my gratitude to Dr. Meng Tao for his invaluable advice, inspiration and support throughout my graduate study. Without his enlightenment and guidance, this work would not be completed. What he has taught me is greatly helpful not only for my career but for my whole life.

I am very grateful to my committee members, Dr. Efstathios Meletis, Dr. Qiming Zhang, Dr. Roger D. Goolsby and Dr. Shashank Priya for their encouragement and support. Also, I would like to thank Dr. Pranesh B. Aswath for his advice and help for my graduate study. I appreciate Dr. K. Rajeshwar, Dr. N.R. de Tacconi and Dr. C. R. Chenthamarakshan for their advice and guidance in electrochemistry. I am glad to express my appreciation to Dr. Choong-Un Kim and Dr. Ping Liu for allowing me to use instruments in their laboratories. Also I would like to thank Dr. Nasir Basit for training me on various instruments and helping me with SEM characterization. I would like to thank my group members and friends, Dr. Jinggang Zhu, Dr. Guilhem Larrieu, Mr. Guanghua Song, Mr. Xiaolong Yang, Mr. Kunhee Han and Mr. Yusuf Muhammad Ali for their help and friendship. Finally, I would like to express my appreciation to my parents and my sister for their love, constant encouragement and support.

This research is supported by a grant from the Petroleum Research Fund.

November 3, 2006

ABSTRACT

PREPARATION AND CHARACTERIZATION OF PROPERTIES OF ELECTRODEPOSITED COPPER OXIDE FILMS

Publication No. _____

LONGCHENG WANG, PhD.

The University of Texas at Arlington, 2006

Supervising Professor: MENG TAO

Copper oxides, including cuprous oxide and cupric oxide, are prepared by electrochemical deposition. The structural, optical and electrical properties of as-deposited copper oxides are evaluated, based on which cuprous oxide is selected as a promising material for photovoltaic applications.

Electrodeposited cuprous oxide is a p-type semiconductor with a direct band gap of 2.06 eV. The mechanism of how pH affects the structural and electrical properties of electro-deposited cuprous oxide films is studied. In the pH range of 7.5 to 12.0, there are three different preferred crystal orientations: (100), (110) and (111). With different orientations, cuprous oxide shows different surface morphology and

grain size. Bath pH effect on structural properties is explained by its effect on the growth rate of different crystallographic planes with different Cu^{+}/O^{2-} ratios. Capacitance-voltage measurements are performed to study electrical properties of differently oriented cuprous oxide films. The results show that the flat band potential shifts negatively as the bath pH increases.

Electrodeposited cupric oxide is a p-type cupric oxide with an indirect band gap of 1.32 eV. Different cleaning methods are used to clean the substrate surface for electrodeposition of cupric oxide. Electrochemical etching is proven to be an effective method for Cu substrate cleaning in cupric oxide deposition. In particular, in-situ electrochemical etching is developed, which prevents the cleaned substrate from exposure to air. Current-voltage characterization shows that cupric oxide deposited on electrochemically etched Cu substrates has favorable electrical properties and better rectification behavior.

Cuprous oxide is selected for the fabrication of p-n homo-junction because it has better crystallinity, bigger grains, better control over crystal quality and a direct band gap. Based on the model that bath pH can control the stoichiometry and native point defects in electrodeposited cuprous oxide films, both p-type and n-type cuprous oxides are successfully deposited at different bath pH values. For samples deposited at pH below 7.5, cuprous oxides are n-type semiconductors, while at bath pH above 9.0, cuprous oxides are p-type semiconductors. Furthermore, a two-step deposition process is developed to fabricate a p-n homo-junction in cuprous oxide. Current-voltage measurements show a typical rectification behavior of a p-n junction for these samples,

which suggest that a p-n homo-junction of cuprous oxide is achieved, which is, to our knowledge, the first p-n homo-junction of cuprous oxide prepared by any method. The significance of this invention is because it enables the fabrication of solar cell with a reasonable high conversion efficiency (~10%) at a very low cost.

TABLE OF CONTENTS

LIST OF ILLUSTRATIONS

LIST OF TABLES

CHAPTER 1

INTRODUCTION

Nowadays, energy is used at a rate of approximately 4.1×10^{20} joules/year, equivalent to a continuous power consumption of 13 terawatts (Fig 1.1).[1-3] As projected, the increasing population, combined with rapid technology development and economic growth, will raise the demand for energy to 30 TW by 2050, and more than triple the demand to 45 TW by the end of the century.[3] According to this projection, any prospective energy resource has to have the capability to provide at least 1~10 TW power to make a primary contribution to the future energy supply.

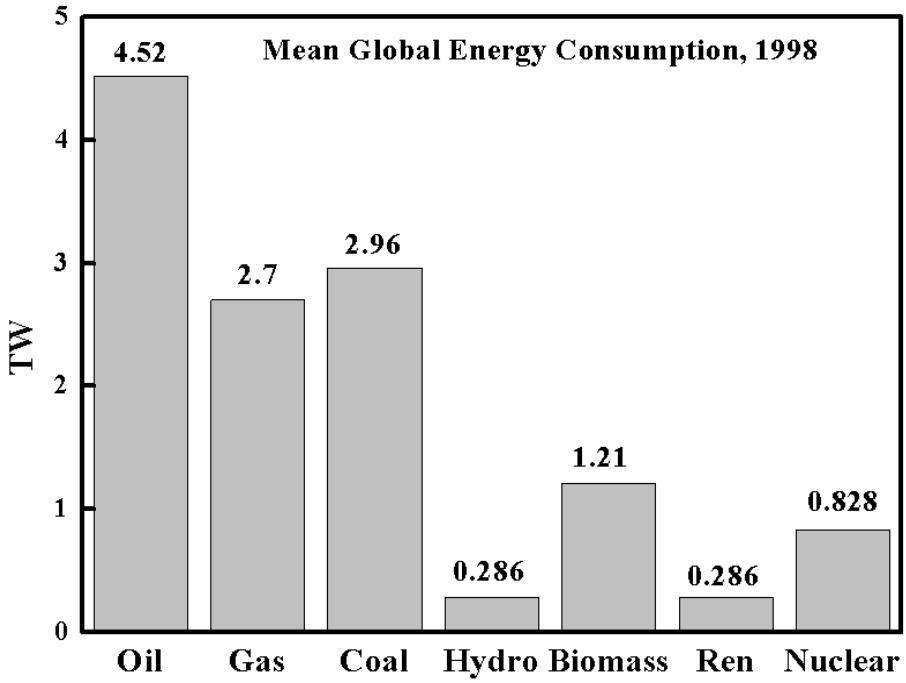

Fig. 1.1 Mean global energy consumption, 1998

Besides the capacity, another critical factor should be also taken into consideration: environmental effect. Fossil fuels generate severe adverse effects on environment such as pollutions and greenhouse gases associated with global warming. Since the industrialization, the level of carbon dioxide (CO_2) has increased dramatically due to the use of fossil fuels (Fig. 1.2).[3, 4] At the present CO_2 releasing rate, even before fossil fuels run out, the Earth may not be livable any more. To avoid this, another critical requirement on prospective energy sources must be satisfied, which is they must not generate any greenhouse gases.

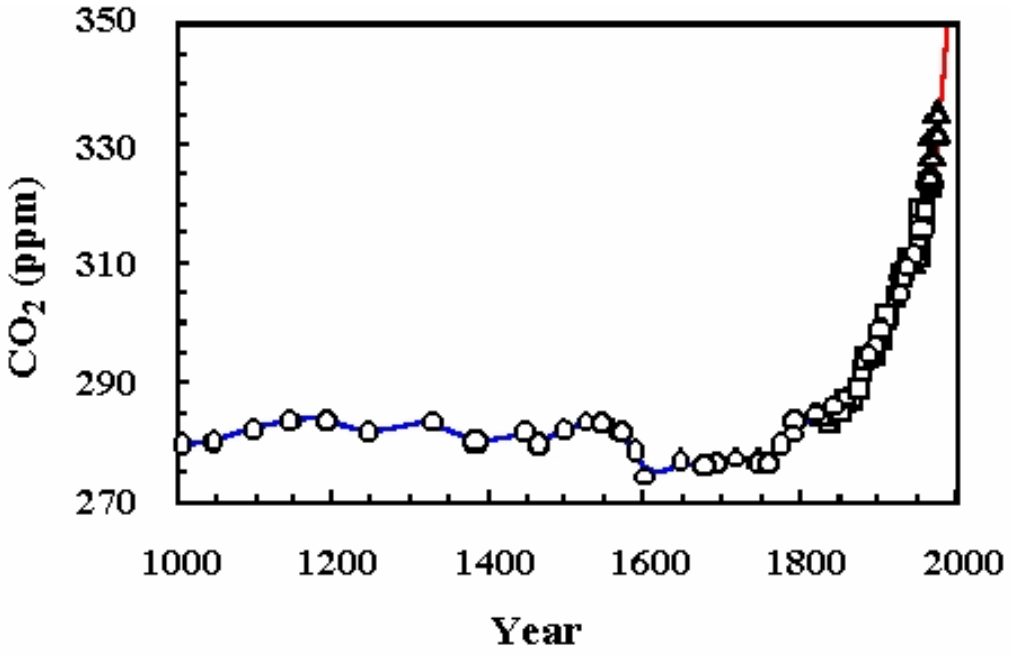

Fig. 1.2 CO_2 level in the atmosphere

As shown in Fig. 1.3,[2] fossil fuels are still the dominant energy sources, which provide almost 80% of total energy supply. In order to stabilize and/or decrease the CO_2 level in the atmosphere, it requires around 20 TW carbon-free power by 2050. Out of all the renewable energy sources, there are three promising options to meet this

requirement: fossil fuels use in conjunction with carbon sequestration, nuclear power, and solar power.

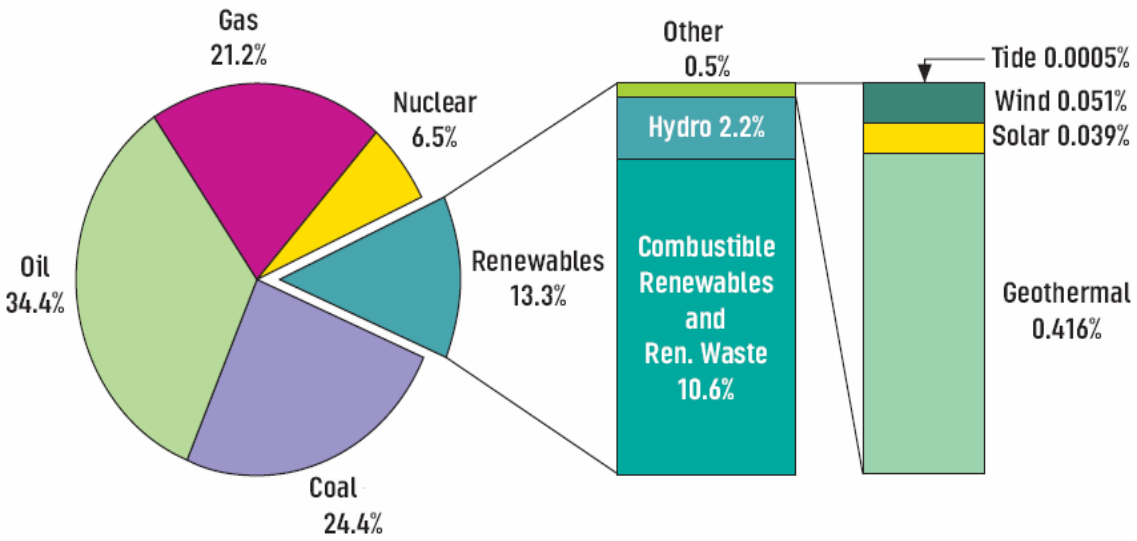

Fig. 1.3 Fuel shares of world total primary energy supply, 2003

Carbon sequestration is to convert fossil fuels into carbon-free fuel such as hydrogen. The challenge for carbon sequestration is finding secure storage for the 25 billion metric tons of CO_2 produced annually on the Earth. Prevention of CO_2 leakage is another critical issue because even with 1% leakage the CO_2 level in the atmosphere will increase dramatically and cause severe changes in the climate. Up to now, carbon sequestration on the required power scale has not yet been realized.

Nuclear power is the second theoretical option, while it has its own limitation. To produce 10 TW power, it would require construction of 10,000 new one-gigawatt nuclear power plants in the next 50 years. With this amount of energy production, the terrestrial uranium resource would be exhausted in 10 years. The required source

materials would have to be mined from seawater. Also storage of nuclear waste is another important issue.

The third option is to exploit renewable energy sources, which include hydroelectricity, tides and ocean energy, geothermal energy, biomass energy, wind energy and solar energy. It seems there are lots of options, while most of them are not practically exploitable. In table 1.1, some of renewable energy sources are listed with the theoretical and practical capacity.[1-3] Clearly, solar energy is the most promising energy source. Solar energy has a capacity of 170000 TW, of which, on average, 120,000 TW strikes the Earth.[5] Therefore, solar energy can be exploited on the needed scale to meet global energy demand in a carbon-free manner.

Table 1.1 Capacity of renewable energy sources

Renewable energy source	Theoretical capacity (TW)	Practically exploitable (TW)
Hydroelectric energy	4.6	1.5
Tides and ocean energy	<2.0	<<2.0
Geothermal energy	42.0*	Very small faction of 42
Wind energy	50	2.0~4.0
Solar energy	170000	600

*: Including geothermal energy at the surface of the Earth and in the ocean

Compared with fossil fuels, the cost for solar energy is way too high. To make solar energy competitive, the most import key issue is to lower the cost.

CHAPTER 2

OBJECTIVES

Efficiency and cost are two key issues for solar cell to become a house-hold energy source. Copper oxides, including cuprous oxide and cupric oxide, have the advantages of abundant source materials, low cost and low energy fabrication, which makes them promising candidates for next generation photovoltaic applications. However, both cuprous oxide and cupric oxide are intrinsically p-type semiconductors. Since a solar cell is basically a p-n junction, copper oxides solar cells have been fabricated with p-n hetero-junctions, i.e., an n-type metal oxide on p-type cuprous oxide. These hetero-junction solar cells have shown low conversion efficiency (<2%). One way to improve the efficiency is to fabricate p-n homo-junctions of copper oxides. The objectives of this work are listed as follows:

1. Study structural, optical and electrical properties of cuprous oxide and cupric oxide.
2. Identify more suitable copper oxide for photovoltaic applications.
3. Achieve both n-type and p-type copper oxide.
4. Fabricate p-n homo-junction in copper oxide.

CHAPTER 3

BACKGROUND

3.1 Development of solar cells

3.1.1 Fundamental mechanism of solar cell operation

There are different ways to exploit solar energy, including solar thermal system (converts solar energy into heat), solar fuel system (converts solar energy into chemical energy) and solar electrical system (converts solar energy into electricity). Here we'll just focus on solar electrical system.

Photovoltaic (PV) effect, which was first reported by Edmond Becquerel in 1839,[6] is the fundamental mechanism for solar cells. Practically, all the commercial solar cells involve a semiconductor p-n junction. A typical structure of a solar cell is shown in Fig. 3.1.[7]

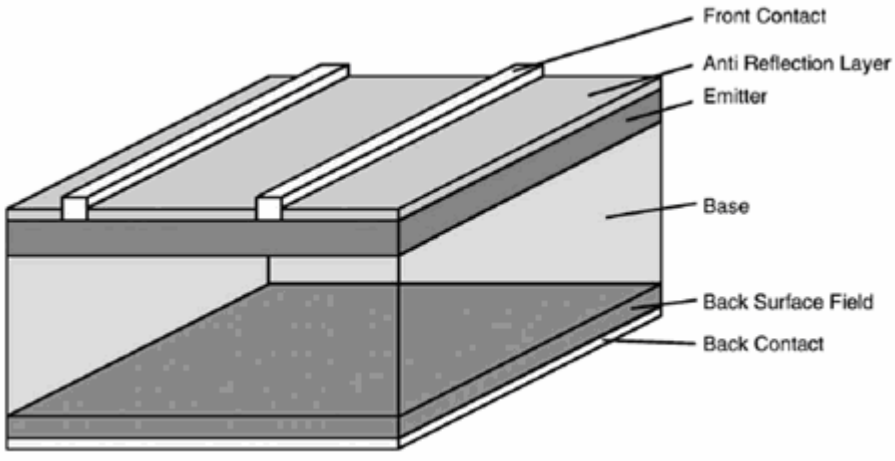

Fig. 3.1 Typical structure of a solar cell

When light is shed on a semiconductor, photons with energy higher than the semiconductor band-gap will generate electron-hole pairs. If electrons and holes can reach the junction before recombination, they will be separated by the built-in electrical field and generate a current or voltage within the circuit. This process is schemed in Fig. 3.2.

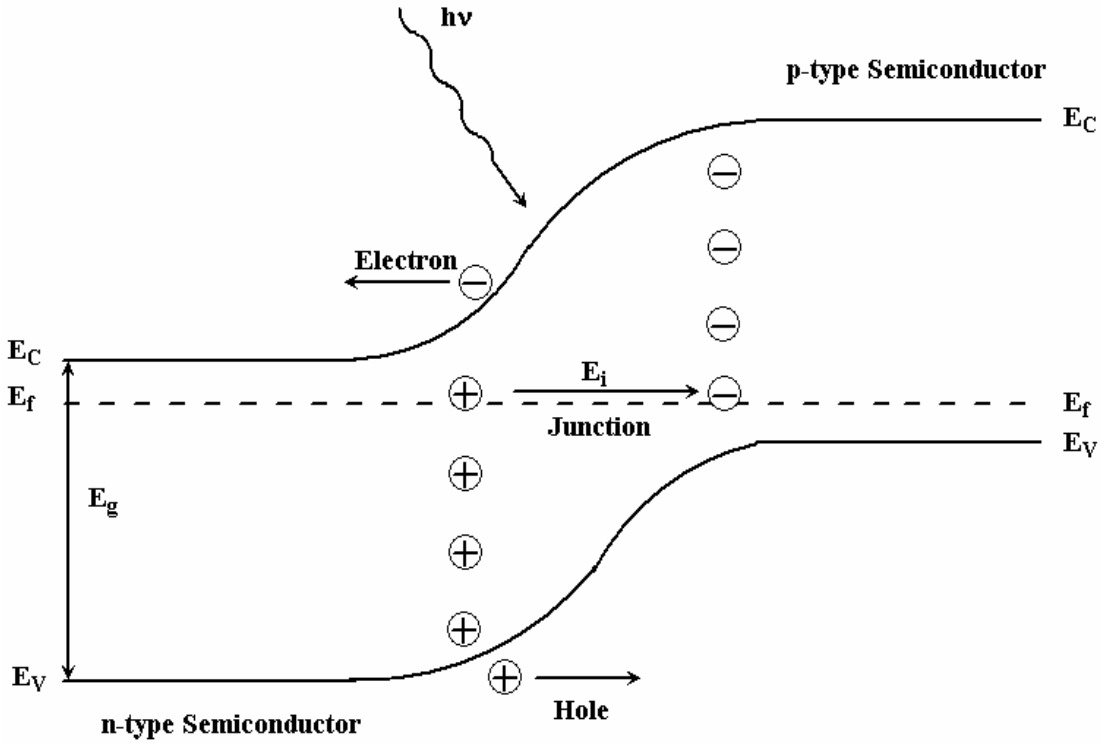

Fig. 3.2 Photovoltaic process in a p-n junction

3.1.2 World market of PV module

Through the past couple of decades, the world market of solar cells has shown continuous growth as shown in Fig. 3.3.[8] However, even with such a high growth rate, production of solar electricity is far away from being a significant contribution to future energy supply.

3.1.3 Requirements for solar cell materials

Despite the complicated fabrication process and high cost, crystalline silicon is still the dominant PV material, which takes ~85% market share as shown in Fig. 3.4.[7]

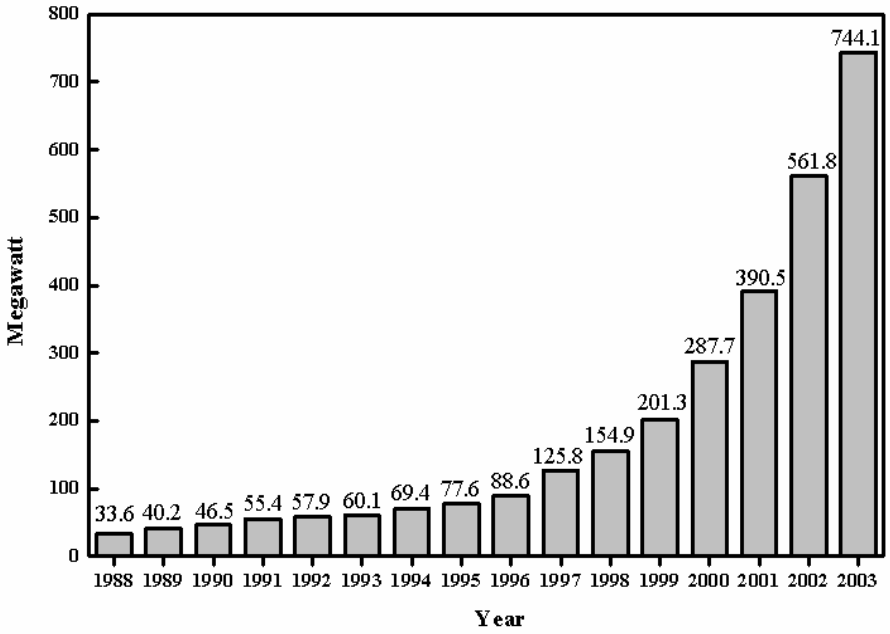

Fig. 3.3 Annually PV power production from 1988 to 2003

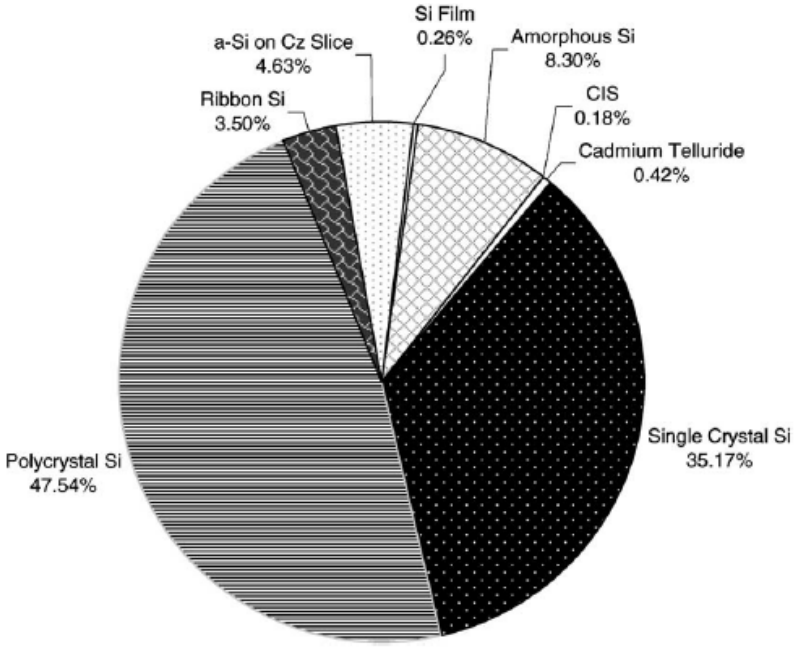

Fig. 3.4 Market share of different photovoltaic materials, 2001

From the viewpoint of semiconductor physics, photovoltaic materials should satisfy the following requirements:[7]

- Band-gap between 1.1 eV to 1.7 eV (Fig. 3.5)[7]
- Direct band gap
- Have both p-type and n-type
- Abundant source materials
- Simple preparation method, suitable for large area preparation
- Non-toxic
- Good physical and chemical stability

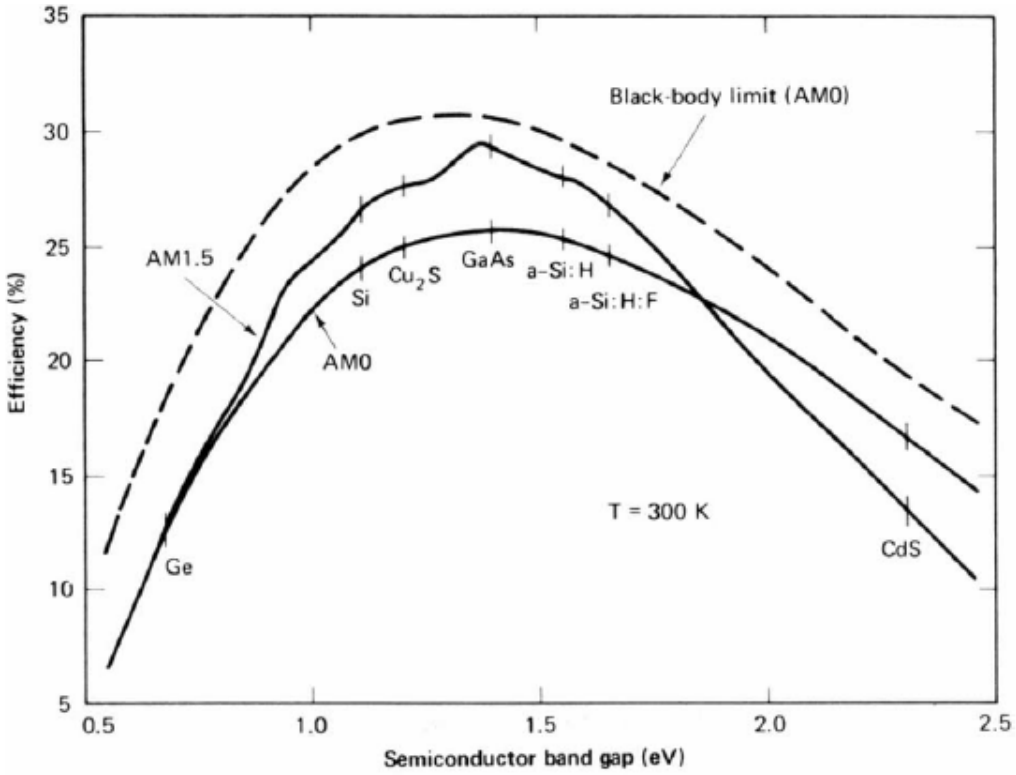

Fig. 3.5 Dependency of conversion efficiency on semiconductor band-gap

Therefore, silicon is not a perfect material for PV application due to its indirect band gap and high cost of fabrication. Lots of efforts have been and are being dedicated to develop new materials for PV application.

3.2 Copper oxides-new photovoltaic material

Copper oxides have two stable forms: cuprous oxide (Cu_2O) and cupric oxide (CuO). These two oxides have very different colors, crystal structures, physical properties and electrical properties, which will be reviewed in details in following sections.

There are several reasons copper oxides are chosen for photovoltaic applications. First, copper oxides have abundant non-toxic source materials. Second, copper oxides can be prepared with simple methods at very low cost. Third, copper oxides have reasonable band-gap values, which can be possibly adjusted by controlling the compositions.

3.2.1 Cuprous oxide (Cu_2O)

3.2.1.1 Crystal structure of cuprous oxide

Cuprous oxide has a quite simple cubic structure (Fig. 3.6), which belongs to space group $\boldsymbol{O_h^4}$.[9] It can be described as a cubic unit cell with a lattice constant of 0.427 nm, of which oxygen atoms are at corners with a tetrahedral unit of Cu_4O at the center. In the lattice, each copper atom coordinates with two oxygen atoms and each oxygen atom is surrounded by four copper atoms, which makes the stoichiometry 2:1.

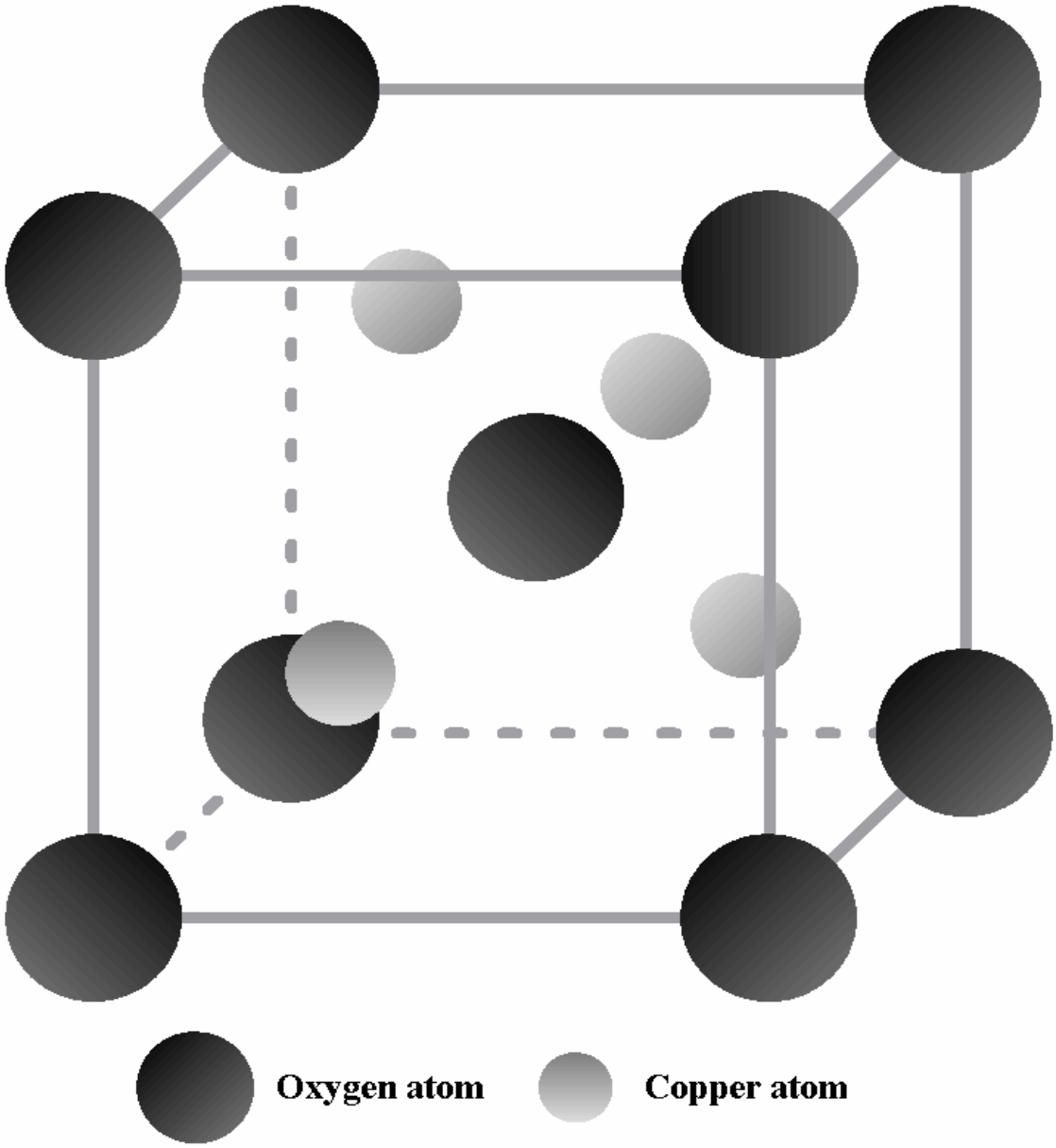

Fig. 3.6 Crystal structure of cuprous oxide

3.2.1.2 Properties of cuprous oxide

Cuprous oxide is a reddish solid with density of 6.0 g/cm^3. It has a quite high melting point of 1235 ºC and does not dissolve in water. Unlike most of other metal oxides, Cu_2O is a p-type semiconductor[10-15] and the majority carriers (holes) are

generated by native copper atom vacancies.[12, 14-17] It has a direct band-gap of 1.9~2.1 eV.[18-27] Single crystalline cuprous oxide can be prepared by thermal oxidation,[10, 19, 28] floating zone (FZ) method,[16, 29] and from the melt.[30] Polycrystalline cuprous oxide can be synthesized by anodic oxidation,[31, 32] sputtering deposition,[33, 34] and electrochemical deposition.[35-41] Electrical properties of cuprous oxide films such as carrier mobility and concentration vary dramatically with preparation methods, which result in large variation in resistivity of Cu_2O films. Table 3.1 shows some previous data on electrical properties of cuprous oxide.[11-14, 17, 25, 42]

Table 3.1 Electrical properties of cuprous oxide

Preparation method	Crystallinity	Conduction type	Resistivity (ohm•cm)	Mobility ($cm^2/V•s$)	Carrier concentration (cm^{-3})
Thermal oxidation	Single crystal	p-type			1.03 to 3×10^{18}
Thermal oxidation	Single crystal	p-type		0.08 at 300K 1.0 at 500K	8.5×10^{16} at 300 K 2.5×10^{17} at 500 K
Floating zone	Single crystal	p-type		1.8×10^{5} at 4.2K	
Electro-deposition	Polycrystalline	p-type	10^{6}~10^{8}		
Thermal oxidation	Polycrystalline	p-type	Un-annealed: 3.7×10^{3} Annealed: 5.6×10^{2} HCl doped: 2.5×10^{2}	Unannealed: 75 HCl doped and annealed: 130	
Galvanostatic deposition	Polycrystalline	p-type	5×10^{7} at RT 3×10^{4} after annealing		
Sputtering	Polycrystalline	p-type	10^{4}~10^{6}		

3.2.1.3 Work done on cuprous oxide

Interest in cuprous oxide as a semiconductor began with the invention of Cu_2O rectifier by Grondhal in the 1920s.[43] Considerable work on preparation and characterization of Cu_2O, especially on rectifiers, was done from 1930 to 1940.[44] After 1940 interest was shifted to selenium and later to germanium, silicon and other materials.

In the 1970s, cuprous oxide became popular again due to its potential applications in photovoltaic area. Two research groups from the United States did extensive work on cuprous oxide based PV devices. One is from the Wayne State University (Detroit), and the other is the Joint Center for Graduate Study (Richland, WA). They have studied Schottky diodes, MIS (metal insulator semiconductor) and hetero-junction PV devices mainly based on high-temperature prepared cuprous oxide.[17, 28, 45-47] Other groups around the world also did some similar studies.[18, 20-22, 48-50] From the reported data, no cell had efficiency over 2%. The common conclusion of most of these studies is: the only way to increase the efficiency is to fabricate homo-junction of cuprous oxide.

Since the 1980s, low temperature methods, such as sputtering, anodic oxidation and electrochemical deposition, have been developed for cuprous oxide preparation. Electrochemical method shows advantages over other methods. It offers better control on film quality and can be performed at very low temperature (<100 ºC). Rakhshani et al[35-37] and Zhou et al[38-40] both reported that cuprous oxide films electro-deposited at different pH values showed two preferred orientations: (100) and (111). Siripala et al[23,

[51, 52] reported n-type behavior of cuprous oxide prepared by electrochemical deposition, which makes cuprous oxide based homo-junction PV cells feasible.

3.2.2 Cupric oxide (CuO)

3.2.2.1 Crystal structure of cupric oxide

Cupric oxide has a much more complicated tenorite crystal structure.[53] The mono-clinic unit cell (space group $\boldsymbol{C_{2h}^{6}}$) contains four CuO molecules. Lattice constants are: a=0.47 nm, b=0.34 nm, c=0.51 nm and β=99.54º, as shown in Fig. 3.7.[53-55] The coordination of atoms in CuO is that each atom has four nearest neighbors of the other kind. In the (110) plane, each Cu atom is linked to four nearly coplanar O atoms at the corner of an almost rectangular parallelogram. The O atom is coordinated to four Cu atoms in the form of a distorted tetrahedron.

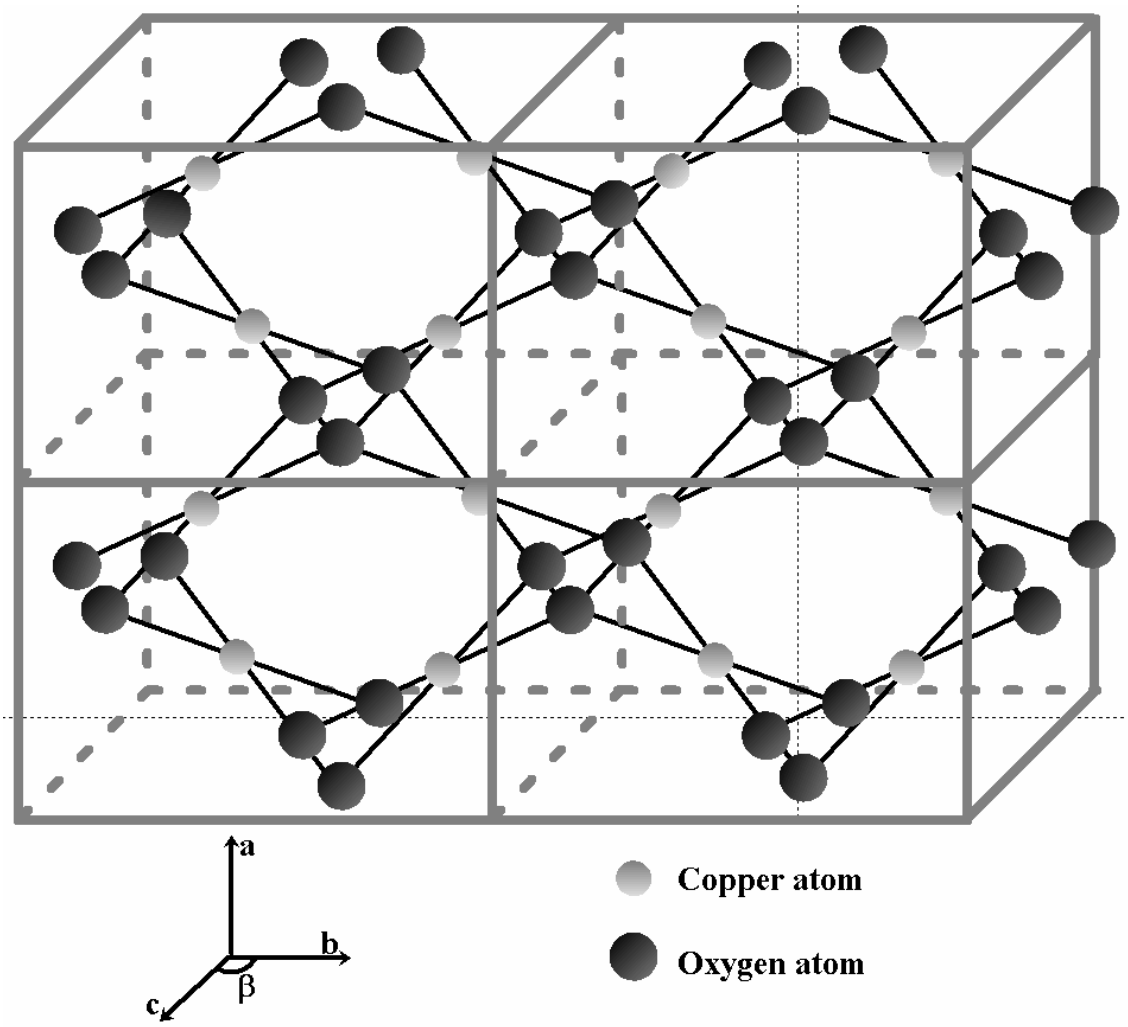

Fig. 3.7 Crystal structure of cupric oxide

3.2.2.2 Properties of cupric oxide

Pure cupric oxide is a black solid with a density of 6.4 g/cm^3. It also has a high melting point of 1330 ºC and is insoluble in water. Same as cuprous oxide, native copper vacancy in CuO makes it a p-type semiconductor.[55-59] Different from cuprous oxide, cupric oxide has an indirect band-gap of 1.4 eV to 1.9 eV.[56, 59-64] Many methods can be used to prepare cupric oxide such as thermal oxidation,[65, 66] sintering,[67-69] precipitation,[70] sputtering,[33, 59, 64] CVT (chemical vapor transport),[55, 71, 72] and

electrochemical deposition.[58, 73-75] Cupric oxide prepared by different methods also shows large variations in electrical properties, which are listed in Table 3.2.[33, 55, 56, 68, 71]

Table 3.2 Electrical properties of cupric oxide

Preparation method	Crystallinity	Conduction type	Resistivity (ohms•cm)	Carrier concentration (cm^{-3})
Sintering	Polycrystalline	p-type	16.0	4×10^{18}
Sputtering	Polycrystalline	p-type	10^{-2}~10	
Sintering	Polycrystalline	p-type	2400 at 300 K 15 at 773 K	
CVT	Single crystal	p-type	2×10^{5}	
CVT	Single crystal	p-type	~10^{5}	

3.3 Electrochemical deposition method

Both cuprous oxide and cupric oxide can be prepared by many methods, such as thermal oxidation, sputtering, anodic oxidation and electrochemical deposition. Compared with other deposition methods, electrochemical deposition has advantages of low cost, low temperature, easy control over parameters and large area deposition.

Generally, the overall electrochemical reaction in a cell consists of two independent half-reactions. Most time one is only interested in one half-reaction, and the electrode at which it happens is referred as working (or indicator) electrode (WE). The potential of the working electrode is observed or controlled with respect to a reference electrode (RE). Since the reference electrode has a constant makeup, so its potential is fixed. Fig. 3.8[76] shows how reactions are controlled by the potential applied to the working electrode. When a negative potential is applied, energy of electrons in

working electrode is increased. At certain potential, electrons will transfer to the vacant electronic states of the species in the solution. Therefore, electrons will flow from working electrode into solution and form a cathodic current, which causes reduction of the species in the solution at the surface of the working electrode. Similarly, as a positive potential is applied, energy of electrons in working electrode will be lowered. At certain point, electrons will flow from solution species to working electrode and form an anodic current, which results in the oxidation of the species in the solution. The critical potential, at which the reaction happens, is called the standard potential (E^0) for the related species in the solution.

From the thermodynamics point of view, an electrochemical reaction is simple, while practically, it's much more complicated. An electrode reaction is a heterogeneous reaction since it happens at the interface between electrode and electrolyte. Generally, an electrode reaction includes four steps (Fig. 3.9):[76]

1. Mass transfer (reactive species transferred to electrode surface)
2. Electron transfer at the electrode surface
3. Chemical reactions preceding or follow the electron transfer
4. Other surface reactions, such as desorption or adsorption

Therefore, an electrode reaction will not be only controlled by applied potential but also by many other factors as shown in Fig. 3.10.[76]

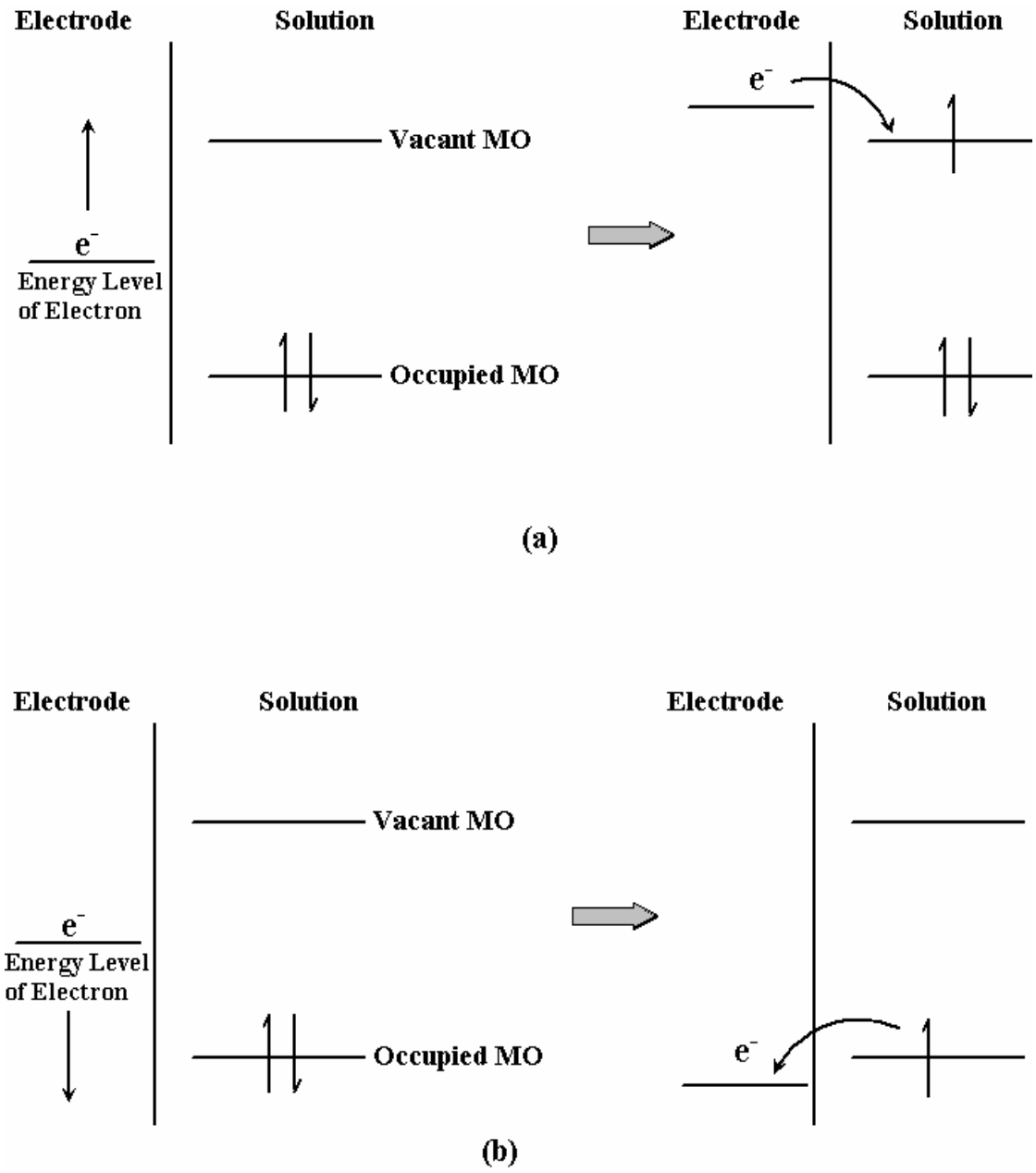

Fig. 3.8 (a) reduction, (b) oxidation process of a species in solution

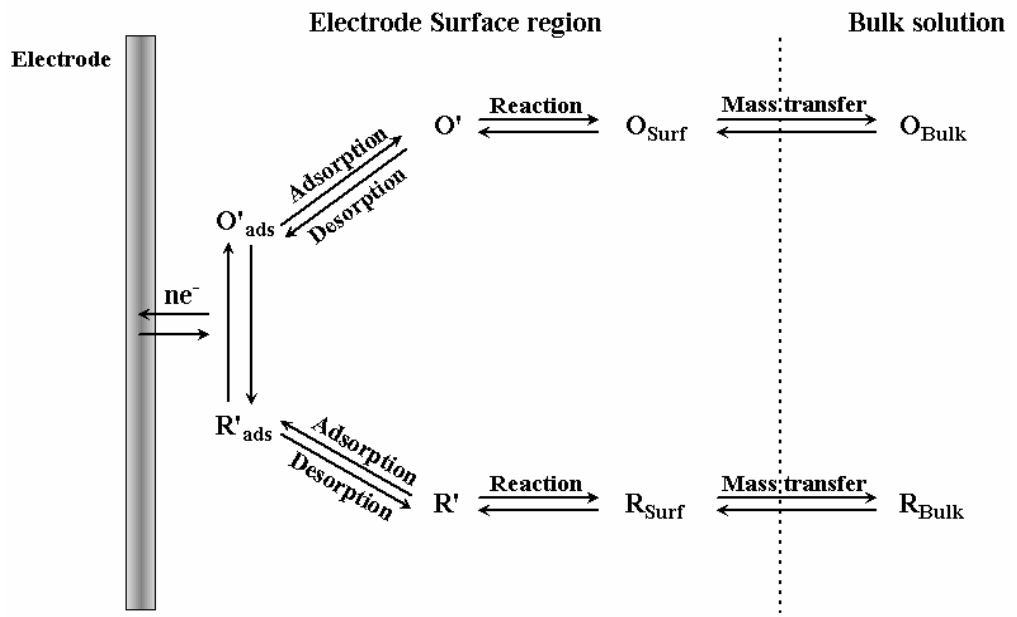

Fig. 3.9 Pathway of a general electrode reaction

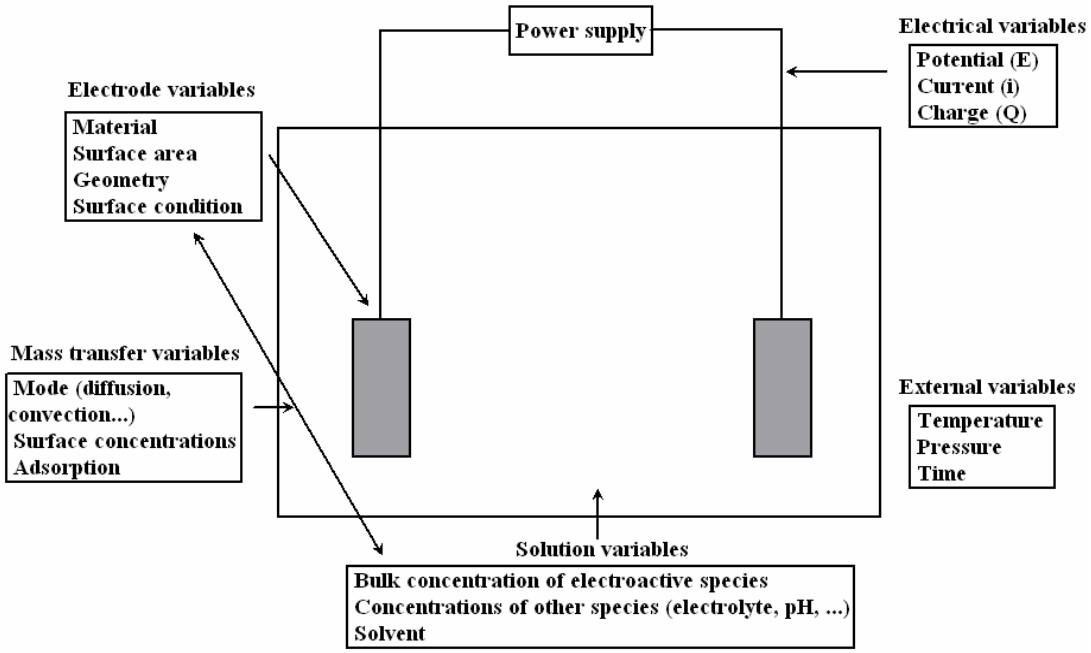

Fig. 3.10 Variables affecting the electrode reaction

Nowadays, instead of a two electrode cell (WE and RE), a three-electrode cell is preferable. A counter (or auxiliary) electrode (CE) is placed into the cell and current will flow between working electrode and counter electrode (instead of reference electrode). Reference electrode is placed near the working electrode surface. The device used to observe or control the potential difference between working electrode and reference electrode generally has very high impedance, so that a negligible current is flowing through the reference electrode. Therefore, its potential will remain constant.

3.4 Work in this dissertation

As mentioned in previous sections, copper oxides have advantages to make the promising candidates for photovoltaic applications, to which lots of work has been dedicated. However, both cuprous oxide and cupric oxide are intrinsically p-type semiconductors. Since solar cells are basically p-n junctions, cuprous oxide based solar cells are hetero-junctions, which have shown low conversion efficiency (<2%). The only way to improve the efficiency is to fabricate p-n homo-junction in copper oxides. Chapter 5 and chapter 6 mainly focus on the study on structural, optical and electrical properties of cuprous oxide and cupric oxide, respectively. And chapter 7 covers the fabrication of p-n homo-junction in cuprous oxide.

The content covered in chapter 5 provides a more detailed study on structural properties of electrodeposited cuprous oxide compared with work done by other groups. Electrodeposited cuprous oxide is found to be a p-type semiconductor with a direct band-gap of 2.06 eV. Structural properties, including film orientations and grain size, can be well controlled by deposition pH. Besides the two reported orientations of

cuprous oxide, the third orientation (110) is achieved, which is a very useful complement to previous work. Based the results and the understanding on cuprous oxide crystal structure, a new model for the mechanism of bath pH effect is proposed as follows: the bath pH controls the orientation of cuprous oxide film by affecting the growth rate of crystallographic planes with different Cu^{+}/O^{2-} ratio. This model reasonably explains bath pH effect on structural properties of cuprous oxide and paves the way for the development of fabrication of p-n homo-junction in cuprous oxide. Besides the structural properties, electrical properties such as the flat band potential (V_{fb}) are found to shift with the orientations. To our knowledge, this is the first report of how the bath pH has a profound influence on the subsequent interfacial behavior of an electrodeposited film.

Chapter 6 focuses on structural, optical and electrical properties of electrodeposited cupric oxide. Cupric oxide is found to be a p-type semiconductor with an indirect band gap of 1.32 eV. While compared with cuprous oxide, cupric oxide film has no preferred orientation and grain size is much smaller. Different cleaning processes, including chemical etching and electrochemical etching processes, are applied to copper substrates to investigate effects of starting surface conditions on electrical properties of cupric oxide. Here, a new in situ electrochemical etching process is developed for cupric oxide deposition, which is of great importance because it prevents the exposure of the cleaned substrates to the air or other contaminations before deposition. Current-voltage characterization proves electrochemical etching processes

are effective cleaning method and it shows that cupric oxide deposited on electrochemically etched substrate has favorable electrical properties.

After the studies on both cuprous oxide and cupric oxide, it's found that, compared with cupric oxide, cuprous oxide has much better crystallinity, bigger grains, better control over crystal quality and a direct band gap structure. Therefore, cuprous oxide is selected for the fabrication of p-n homo-junction, which is covered in chapter 7. Based on the results in chapter 5, it's found that bath pH may control the native point defects in cuprous oxide by controlling the oxygen content incorporated into the film. Cuprous oxides deposited at bath pH below 7.5 are characterized to be n-type semiconductor, while cuprous oxides deposited at bath pH above 9.0 show p-type semiconductor behavior. To our knowledge, this is the first report on the control of conduction types of cuprous oxide, which is of great importance not only for cuprous oxide but also for other semiconductor metal oxides. A two-step deposition process is developed to fabricate p-n homo-junction in cuprous oxide. Photocurrent and current-voltage measurements demonstrate a successful fabrication of the first p-n homo-junction in cuprous oxide ever made by any method. This invention is of great significance because it enables the fabrication of cuprous oxide solar cell with a reasonable high conversion efficiency (~10%) at a very low cost.

CHAPTER 4

EXPERIMENTAL

4.1 Sample Preparation

Cuprous oxide and cupric oxide films were deposited under different conditions including substrates, solutions and applied potentials.

4.1.1 Preparation of working electrode

Two kinds of substrates are used for different purposes: ITO (indium tin oxide) coated glass and metal (copper, titanium) sheets. ITO coated glass has a sheet resistance of 30 ohms/□ and is specially used for optical characterization. Metal substrates (99.9% pure), which are mainly used for electrical characterization, are cut into 1 cm × 4 cm stripes. Before any deposition, the surface of working electrode is cleaned by a degreasing process and an etching process.

The degreasing process is to remove organic contamination on the surface. The substrates are immersed into acetone, ethanol or isopropanol and ultrasonicated for 15 minutes. After degreasing process, the substrates are rinsed in de-ionized water.

The etching process is to remove inorganic contamination and native oxides on the surface. Suitable etching processes are selected for different substrates. ITO (indium tin oxide) coated glass is etched in diluted HCl (hydrochloride) for 2 minutes, while

copper substrate (and other metal substrates) are etched in diluted HNO_3 (nitric acid) for 2 minutes.

Besides the chemical etching, electrochemical etching process is used for cupric oxide deposition. Copper substrate is set as working electrode in a 3-electrode cell (counter electrode: platinum foil, reference electrode: Ag/AgCl/saturated NaCl). By applying a certain current through the cell, copper atoms at the surface are oxidized to soluble Cu^{2+} ions and fresh clean surface is formed for following deposition.

4.1.2 Preparation of solution

4.1.2.1 Solution for cuprous oxide deposition

Cuprous oxide films are electrodeposited from solution containing 0.4 M copper (II) sulfate and 3 M lactic acid.[35-39] Lactic acid is used to stabilize Cu (II) ions at bath pH higher than 7. The bath pH is carefully adjusted between 5.8 and 12.0 by controlled addition of 4 M NaOH.

4.1.2.2 Solution for cupric oxide deposition

The solution for cupric oxide deposition contains 0.15~0.2 M copper (II) sulfate and 0.2 M tartaric acid.[73, 75] Tartaric acid acts as a stabilizer for Cu (II) ions to prevent its precipitation at pH higher than 7. The bath pH is adjusted to 13.0 by controlled addition of 4 M NaOH.

4.1.3 Deposition process

Both cuprous oxide and cupric oxide are deposited from a custom-designed 3-elctrode cell, as shown in Fig. 4.1. Electro-deposition is carried out with a Princeton

Applied Research Versastat II potentiostat. Deposition bath temperature is controlled between 20 °C and 60 °C with a Precision 280 water bath.

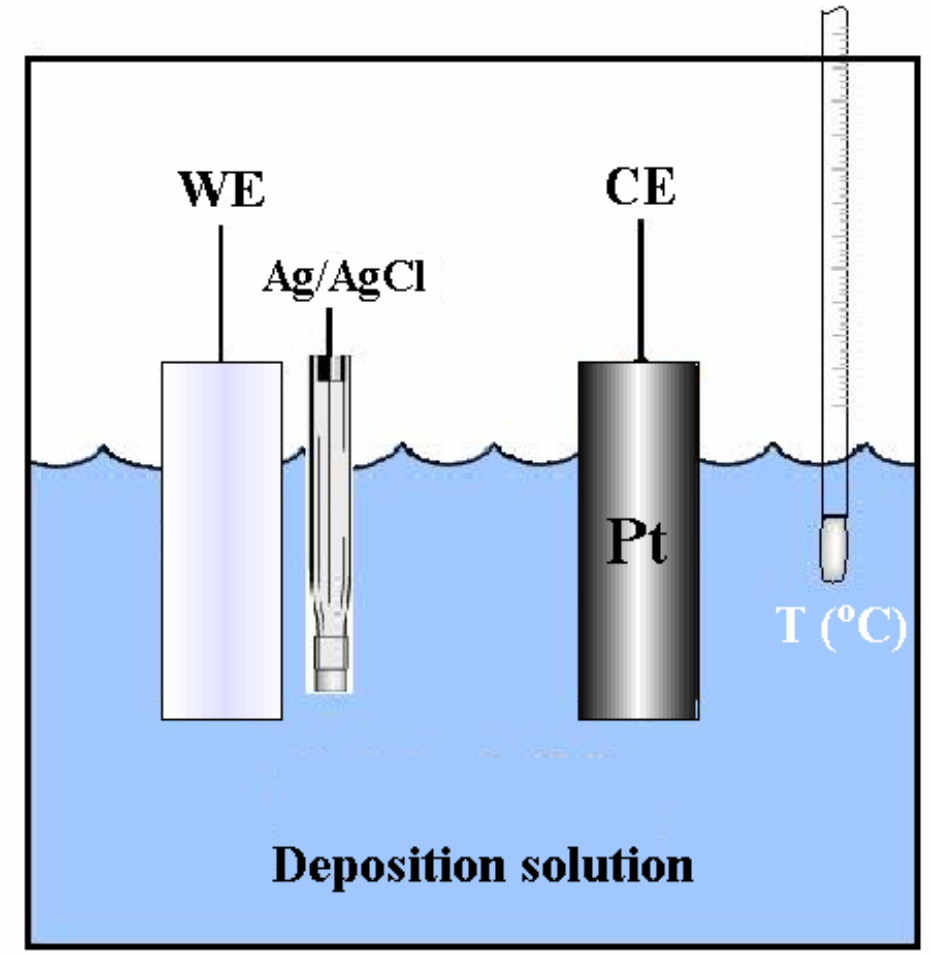

Fig. 4.1 Arrangement of the deposition cell

For cuprous oxide deposition, solution pH is set from 5.7 to 12.0, and bath temperature is kept at 60 ºC. Cuprous oxide is deposited at a constant potential between -0.2 V and -0.4 V (vs. Ag/AgCl/saturated NaCl).

For cupric oxide deposition, solution pH is kept at 13.0, and bath temperature is kept at 50 ºC. Cupric oxide is deposited at a constant current -5 mA or a constant potential 0.5 V (vs. Ag/AgCl/saturated NaCl).

4.2 Characterization

Different methods were used to characterize the structural, optical and electrical properties of electrodeposited cuprous oxide and cupric oxide.

4.2.1 Cyclic voltammetry (CV)

Cyclic voltammetry is one of the most versatile electro-analytical techniques for the study of electroactive species. Its versatility combined with ease of measurement has resulted in extensive use of CV in the fields of electrochemistry, inorganic chemistry, organic chemistry and biochemistry. Cyclic voltammetry is often the first experiment performed in an electrochemical study.

CV is a simple and direct method to measure the current flowing through a working electrode as a function of applied potential. A typical CV curve is shown in Fig. 4.2 for a platinum working electrode in a solution containing 6.0 mM $K_3Fe(CN)_6$ (electroactive species) and 1.0 M KNO_3 (supporting electrolyte).[77, 78] Saturated calomel electrode (SCE) is used as the reference electrode. Potential starts to scan negatively from 0.8 V (initial potential, E_i). When potential is sufficiently negative to reduce $[Fe^{3+}(CN)_6]^{3-}$, a cathodic current occurs as indicated by letter (a) due to the reaction:

$$[Fe^{3+}(CN)_6]^{3-} + e \rightarrow [Fe^{2+}(CN)_6]^{4-} \qquad (4\text{-}1)$$

The cathodic current increases rapidly (a→b) until the concentration of $[Fe^{3+}(CN)_6]^{3-}$ at electrode surface is substantially diminished, which results in a peak current (b). Then the current decreases (b→c) as the solution surrounding electrode is depleted of $[Fe^{3+}(CN)_6]^{3-}$. The scan direction is switched at point c (switch potential) for reverse scan. As the potential is still negative enough, the cathodic current still flows

although the scan is reversed. When the potential is positive enough (d), $[Fe^{2+}(CN)_6]^{4-}$ are oxidized by the following electrode process:

$$[Fe^{2+}(CN)_6]^{4-} - e \rightarrow [Fe^{3+}(CN)_6]^{3-} \qquad (4\text{-}2)$$

This process causes an anodic current (d→e) and it goes through a same increase (d→e), peak (e), and decrease (e→f) process as that of the cathodic current. As potential goes back to 0.8 V, a cycle is done. From the curve shown, parameters such as the cathodic and anodic peak potentials, and the cathodic and anodic peak currents, can be extracted.

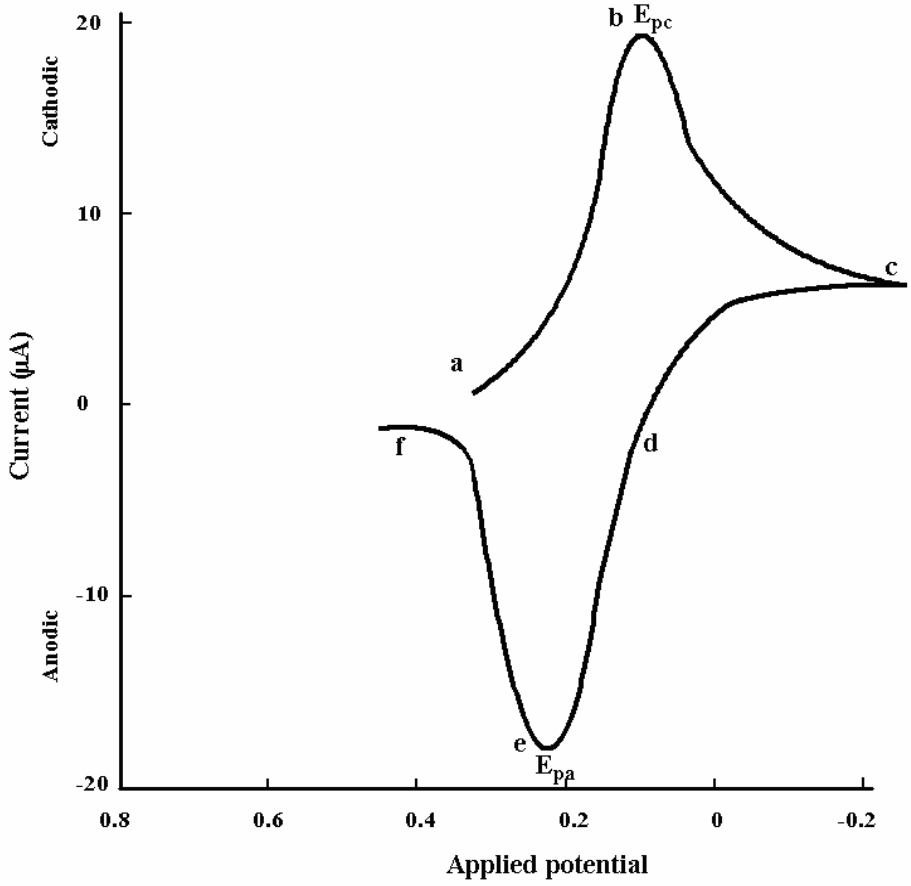

Fig. 4.2 Cyclic voltammety curve of a $K_3Fe(CN)_6$ system

Therefore, a well done CV experiment is crucial for any electrochemical study, which is the reason why CV measurements are performed before any deposition of copper oxide.

4.2.2 UV-Vis transmittance spectrum and band-gap calculation

Generally, UV-Vis transmittance spectrum is an effective method used for characterization of band-gap of semiconductor.

4.2.2.1 Instrumentation

All UV-Vis transmittance spectra are measured with a V570 Spectrophotometer from Jasco Co., of which the schematic is shown in Fig. 4.3.

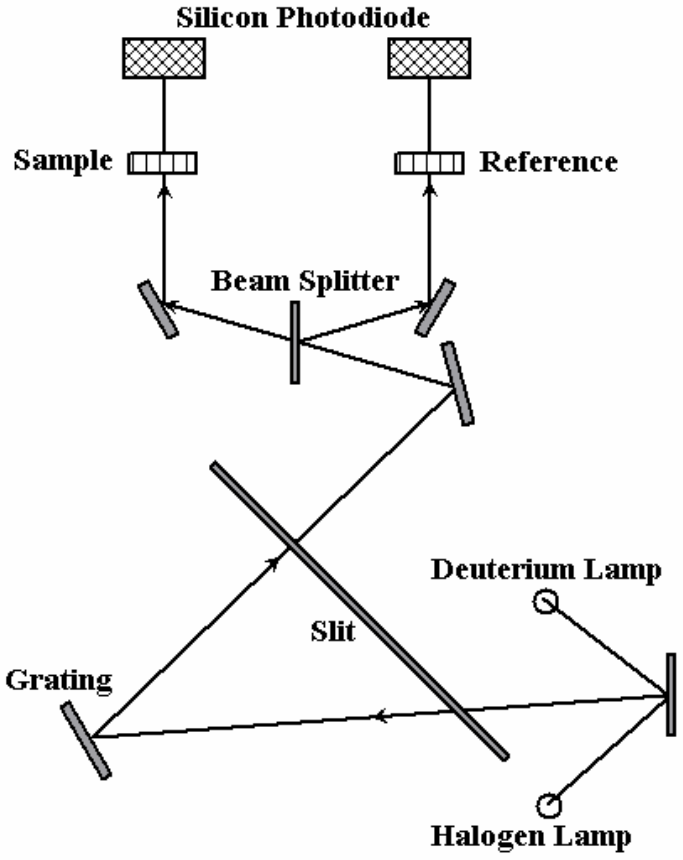

Fig. 4.3 Schematic of V-570 Spectrophotometer

Light with wavelength of 400nm-1100nm is generated by a halogen lamp and a deuterium lamp. Then the light is divided into two equal-intensity beams and passes through a prepared sample and a reference sample, respectively. A silicon photodiode is used to record the intensity of the transmitted light.

4.2.2.2 Calculation of band-gap

From a UV-Vis transmittance spectrum, the band-gap of a semiconductor can be calculated with the following equations:

$$I = I_0 \times e^{-\alpha t} \quad (4\text{-}3)$$

$$(\alpha h\nu)^n = A(h\nu - E_g) \quad (4\text{-}4)$$

In equation 4-3, I is the intensity of the transmitted light, I_0 is the intensity of the incident light, t is the thickness of as-deposited film and α is the absorption coefficient. In equation 4-4, $h\nu$ represents the photon energy, E_g is the band-gap and A is a constant. n depends on the nature of the band-gap (n = 1/3 for indirect forbidden transition, n = 1/2 for indirect allowed transition, n = 2/3 for direct forbidden transition, and n = 2 for direct allowed transition). The intercept of a $(\alpha h\nu)^n$-$h\nu$ plot with the $h\nu$ axis determines the band-gap of the semiconductor.

4.2.3 X-ray diffraction (XRD)

Structural properties of as-deposited copper oxide, such as orientation of films, were studied by thin film X-ray diffraction method, which was carried out with a Siemens D-500 powder diffractometer. The incident X-ray is copper K_α (1.54 Å) radiation and the diffracted X-ray is collected by an X-ray detector. The scan range for

2θ is 25 degrees to 90 degrees.

4.2.4 Scanning electron microscopy (SEM)

A Zeiss Supra 55 scanning electron microscopy was used to characterize surface morphology and grain size of our samples. Energy of incident electron beam was kept between 5 kV to 10 kV.

4.2.5 Atomic force microscopy (AFM)

A Nanoscope IIIa microscope from Digital Instruments Co. was used to characterize the surface roughness of the copper substrates for the deposition of cupric oxide. It operated at a tapping mode and the cantilever oscillates at a frequency around 215.0 KHz.

4.2.6 Profiler

In this dissertation, an Alpha-Step IQ stylus-based surface profiler was used to measure the thickness of as-deposited cuprous oxide.

4.2.7 Photocurrent characterization

Photocurrent characterization is a very simple method that can be used to identify the conduction type of semiconductor electrode.

4.2.7.1 Instrumentation

Photocurrent characterization is carried out in a custom-built system, which includes a light source, an illumination switch, a three-electrode cell and a controlling system (Fig. 4.4). A 100W tungsten/halogen lamp is used to provide broad spectrum light. The illumination switch is actually a manually controlled light chopper with certain time intervals. In the three-electrode cell, the working electrode is as-deposited

cuprous oxide film facing the light source, the counter electrode is a platinum foil and the reference electrode is Ag/AgCl/saturated KCl. The cell solution is 0.5 M sodium sulfate (Na_2SO_4) with 0.1 M sodium formate (HCOONa). A PAR 264A polarographic analyzer/stripping voltammeter is used to control the applied potential and scan rate.

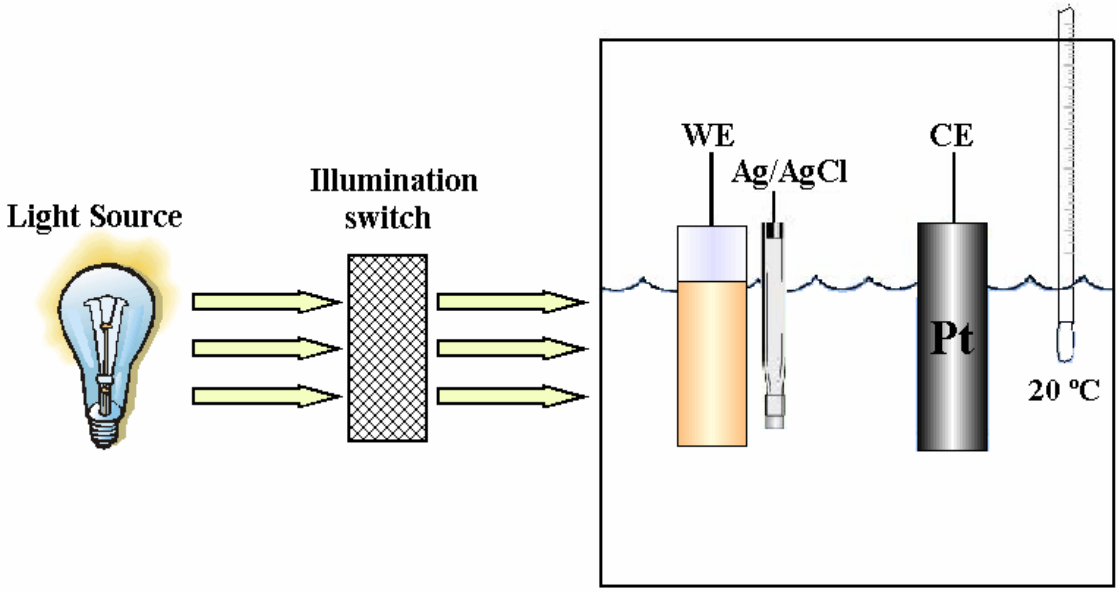

Fig. 4.4 Arrangement of a photocurrent characterization system

4.2.7.2 Mechanism

As a semiconductor electrode in contact with a solution, a depletion layer is formed at the electrode surface. Since there are few free carriers available, the current (dark current) is very small. When light is shed on the electrode, electron-hole pairs are generated and separated in space charge region, which generates a photo current. The magnitude of a photocurrent depends on the electrode properties, applied potential, and solution composition, which provide information about the nature of the photo-process. In this dissertation, the photocurrent is mainly used to characterize the conduction types of our cuprous oxide films.

For an n-type semiconductor electrode at open circuit, the Fermi level is typically higher than the redox potential of the electrolyte (Fig. 4.5 (a)), and electrons will transfer from the electrode into the solution. Therefore, a positive space charge region (depletion layer) is formed at the semiconductor surface (Fig. 4.5 (b)). When the interface is irradiated with light of energy greater than the band gap, photons are absorbed and electron-hole pairs are created. Those pairs formed beyond the space charge region will recombine quickly with evolution of heat. However, electron-hole pairs formed in the space charge region will be separated by the built in electrical field (E_i). Holes move into solution and electrons move into semiconductor (Fig. 4.5 (c)). Therefore, irradiation on an n-type semiconductor will promote a photo-anodic current. The behavior of p-type semiconductor is different from that of n-type semiconductor. In a p-type semiconductor, the depletion layer is negatively charged, so under irradiation, holes move into semiconductor and electrons move into solution, which generates a photo-cathodic current (Fig. 4.5 (d, e, f)).

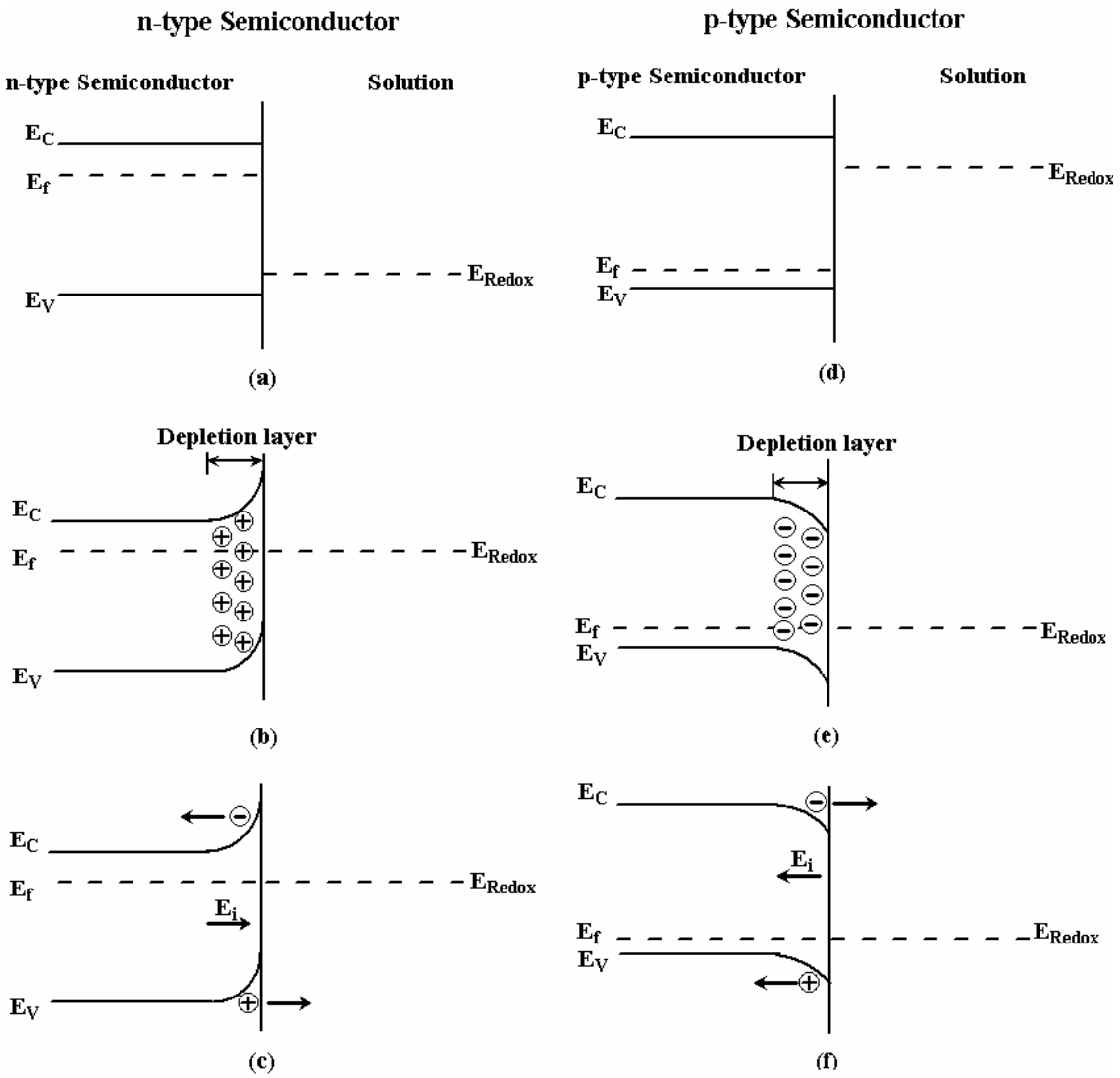

Fig. 4.5 Junctions of n-type and p-type semiconductors formed with solution: n-type: (a) before contact, (b) after contact, (c) under irradiation and p-type: (d) before contact, (e) after contact, (f) under irradiation

A typical photocurrent-voltage curve of an n-type semiconductor is shown in Fig. 4.6.[76, 80, 81] In the darkness (curve 1), no current flows when the potential on the semiconductor electrode is made positive to the flat band potential (E_{fb}) because there are few free charge carriers available in the depletion layer. Under irradiation (curve 2),

electron-hole pairs generated in the depletion layer are separated by the built in electrical field (E_i) and a photo-anodic current is generated.

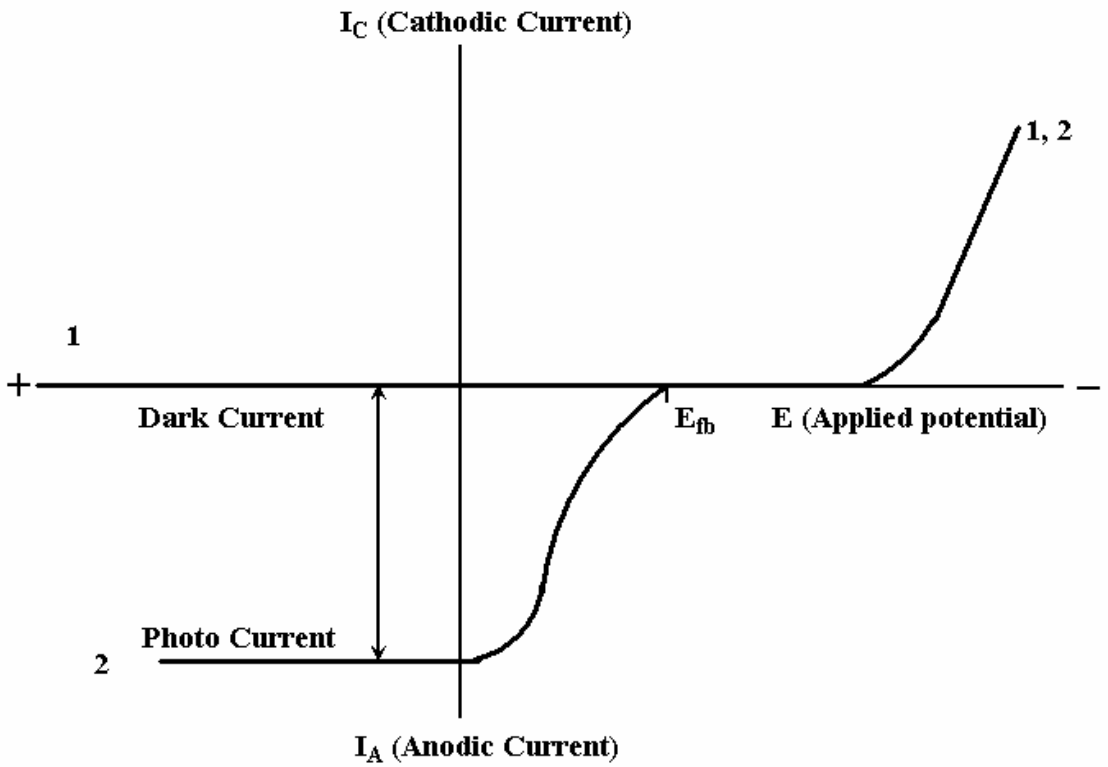

Fig. 4.6 A typical photocurrent-voltage curve of an n-type semiconductor

4.2.8 Current-voltage (I-V) characterizations

Current-voltage characteristics can supply information about properties of a metal/semiconductor contact. When a semiconductor is in contact with a metal, the Fermi levels of both materials should be equal at thermal equilibrium, which results in band bending and formation of an energy barrier (Schottky barrier).

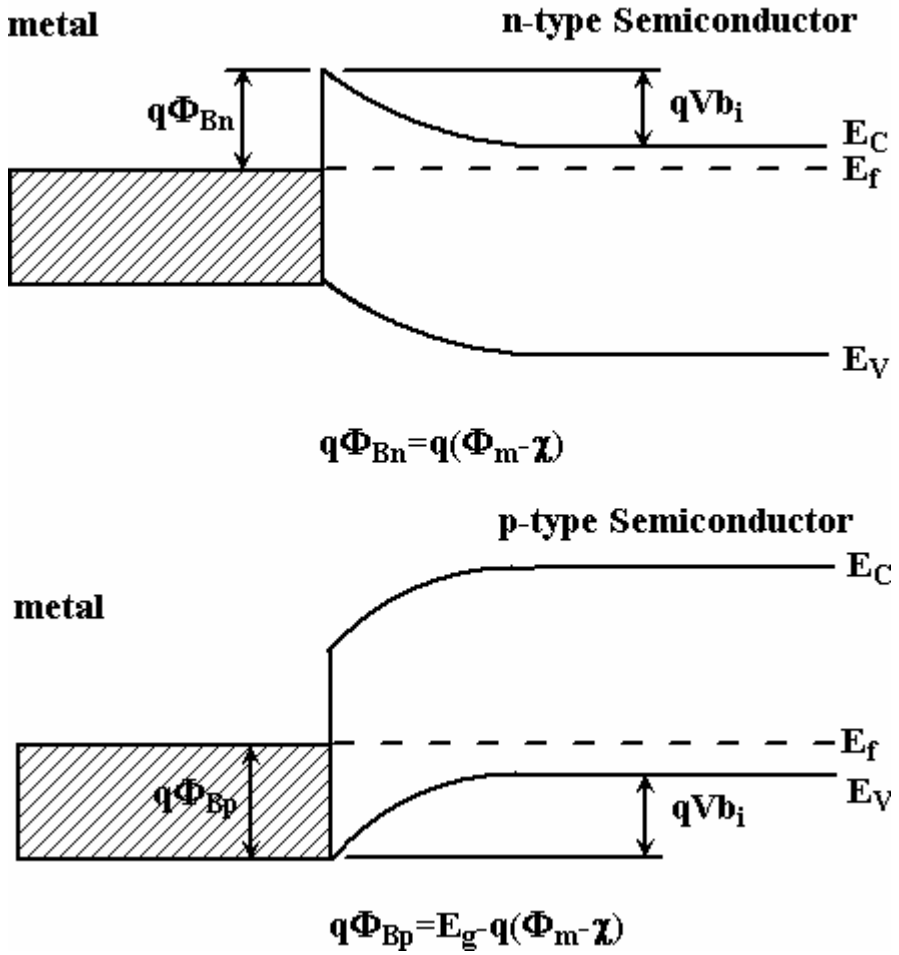

Fig. 4.7 Formation of Schottky barrier for a metal in contact with a semiconductor

Theoretically, the Schottky barrier height is only determined by the work function of metal and the electron affinity of n-type semiconductor. The equations used to calculate the barrier height are given in the figure.

For I-V characterization, Al, Ni, and Cu are deposited on copper oxide by thermal evaporation through a shadow mask with a dot area of 3.6×10^{-4} cm^2. The metal dots are used as the mask for etching copper oxide in 0.25 M H_2SO_4. After etching, metal/copper oxide diodes are ready for I-V measurements, which are performed with a HP 4145A probe station.

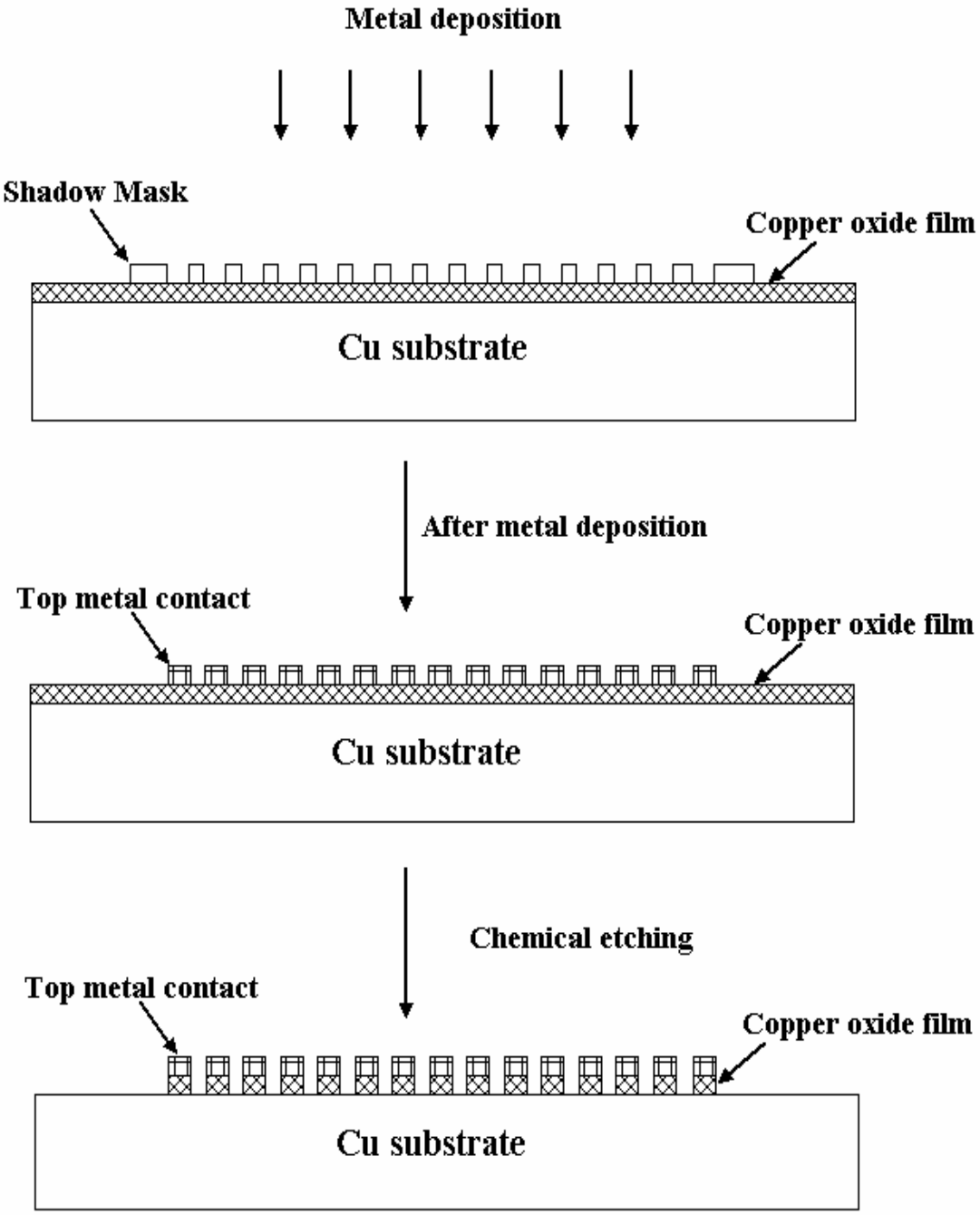

Fig. 4.8 Fabrication of metal/copper oxide Schottky diodes

4.2.9 Capacitance-voltage (C-V) characterization

Capacitance-voltage (C-V) characterization is performed in a three-electrode cell, of which the working electrode is cuprous oxide, the counter electrode is a platinum foil and the reference electrode is Ag/AgCl/saturated KCl. Solution used is a non-aqueous solution of 0.1 M tetrabutylammonium hexafluorophosphate in acetonitrile. All the measurements are controlled and recorded by a PARSTAT 273 system.

C-V method involves measuring capacitance as a function of applied voltage under depletion condition. There are two capacitances to be considered: capacitance of the space charge region and capacitance of the double layer, which are in series. Since the space charge capacitance is much smaller than the double layer capacitance, the contribution of the double layer capacitance is negligible. Capacitance-voltage data is generally analyzed by the Mott-Schottky equations[82] shown as follows:

$$\text{n-type: } \frac{1}{C_{sc}^2} = \frac{2}{e\varepsilon\varepsilon_0 A^2 N_D}(V - V_{fb} - \frac{KT}{e}) \qquad (4\text{-}6)$$

$$\text{p-type: } \frac{1}{C_{sc}^2} = -\frac{2}{e\varepsilon\varepsilon_0 A^2 N_A}(V - V_{fb} + \frac{KT}{e}) \qquad (4\text{-}7)$$

where C_{sc} represents the capacitance of the space charge region, ε is dielectric constant of the semiconductor, ε_0 is permittivity of free space, A is the area of the working electrode, N_D and N_A are the doping concentration, V is the applied voltage, V_{fb} is the flat band potential, K is the Boltzmann constant (1.38×10^{-23} J/K), T is the absolute temperature (298 K) and e is the electronic charge (1.6×10^{-19} C).

The Mott-Schottky plot ($1/C^2$ vs. V) can supply information related to electrical properties, such as conduction type, flat band potential and doping concentration of the

semiconductor. Positive slope refers to an n-type semiconductor, while negative slope refers to a p-type semiconductor. Also from the slope (S), doping concentration can be calculated according to equation (4-8):

$$N = \frac{2}{e\varepsilon\varepsilon_0 A^2 S} \tag{4-8}$$

From the intercept (V_0), the flat band potential can be calculated by equation (4-9), where "-" refers to n-type and "+" refers to p-type.

$$V_{fb} = V_0 \mp \frac{KT}{e} \tag{4-9}$$

CHAPTER 5

EFFECT OF DEPOSITION CONDITIONS ON PROPERTIES OF CUPROUS OXIDE

Cuprous oxide (Cu_2O) is a p-type semiconductor that has attracted increasing attention in recent years as an active component in solar cells and photodiodes. It has also been used to form junctions with other n-type oxide semiconductors such as TiO_2 and ZnO for various applications.[83-86] Cuprous oxide has a band-gap of 1.9~2.1 eV and a high absorption coefficient over the wavelength range of the solar spectrum.[18-27] Its component elements are non-toxic and are highly abundant. Cuprous oxide can be synthesized by thermal oxidation, anodic oxidation, electrochemical deposition, sol-gel chemistry, and sputtering deposition.

Electrodeposition is a versatile and low-cost technique for preparing thin films of oxide semiconductors. Lots of work has been done on electro-deposition of cuprous oxide. An interesting aspect of electrodeposited Cu_2O is how the bath pH influences grain orientation in the film. In an early report[35], films deposited from an alkaline bath (pH ~9) were found to be highly oriented along the (100) plane regardless of the deposition history and the type of substrate. Subsequent work by the same group[36, 37] revealed that at bath pH value higher than ~9.5, the (111) preferred orientation was observed. Another group[38, 40] reported a transition of the preferred orientation from (100) to (111), which occurs around pH of 11.0.

In this chapter, the influence of the bath pH on grain orientation and crystallite shape in Cu_2O films is carefully re-examined. In addition to the (100) and (111) preferred orientations identified in previous studies, a third preferred orientation, (110), is identified in a narrow pH range, ~9.4- ~9.9. A new theory is developed to explain how bath pH affects the orientation and the crystallite shape of as-deposited cuprous oxide films. Besides the structural properties, electrical properties such as the flat band potential (V_{fb}) are found to shift with the orientations. To our knowledge, this is the first report of how the bath pH has a profound influence on the subsequent interfacial behavior of an electrodeposited film as manifested by the corresponding variations in V_{fb}.

5.1 Sample preparation

Indium tin oxide (ITO) coated glass with a sheet resistance of 30 ohms/□ is used as the working electrode and a platinum foil is used as the counter electrode. Before deposition, ITO glass and platinum foil are degreased in ultrasonicated acetone, etched in diluted HCl and finally rinsed in de-ionized water.

Cuprous oxide films are electrodeposited from a solution containing 0.4 M copper sulfate and 3 M lactic acid.[35-39] The bath pH is carefully adjusted between 7.5 and 12.0 by controlled addition of 4 M NaOH. Films are grown at -0.40 V (vs. Ag/AgCl/saturated NaCl) for 30 minutes. Deposition temperature is controlled between 20 ºC and 70 ºC with a Precision 280 water bath.

5.2 Cyclic voltammetry

Before any deposition, cyclic voltammetry is performed in the same cell as for deposition to figure out parameters needed for the deposition of cuprous oxide. In Fig. 5.1, a typical CV is shown with the corresponding conditions.

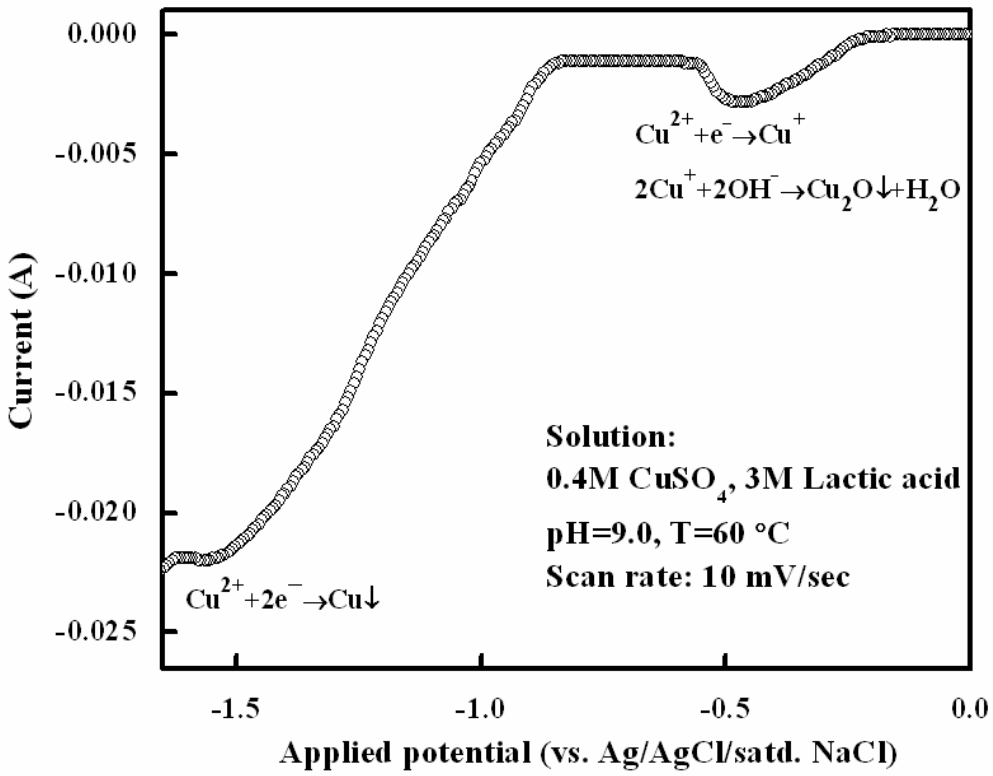

Fig. 5.1 Cyclic voltammetry curve for solution containing 0.4M $CuSO_4$ and 3M lactic acid (pH=9.0, T=60 ºC)

According to the CV curve, deposition of Cu_2O occurs between -0.17 V to -0.56 V. -0.4 V is selected as the deposition potential for a reasonable deposition rate.

5.3 Optical characterization

Optical characterization is performed with a Jasco V570 UV-Vis spectrophotometer. Transmittance spectrum (400nm~1100nm) shows that the bath pH

barely has no effect on the optical properties of as-deposited cuprous oxide films. In Fig. 5.2, a transmittance spectrum is shown with deposition conditions.

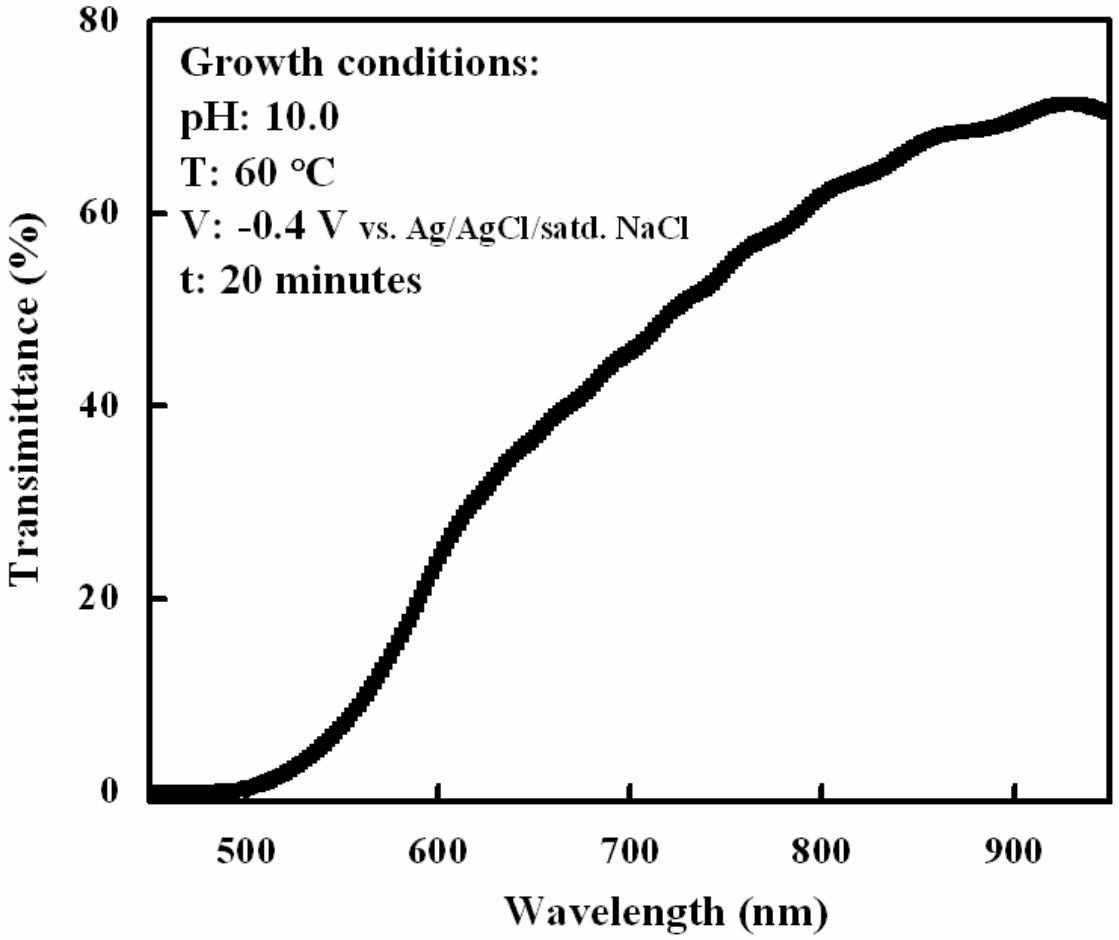

Fig. 5.2 Transmittance spectrum of as-deposited cuprous oxide

To analyze the spectrum, the following equation is used:

$$(\alpha h\nu)^n = A(h\nu - E_g) \qquad (5\text{-}1)$$

where α is the absorption coefficient and n depends on the nature of the band-gap (n = 1/3 for indirect forbidden transition, n = 1/2 for indirect allowed transition, n = 2/3 for direct forbidden transition, and n = 2 for direct allowed transition). We tried all the

values for n and only n = 2 gives a linear $(\alpha h\nu)^n$-$h\nu$ plot as shown in Fig. 5.3, which indicates that electrodeposited Cu_2O has a direct band-gap. The intercept of the plot with the $h\nu$ axis shows that Cu_2O has a band-gap of 2.06 eV, which is consistent with the reported band-gap values for Cu_2O.[18-27]

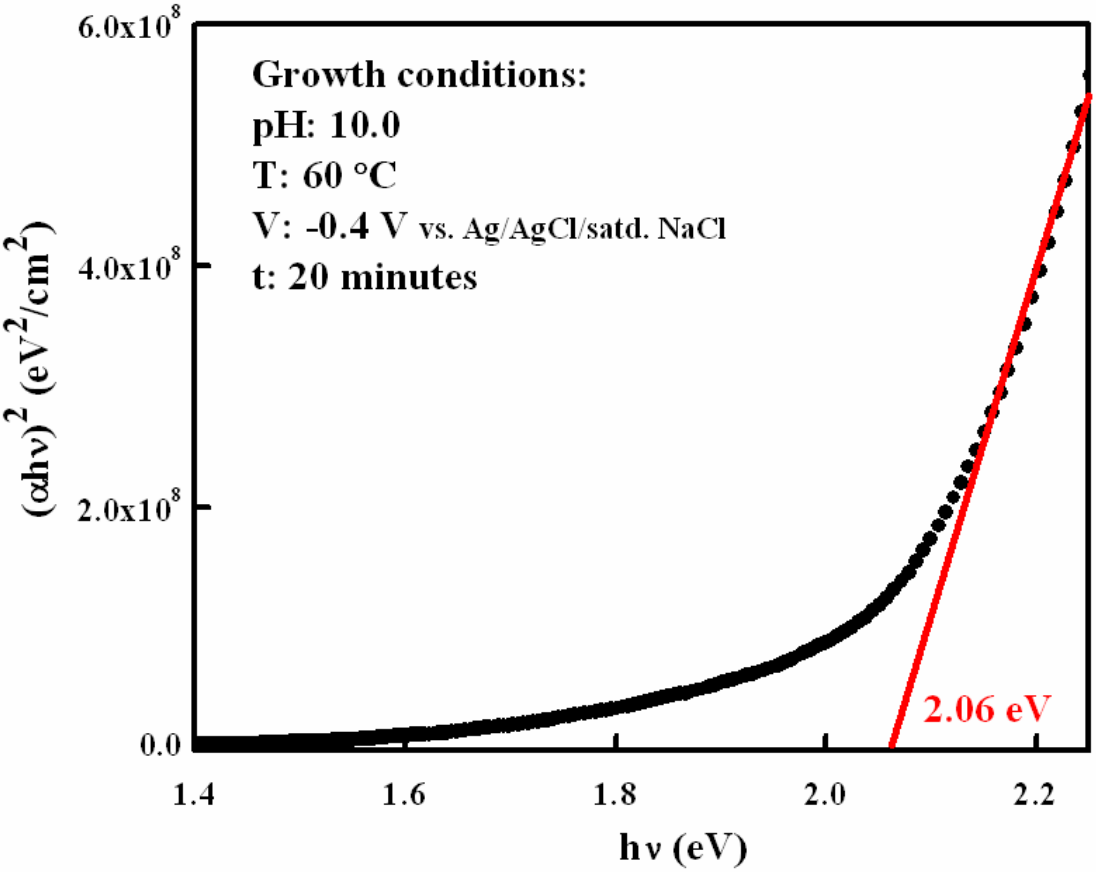

Fig. 5.3 $(\alpha h\nu)^2$-$h\nu$ plot of an electrodeposited cuprous oxide film

5.4 Growth rate

Generally, the growth rate of electro-deposition depends on the applied potential (current), bath temperature, concentration of electroactive species and deposition time.

As a constant potential (-0.4 V) is applied for cuprous oxide deposition, the growth rate is only determined by the last three factors, which are discussed in following sections.

5.4.1 Growth rate as a function of deposition time

Different durations are selected for three sets of samples deposited at different bath pH (9.0, 10.0, and 12.5). Bath temperature is kept at 60 ºC.

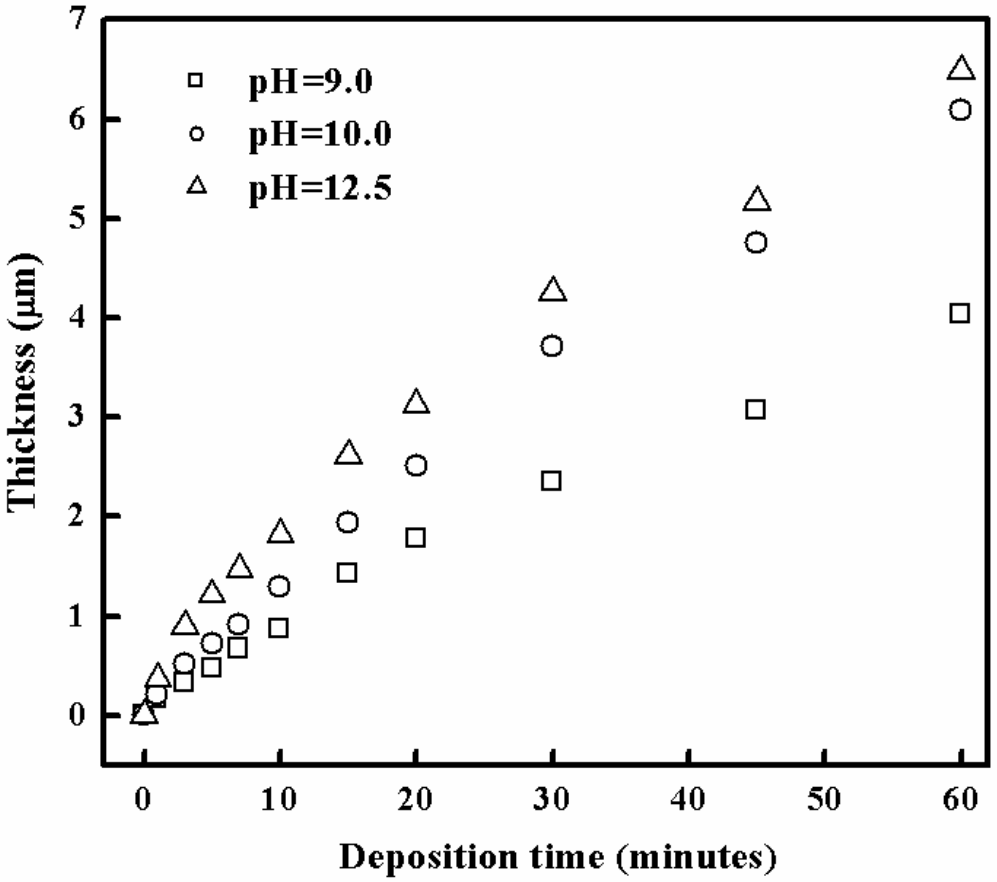

Fig. 5.4 Dependence of film thickness on deposition time

As shown in Fig. 5.4, all curves show a decelerated increasing trend as deposition time increases. Different from other physical deposition methods such as thermal evaporation and sputtering, electro-deposition is closely related with the electron transfer process at the electrode surface. As deposition goes on, ITO substrate

is gradually covered by a cuprous oxide film, which is much less conductive than ITO. Therefore, the transfer rate of electrons at the electrode surface is lowered, which results in a slower growth process.

5.4.2 Bath pH and temperature effect on growth rate

Samples are deposited at bath pH between 8.0 and 12.0 with a step of 1.0 and the bath temperature is adjusted between 20 ºC to 70 ºC with a step of 10 ºC. The growth rate is specified by the film thickness of 30 minutes deposition.

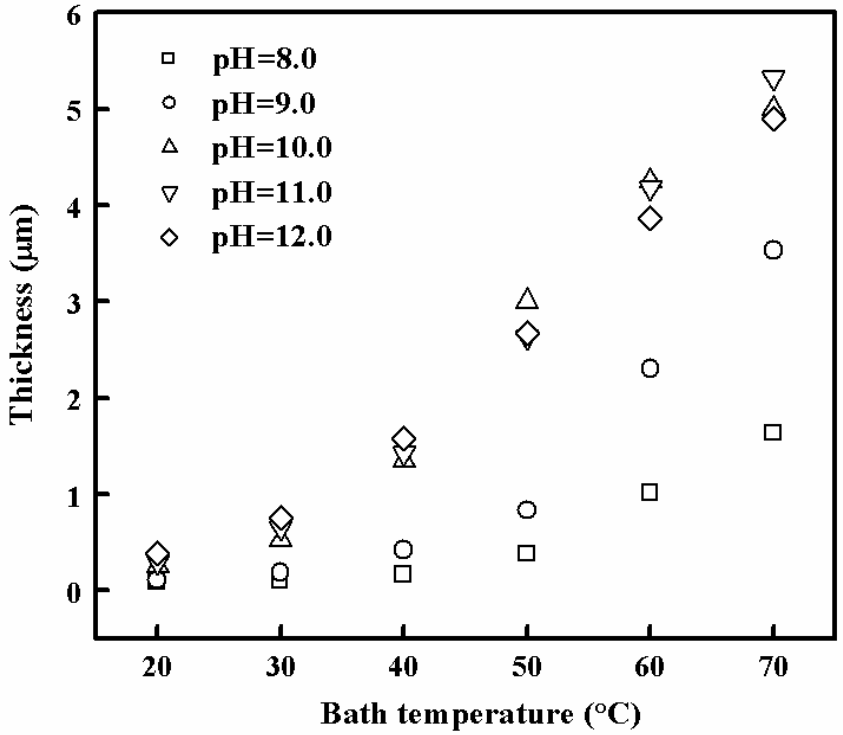

Fig. 5.5 Bath pH and temperature effect on growth rate of cuprous oxide

As shown in Fig. 5.5, the growth rate increases with increasing bath pH or temperature. Generally, crystal growth consists of two steps: nucleation and growth of grain, which mainly depend on growth temperature and concentration of electroactive species. At a given temperature, film thickness is mainly determined by the

concentration of electroactive species: Cu^{2+} and OH^-. As $[Cu^{2+}]$ is kept constant for all depositions, $[OH^-]$, i.e., bath pH, is the dominant factor. As the bath pH increases, it's easier to form nuclei of cuprous oxide at the electrode surface, which leads to higher growth rate.

At a given bath pH value, $[Cu^{2+}]$ and $[OH^-]$ are constant and the growth rate is mainly determined by bath temperature. The higher temperature is, the easier it is to form nuclei and grow grains, which results in higher growth rate.

5.5 pH effect on structural properties

Bath pH not only affects the growth rate of the poly-crystalline cuprous oxide films but also affects the orientation and surface morphology of the films. At different bath pH, as-deposited films show three different preferred orientations, which are characterized by XRD and SEM.

Samples are prepared from a bath containing 0.4 M copper sulfate and 3 M lactic acid at 60 ºC. The bath pH is adjusted from 7.0 to 12.0 with a step of 0.2 by controlled addition of 4M NaOH. Films are grown at -0.40 V (vs. Ag/AgCl/saturated NaCl) for 30 minutes.

5.5.1 pH effect on crystal orientation

XRD patterns of cuprous oxide films deposited at different bath pH are shown in Fig. 5.6 to 5.9.

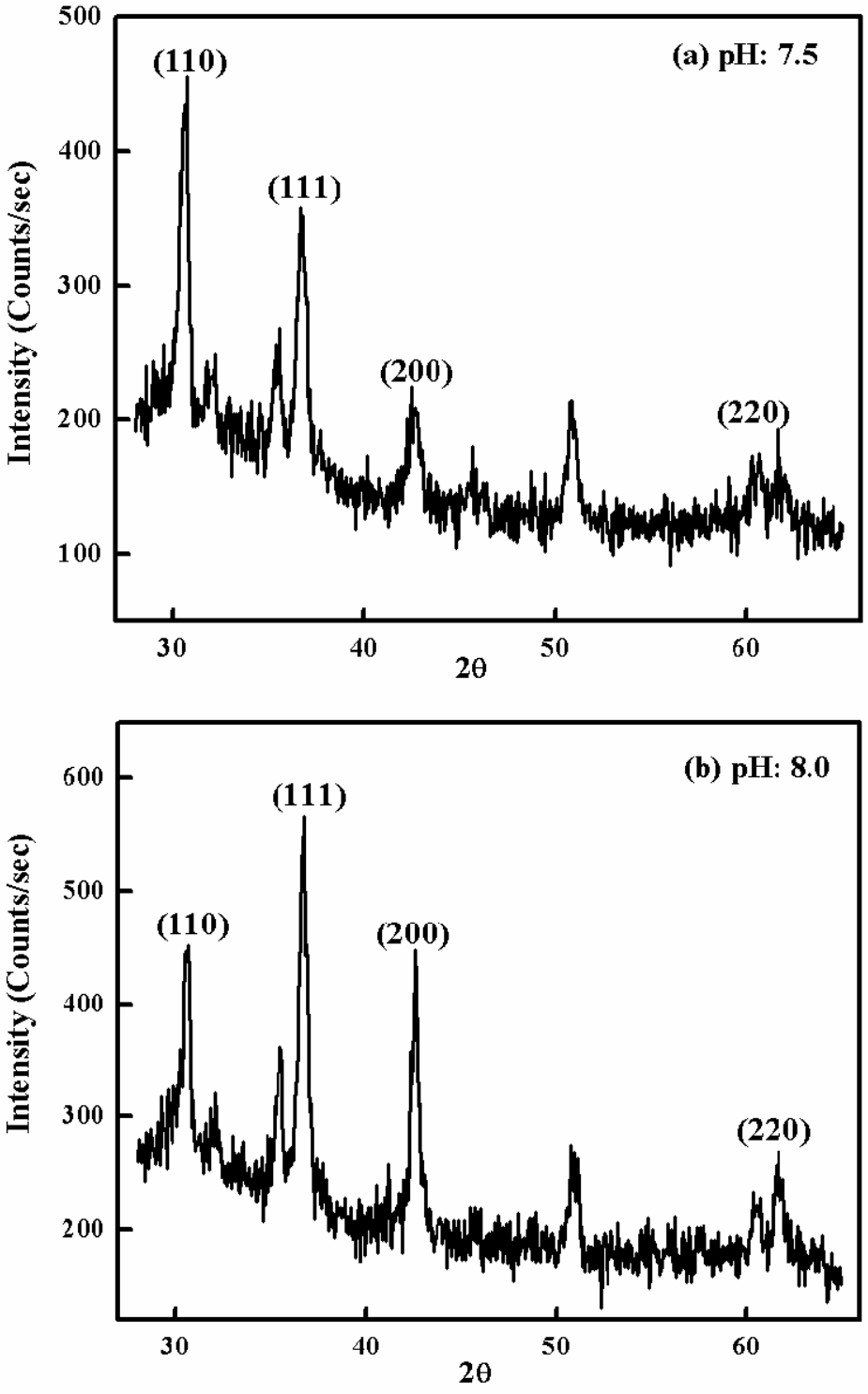

Fig. 5.6 XRD patterns of cuprous oxide films: (a) pH=7.5, (b) pH=8.0

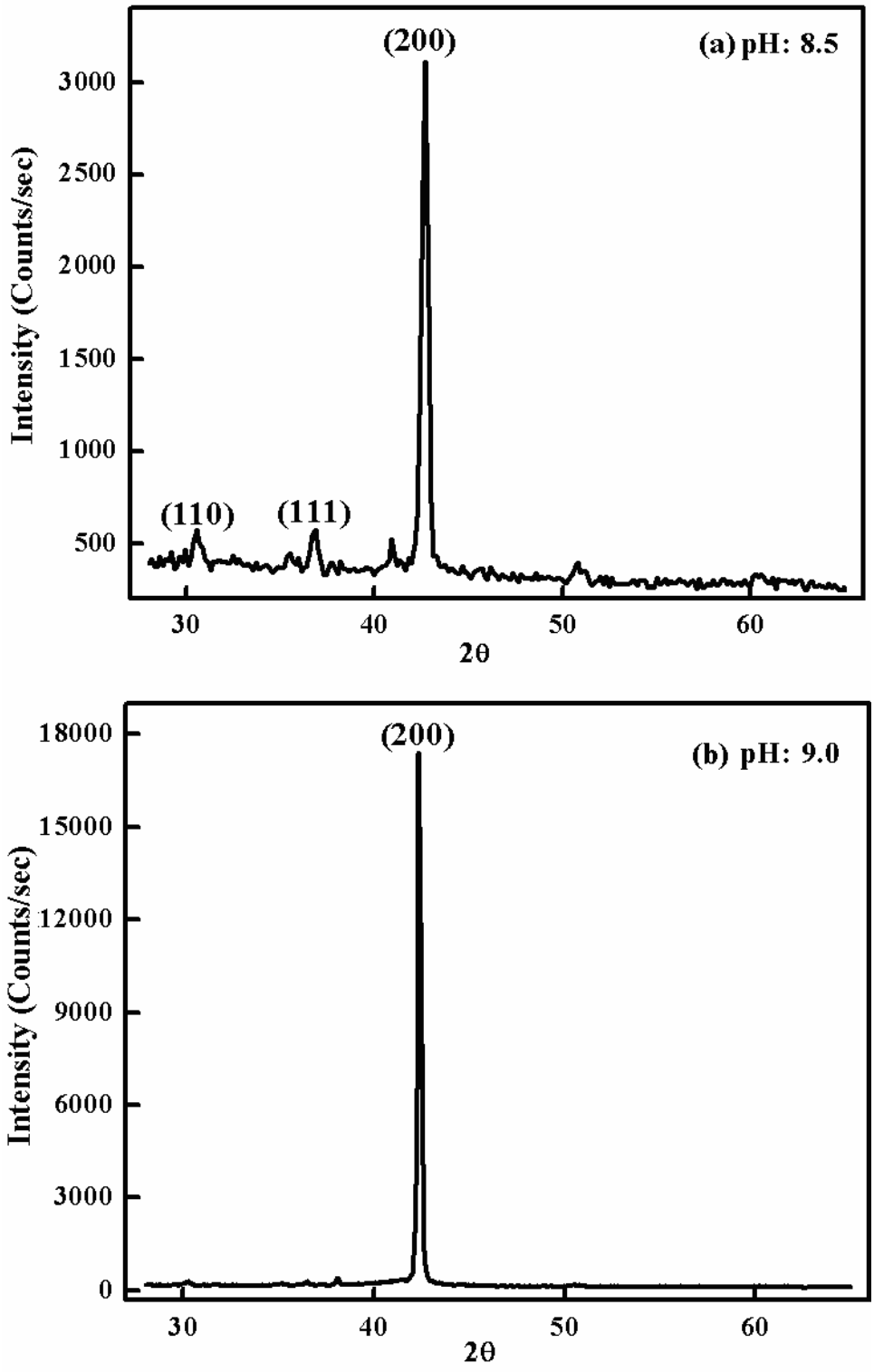

Fig. 5.7 XRD patterns of cuprous oxide films: (a) pH=8.5, (b) pH=9.0

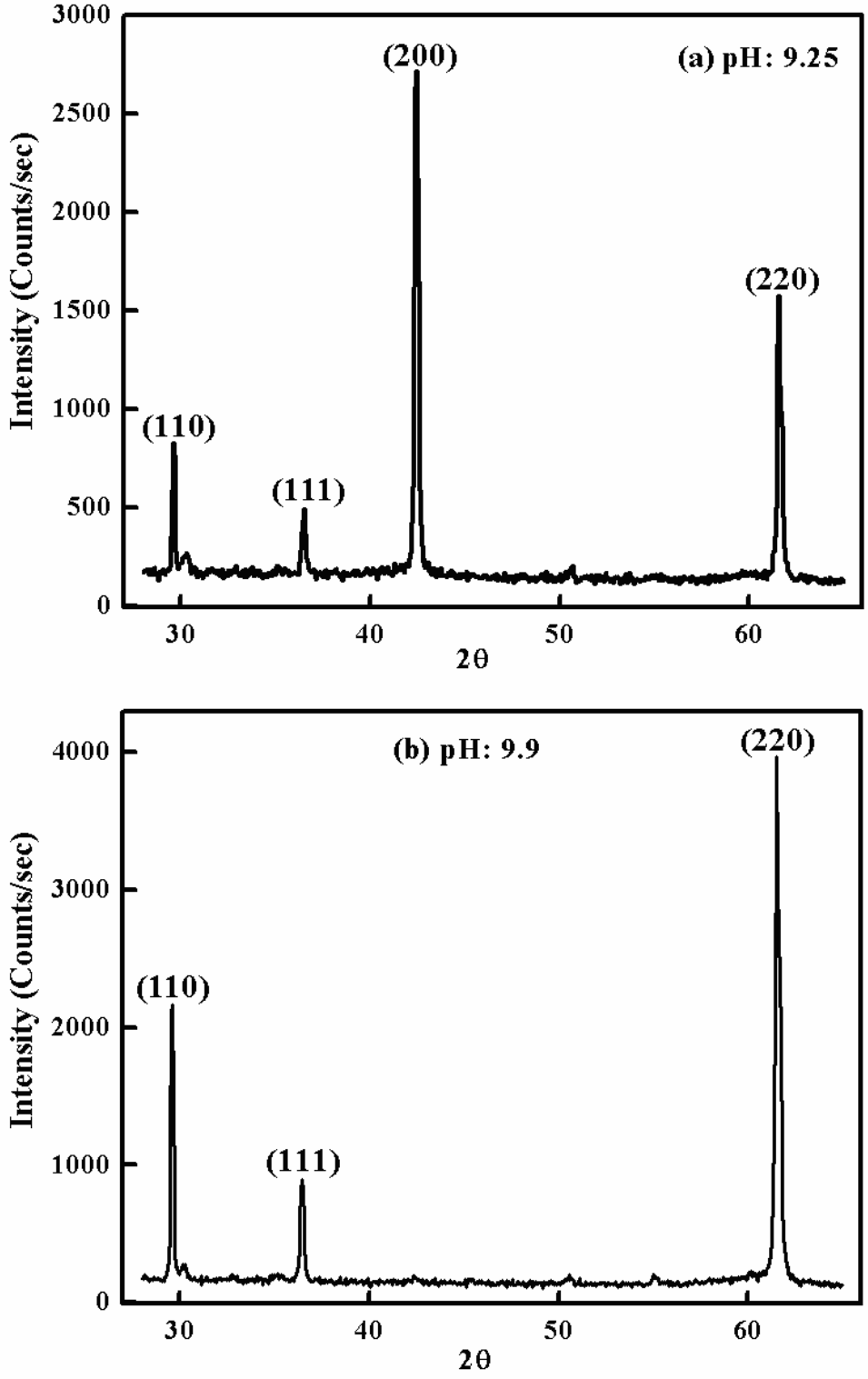

Fig. 5.8 XRD patterns of cuprous oxide films: (a) pH=9.25, (b) pH=9.5

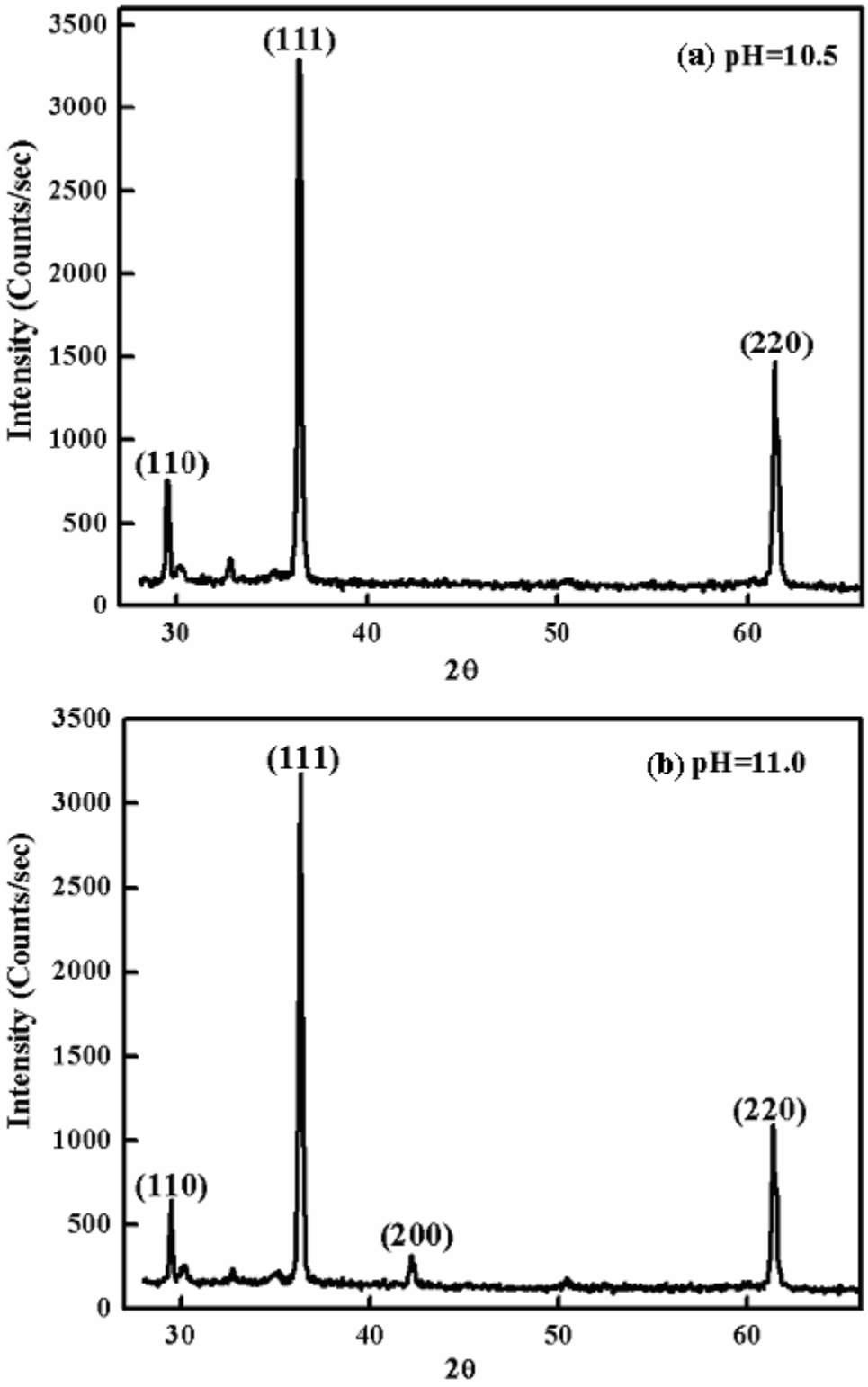

Fig. 5.9 XRD patterns of cuprous oxide films: (a) pH=10.5, (b) pH=11.0

It's found that at lower bath pH (<8.2) cuprous oxide films have quite poor quality, while for pH over 8.2, the crystallinity of cuprous oxide improves dramatically. Besides the crystallinity, the orientations of cuprous oxide films also change with bath pH.

There is no preferred orientation for samples deposited at pH lower than 8.2. When pH increases over 8.2, the intensity of the (200) (equivalent to (100)) peak starts to increase and reaches a maximum at pH around 9.0. As pH keeps on increasing, the (110) orientation replaces (100) as the dominant orientation, and at even higher pH (>10.2), the (111) orientation becomes dominant. To better understand how the bath pH affects the crystal orientation, the relative intensity of each crystal orientation is determined from the corresponding XRD peak area and the calculated result is shown in Fig. 5.10. As shown, the pH range for different crystal orientations is well defined. The (100) orientation dominates between bath pH values of ~ 8.2 and ~ 9.1, while the pH range for the (110) orientation is limited to ~ 9.4 - ~ 9.9. When the bath pH value is above ~ 10.2, the (111) orientation becomes dominant. The rather narrow pH range of the (110) preferred orientation offers a rational reason why this particular orientation has been missed in the previous reported studies.[35-40]

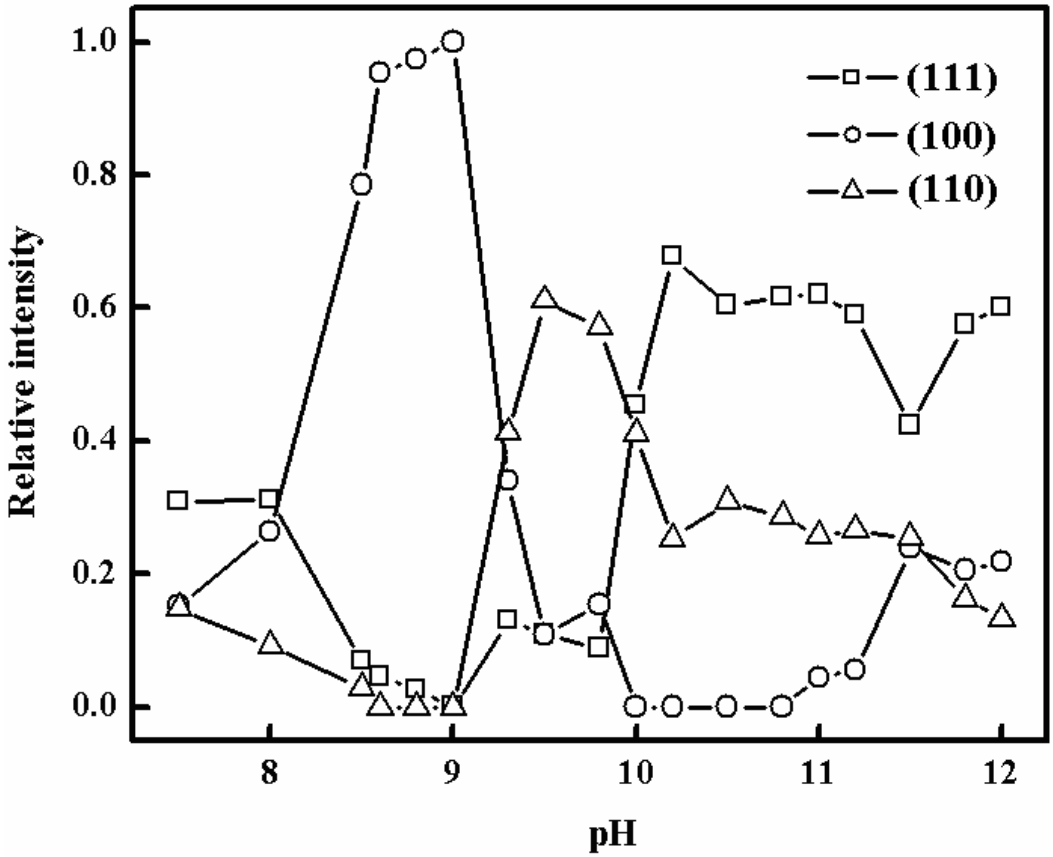

Fig. 5.10 Relative intensity for three preferred orientations: (100), (110) and (111) as a function of bath pH

5.5.2 pH effect on surface morphology

As orientation changes, cuprous oxide film shows different surface morphology. Three samples (deposited at pH=9.0, 9.9, and 12.0, respectively) with different orientations are chosen for SEM characterization.

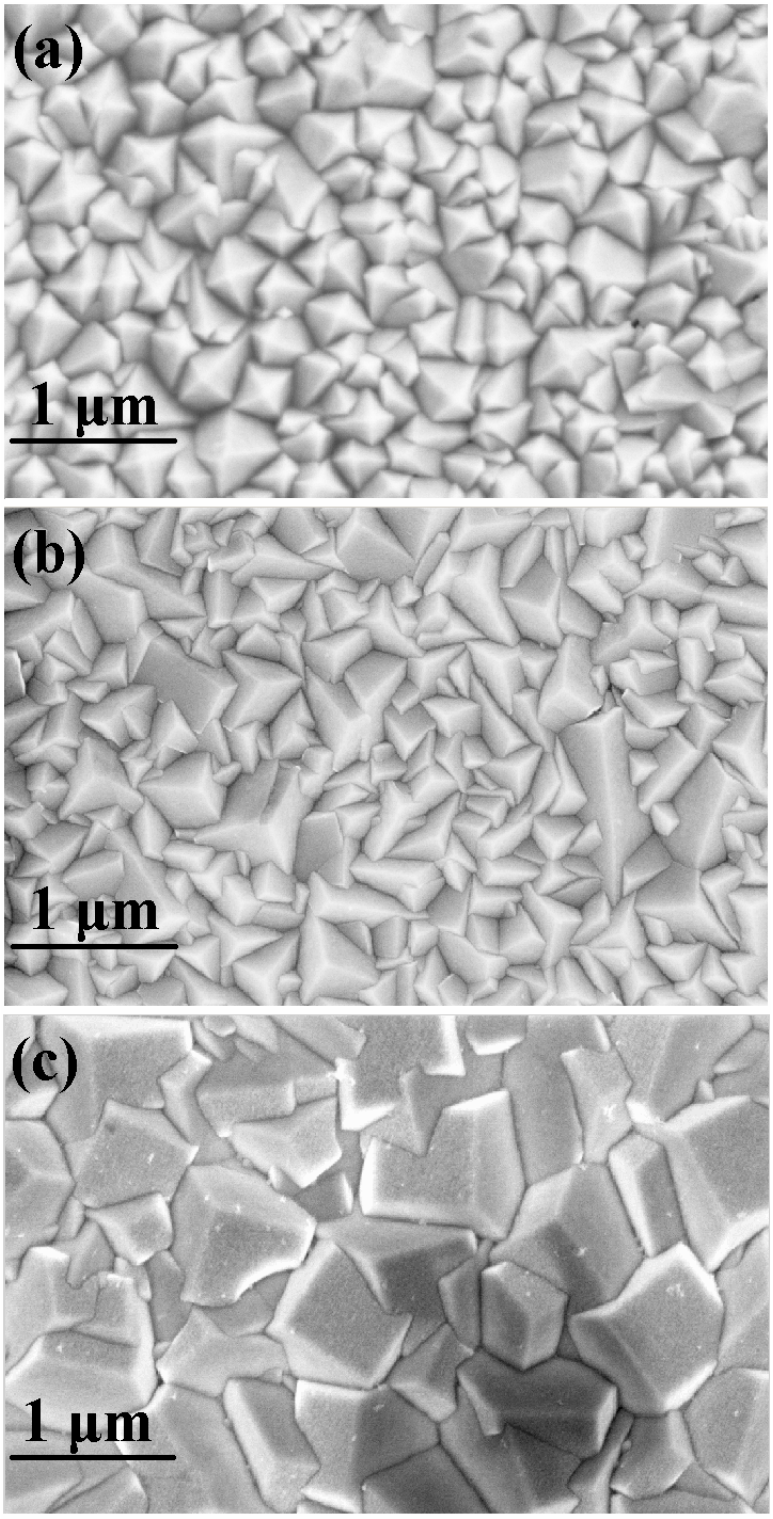

Fig. 5.11 Surface morphology of differently orientated cuprous oxide films: (a) (100), (b) (110), and (c) (111)

For sample with the (100) orientation (Fig. 5.11 (a)), the crystal grains appear as 4-sided pyramids with a 4-fold symmetry, the faces of which should be ascribed to the {111} crystallographic plane. The grains have a relatively uniform size distribution with an average size of ~ 0.3 μm. For sample with the (110) orientation (Fig. 5.11 (b)), the grains show a shape change from 4-sided pyramids to triangular prisms, faces of which should be ascribed to the {100} crystallographic planes. The size distribution is much less uniform compared to the (100) orientated film with a size range from 0.2 μm to 0.8 μm. Fig. 5.11 (c) shows the surface morphology of the (111) orientated films. The grains have a shape of 3-faced pyramid, faces of which should be ascribed to the {100} crystallographic plane. It is also seen that the grain size shows a dramatic change with a much larger average size of ~ 0.8 μm.

5.5.3 Analysis of pH effect on structural properties

To our knowledge, A. E. Rakhshani et al[35-37] first reported bath pH effect on the orientation and surface morphology of electrodeposited cuprous oxide. Both (100) and (111) orientations were reported and as explained, bath pH controlled the structural properties by affecting the deposition rate. Thereafter, Zhou et al[38-40] published similar results and used a computational model to explain the pH effect on crystal growth. The model was based on Donnay-Harker theory[87], which defines that the surface with slowest rate is of the highest morphological importance in the crystal morphology. However, there was no explanation about why pH would affect deposition rate or crystal orientation, which will be addressed in following section.

By correlating experimental results with the understanding of crystal structure of cuprous oxide, we propose a new systematic explanation about how the bath pH affects the orientation and surface morphology of electrodeposited cuprous oxide films.

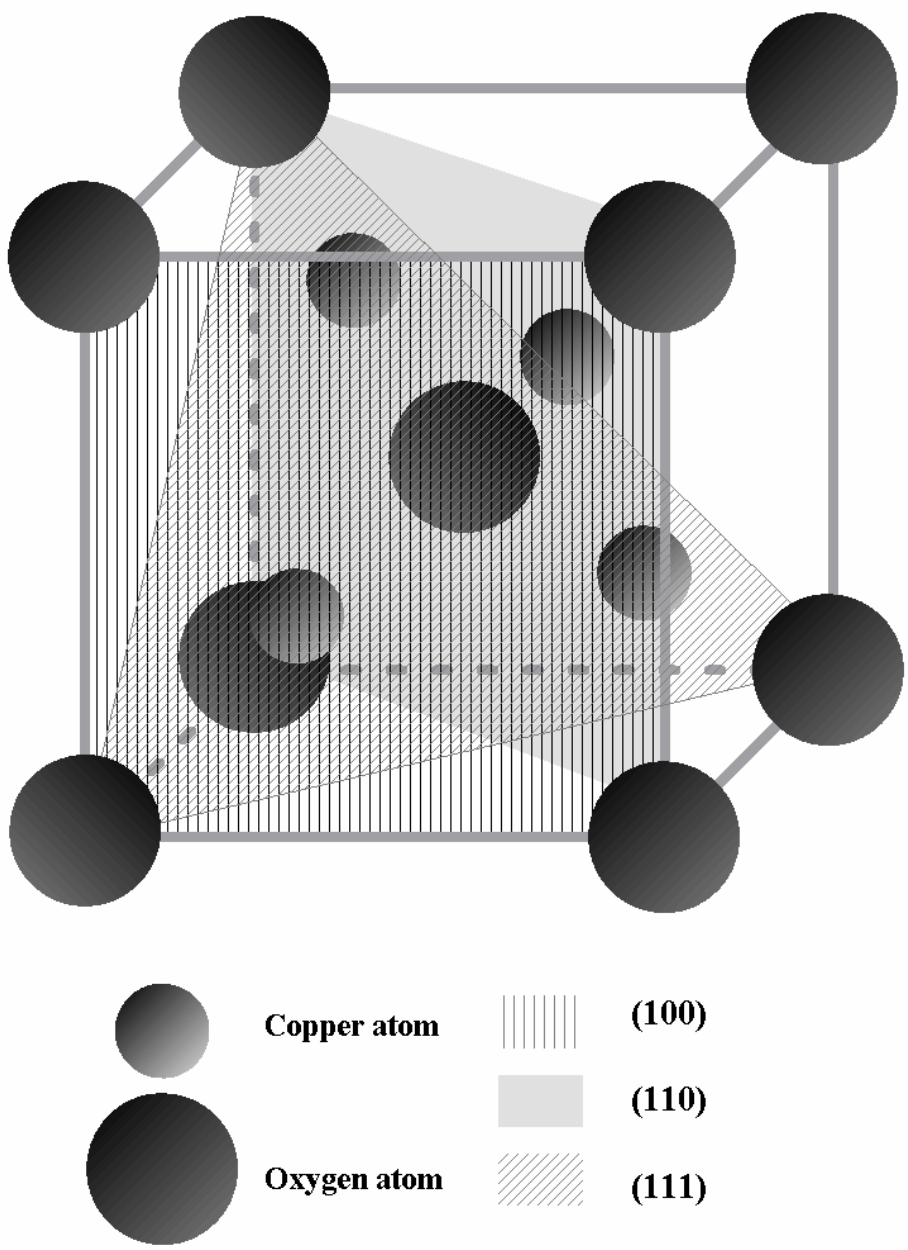

Fig. 5.12 Three major crystallographic planes in a cuprous oxide cell

As shown in Fig. 5.12, the number of oxygen atoms per unit area (N_0) is different for the (100), (110), and (111) planes. N_0 increases from 2.78 nm^{-2} to 5.89 nm^{-2} to 8.83 nm^{-2} for the (100), (110) and (111) plane, respectively. According to the mechanism of cuprous oxide deposition, Cu^{+} comes from the reduction of Cu^{2+} and O^{2-} comes from OH^{-} in the solution. Because $[Cu^{2+}]$ is kept constant throughout the deposition, $[OH^{-}]$, i.e., the pH will determine the growth rate of different crystallographic faces and thus control the orientation.

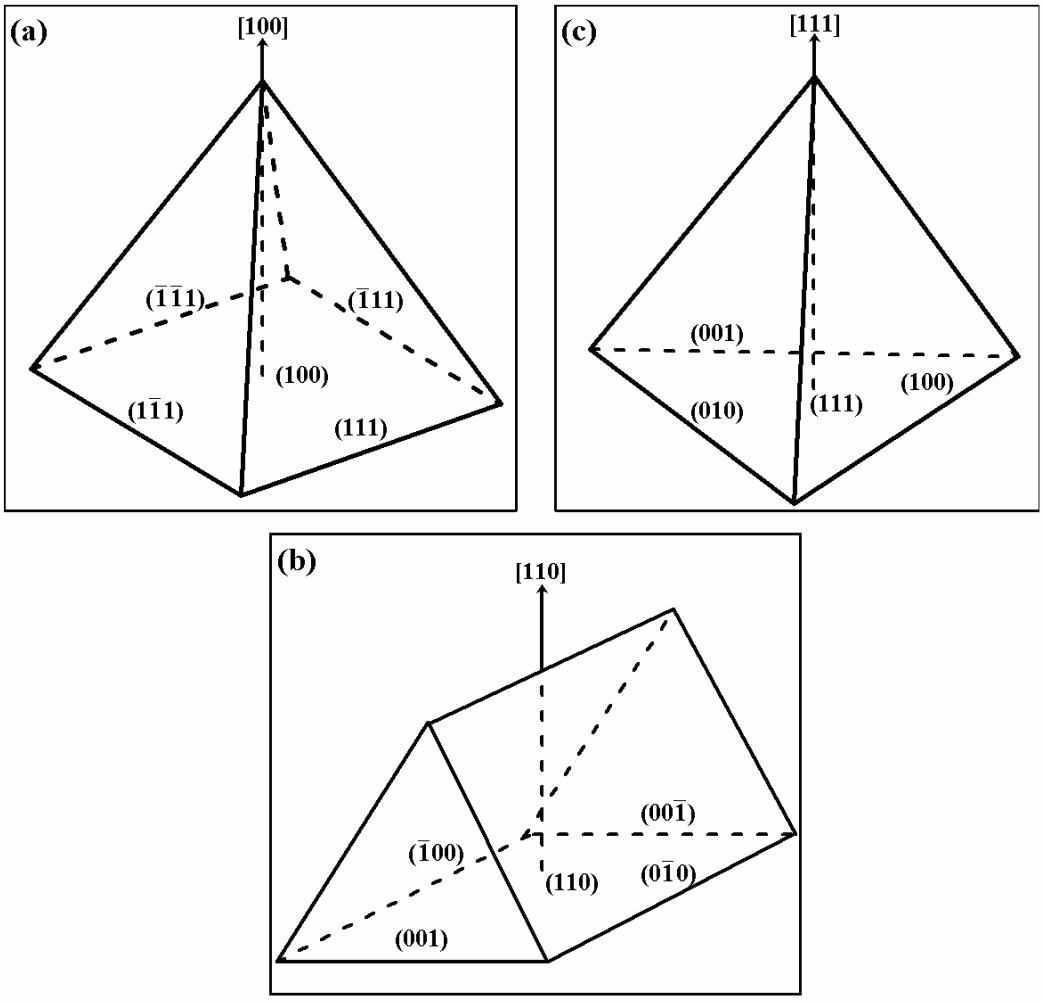

Fig. 5.13 Expected crystallite shape of differently orientated grains: (a) (100), (b) (110), and (c) (111)

At relatively low bath pH (low [OH^-]), the growth rate of the {111} planes (with highest N_0) is the slowest, which defines the grain shape as 4-sided pyramids (Fig. 5.13 (a)). The side faces refer to the {111} planes and the axis perpendicular to the substrate is <100>. As the bath pH value increases, the concentration of hydroxyl ions increases, which favors the growth of crystallographic faces with higher N_0 value, i.e., the growth rate of the (110) and (111) planes exceed that of (100), which in turn changes the grain shapes to triangular prism (Fig. 5.13 (b)) and 3-sided pyramid (Fig. 5.13 (c)), respectively. For the (110) oriented sample, side faces refer to the {100} planes and the axis perpendicular to the substrate is <110>. For the (111) oriented sample, side faces refer to the {100} crystallographic planes and the axis perpendicular to the substrate is <111>.

In conclusion, the bath pH controls the orientation of cuprous oxide film by affecting the growth rate of different crystallographic planes with different O density. In other words, varying the bath pH may control the composition of cuprous oxide films and furthermore control the conduction type, which is discussed in chapter 5.

5.6 pH effect on electrical properties

As the bath pH changes the crystal orientation of electro-deposited cuprous oxide, it may change the electrical properties as well. Cuprous oxide samples with different orientations are selected for capacitance-voltage (C-V) measurements, which are performed in a three-electrode cell. Cuprous oxide is set as the working electrode, and the reference electrode is Ag/AgCl/saturated KCl. The solution used is non-aqueous

solution of 0.1 M tetrabutylammonium hexafluorophosphate in acetonitrile.[88] The Mott-Schottky plots ($1/C^2$ vs. V) are presented in Fig. 5.14.

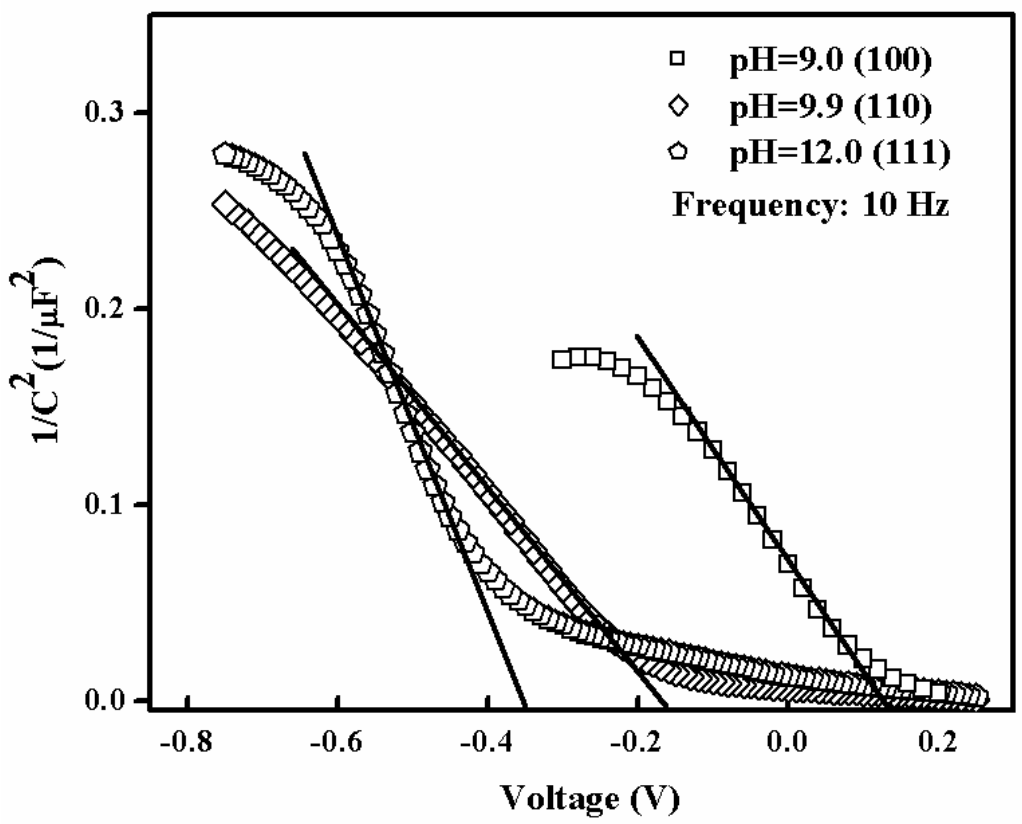

Fig. 5.14 Mott-Schottky plots for cuprous oxide films with different orientations

It's well known that the negative slope of the Mott-Schottky plot indicates a p-type semiconductor behavior. From the plots shown above, it is concluded that cuprous oxide is a p-type semiconductor. Therefore, C-V data is analyzed with the Mott-Schottky equation[82] shown as follows:

$$\frac{1}{C_{sc}^2} = -\frac{2}{e\varepsilon\varepsilon_0 A^2 N_A}(V - V_{fb} + \frac{KT}{e}) \qquad (5\text{-}2)$$

where C_{sc} represents the capacitance of the space charge region, ε is the dielectric constant of cuprous oxide (taken as 8.6[89]), ε_0 is the permittivity of free space, A is the

area of the working electrode, N_A is the carrier concentration, V is the applied voltage, V_{fb} is the flat band potential, K is the Boltzmann constant (1.38×10^{-23} J/K), T is the absolute temperature (298 K) and e is the electronic charge (1.6×10^{-19} C).

From the slope (S) and the intercept (V_0), the carrier concentration and flat band potential (V_{fb}) are calculated according to equations (5-3) and (5-4), respectively.

$$N_A = \frac{2}{e\varepsilon\varepsilon_0 A^2 S} \tag{5-3}$$

$$V_{fb} = V_0 + \frac{KT}{e} \tag{5-4}$$

For the 5 selected samples, N_A fluctuates from 2×10^{18} cm^{-3} to 5.5×10^{18} cm^{-3}, which are several orders of magnitude higher than the carrier concentration obtained with Hall measurements.[90] The calculated V_{fb} is shown in Fig. 5.15.

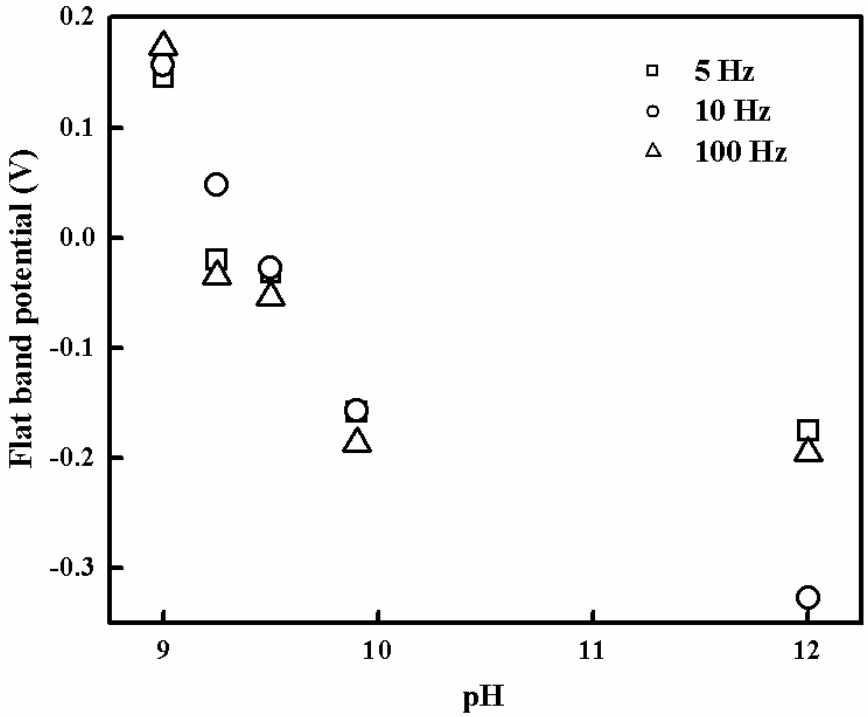

Fig. 5.15 V_{fb} for cuprous oxide deposited at different bath pH.

For different applied frequencies, the flat band potential shows a similar trend with the bath pH (film orientation). The V_{fb} value for the sample deposited at pH=9.0 is in good agreement with that reported in a previous study.[88] As pH increases, the orientation of cuprous oxide films changes from (100) to (110) and (111) and the flat band potential shows a rather remarkable negative shift from 0.157 V to -0.331 V.

V_{fb} is affected by a number of parameters, including the surface state density at the semiconductor/electrolyte interface, surface charge distribution, pH of aqueous electrolyte and ion adsorption on the surface.[91] It must be noted that the present observations of the variation in V_{fb} with bath pH are rooted in the corresponding predominance of specific grain orientations as the bath pH is varied.[92, 93] This trend is entirely different from the (more common) Nernstian variation in V_{fb} observed for oxide semiconductor surfaces as the aqueous electrolyte pH is varied. Such a shift in V_{fb}, which amounts to -60 mV/pH (at 298 K), in fact, has been reported for the cathodically electrodeposited Cu_2O samples by other authors.[94] We performed the C-V measurements in a non-aqueous medium precisely to preclude the interference from this interfacial phenomenon for oxide surfaces in aqueous media. It is reasonable to attribute the variations in V_{fb} to the following possible reasons. The first reason is that different crystallographic planes have different atomic compositions, i.e. the Cu^{+}/O^{2-} ratio, which may suggest that the surface state density is different and thus V_{fb} varies with orientation. The second reason is that adsorption of the $[PF_6]^{-}$ (anions in supporting electrolyte) on different crystallographic planes could result in the V_{fb} shift.

5.7 Summary

In this chapter, pH effect on structural properties and electrical properties of electro-deposited cuprous oxide films is discussed. In the pH range of 7.5 to 12.0, there are three different preferred orientations. Besides the reported (100) and (111) orientations, the (110) orientation is also achieved. To our knowledge, (110) orientation is first reported by us and it is very sensitive to deposition conditions such as solution pH and current density. With different orientations, cuprous oxide shows different surface morphology and grain size. A brand new explanation for the mechanism of bath pH effect on structural properties is proposed as the following. The bath pH controls the orientation of cuprous oxide film by affecting the growth rate of crystallographic planes with different Cu^{+}/O^{2-} ratio. Besides the structural properties, electrical properties such as the flat band potential (V_{fb}) are found to shift with the orientations. To our knowledge, this is the first report on how the bath pH has a profound influence on the subsequent interfacial behavior of an electrodeposited film as manifested by the corresponding variations in V_{fb}. However, optical properties don't show any apparent change with orientation.

CHAPTER 6

SUBSTRATE CLEANING IN ELECTROCHEMICAL DEPOSITION OF CUPRIC OXIDE

Cupric oxide (CuO) is known to be a p-type semiconductor[55-59] with a band-gap of 1.2–1.9 eV,[56, 59-64] which makes it suitable for photovoltaic applications. CuO can be synthesized by thermal oxidation,[65, 66] sputtering,[33, 59, 64] sintering,[67-69] and electrochemical deposition.[58, 73-75] Among these methods, electrochemical deposition is particularly suitable for photovoltaic applications with its low cost, low deposition temperature, and precise control of the red-ox reactions for deposition. Ogura's group[58, 74] reported the structural and electrical properties of CuO deposited from solutions containing Cu(II)-glycine and Cu(II)-amino acid complexes. Poizot et al[73] reported electrochemical deposition of CuO from different solutions with Cu(II)-tartrate complex.

The condition of the starting substrate surface is important in electrochemical deposition.[95] Right treatment of the substrate not only removes contaminations on the surface, but also improves adhesion[96, 97] and affects the properties of as-deposited films.[98, 99] Different methods have been used for substrate cleaning such as chemical etching,[98, 100, 101] plasma etching[102] and electrochemical etching.[98, 103-106] Electrochemical etching can be performed in-situ in the deposition solution or ex-situ in a different solution from the deposition solution. In-situ electrochemical etching is

desirable because it generates a cleaner surface without any air exposure of the cleaned substrate before deposition. A few papers reported in-situ electrochemical etching of substrate for deposition of other materials,[103, 106] but there is no report on in-situ electrochemical etching of Cu substrate and its effect on the electrical properties of electrochemically deposited cupric oxide films, which will be covered in this chapter.

In this chapter, the effect of substrate etching on the electrical properties of CuO films electrochemically deposited on Cu substrates is discussed. Four substrate etching methods are compared in this study: i) no etching; ii) chemically etched in HNO_3; iii) ex-situ electrochemically etched in H_2SO_4; and iv) in-situ electrochemically etched in the deposition solution. The focus of this study is the effect of substrate etching on the current-voltage (I-V) characteristics of CuO/metal (Al, Ni, and Cu) Schottky diodes. The I-V characterization shows that CuO grown on electrochemically etched Cu substrates has favorable electrical properties. Morphological and optical properties of as-deposited CuO films are also investigated.

6.1 Sample preparation

A standard three-electrode electrochemical cell is used for CuO deposition, which contains a Cu mesh as the counter electrode, an Ag/AgCl/saturated NaCl reference electrode, and indium tin oxide (ITO) glass or Cu foil (99.9% pure) as the working electrode. Before deposition, ITO glass and Cu foil is degreased in ultrasonicated acetone and rinsed in de-ionized water. After degreasing, four different surface etching processes are applied to Cu foils: i) no etching; ii) chemically etched in 1.5 M HNO_3 for 3 minutes; iii) electrochemically etched in 0.25 M H_2SO_4 at a constant

current of -50 mA vs. Ag/AgCl/saturated NaCl for 30 seconds; and iv) electrochemically etched in deposition solution at a constant current of -5 mA vs. Ag/AgCl/saturated NaCl for 5 minutes. Conditions for the electrochemical etching processes are optimized with atomic force microscopy (AFM) surface roughness characterization.

After etching, CuO films are electrochemically deposited from a solution containing 0.2 M Cu(II) sulfate and 0.2 M tartaric acid.[73, 75] The bath pH is adjusted to 13.0 by controlled addition of 4 M NaOH. A constant potential of 0.50 V vs. Ag/AgCl/saturated NaCl or a constant current of -5 mA is applied for cupric oxide deposition. A Princeton Applied Research Versastat II potentiostat is used to control the applied potential/current. Deposition time is 30 minutes for all samples. The bath temperature is kept between 20°C and 60°C with a Precision 280 water bath. However, all the films for I-V characterization are deposited at a bath temperature of 50°C.

6.2 Cyclic voltammetry

Different from cuprous oxide deposition, cupric oxide deposition doesn't involve any redox reaction of copper ions. In the given solution, it's believed that cupric oxide comes from the following reactions:

$$[Cu^{2+} \cdot T] \rightarrow T^{n+} + Ne^{-} + Cu^{2+} \qquad (6\text{-}1)$$

$$Cu^{2+} + 2OH^{-} \rightarrow Cu(OH)_2 \rightarrow CuO\downarrow + H_2O \qquad (6\text{-}2)$$

where $[Cu^{2+}\cdot T]$ refers to a Cu(II)-tartrate complex and T^{n+} represents an oxidized tartaric ion.[73] When the applied potential is positive enough, tartaric ions are oxidized

and the Cu(II)-tartrate complex is broken, which results in the precipitation of Cu^{2+} ions and formation of cupric oxide.

Cyclic voltammetry is performed to figure out parameters needed for the deposition of cupric oxide. In Fig. 6.1, a typical CV is shown with the corresponding conditions.

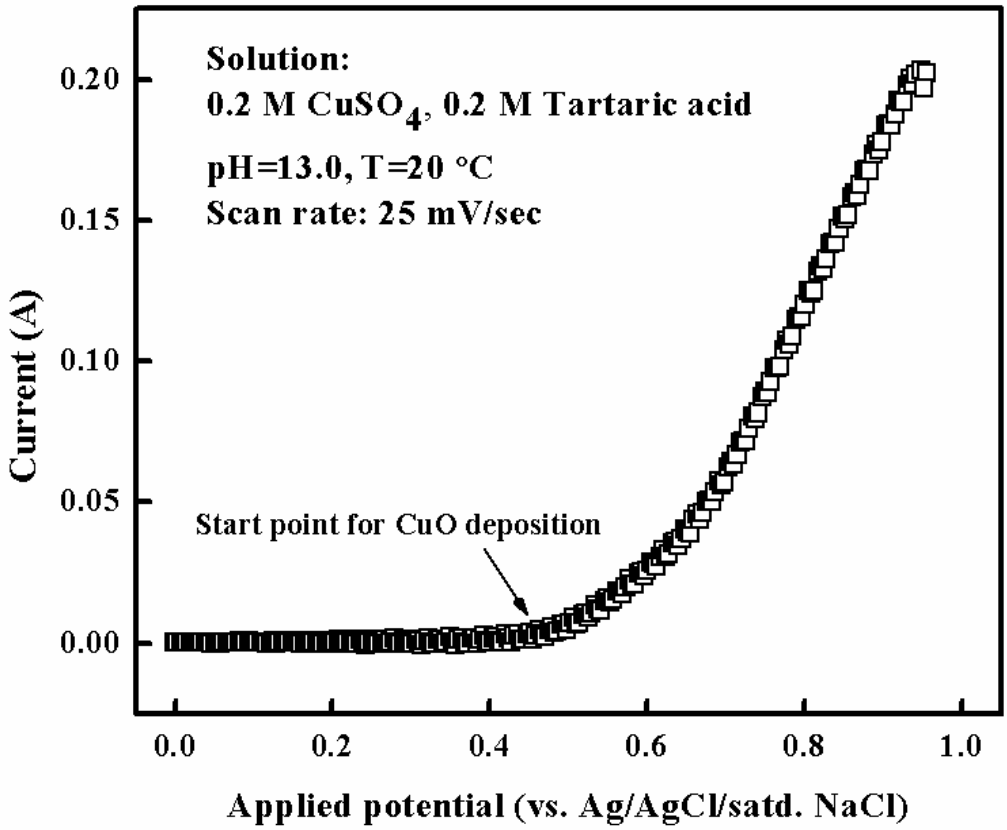

Fig. 6.1 Cyclic voltammetry curve for solution containing 0.2 M $CuSO_4$ and 0.2 M tartaric acid (pH=13.0, T=20 ºC)

According to the C-V curve, deposition of CuO occurs at potential higher than 0.4 V. A constant potential of 0.5 V or a constant current of -5 mA is selected for cupric oxide deposition.

6.3 Optical characterization

CuO films deposited on ITO are used for optical transmission measurement to determine the band-gap. A transmittance spectrum is shown in Fig. 6.2.

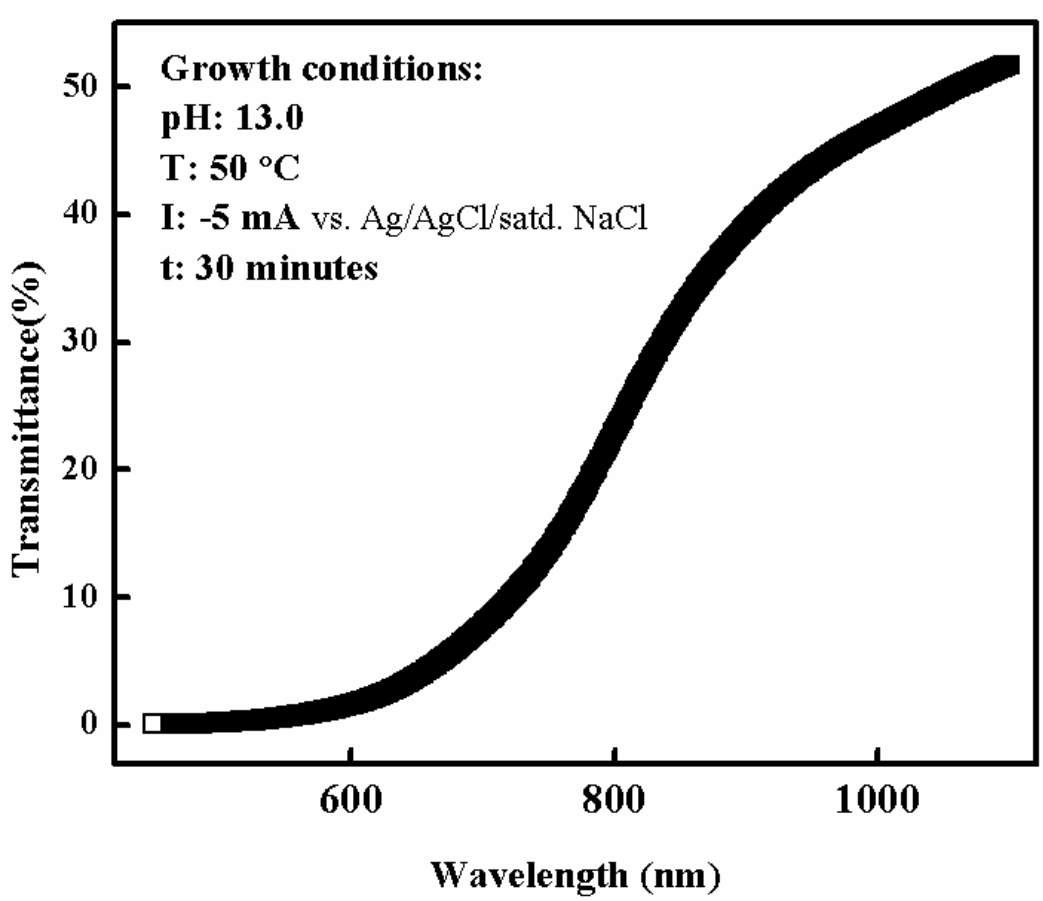

Fig. 6.2 Transmittance spectrum of as-deposited cupric oxide

The same equation used in band gap calculation for cuprous oxide is used to calculate the band gap of cupric oxide.

$$(\alpha h\nu)^n = A(h\nu - E_g) \qquad (6\text{-}3)$$

where α is the absorption coefficient and n depends on the nature of the band gap (n = 1/3 for indirect forbidden transition, n = 1/2 for indirect allowed transition, n = 2/3 for

direct forbidden transition, and n = 2 for direct allowed transition). When all the values for n are tried, only n = 1/2 gives a linear $(\alpha h\nu)^n$-hν plot as shown in Fig. 6.3, which reveals that as-deposited CuO has an indirect band-gap. The intercept of this plot with the hν axis shows that CuO has a band-gap of 1.32 eV, which is consistent with the reported band-gap values for CuO.[59-64]

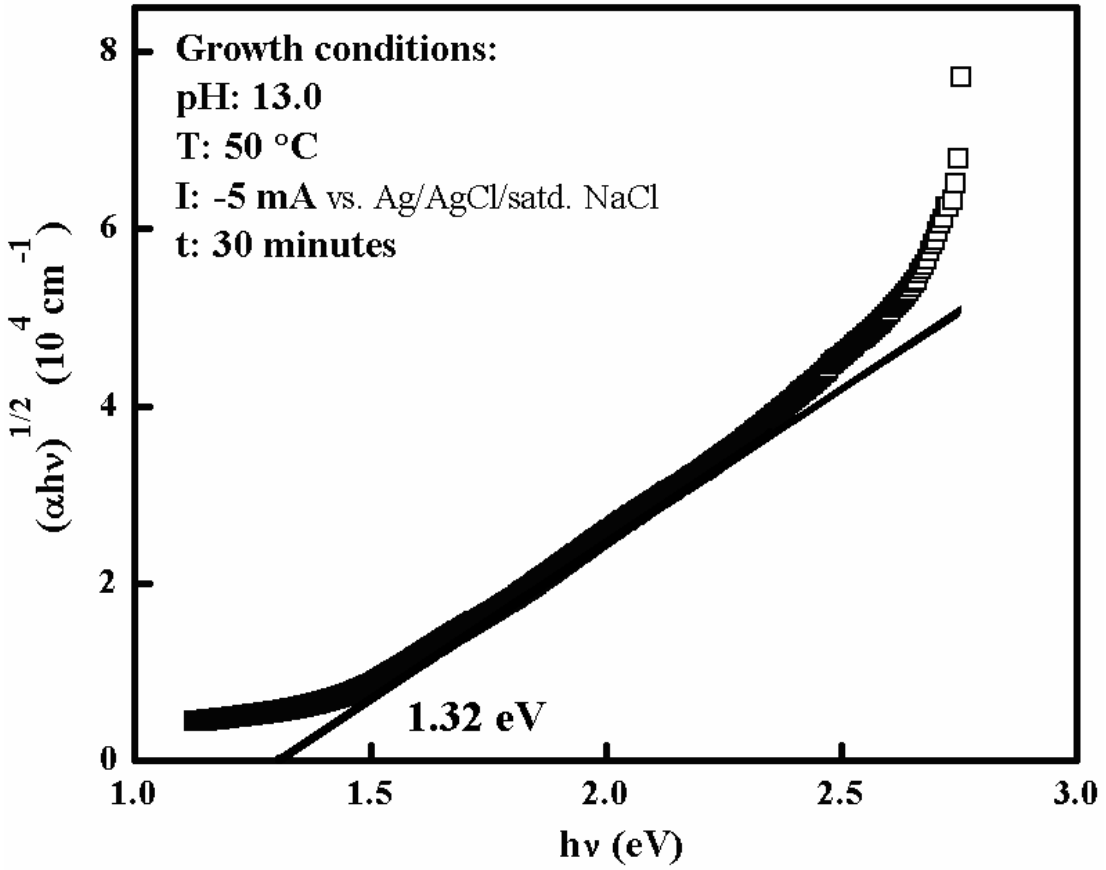

Fig. 6.3 $(\alpha h\nu)^{1/2}$-hν plot of a electrodeposited cupric oxide film

6.4 XRD Characterization

Cupric oxide has a monoclinic lattice, which is much more complicated than the cubic structure of cuprous oxide. XRD pattern of as-deposited cupric oxide film is shown in Fig. 6.4.

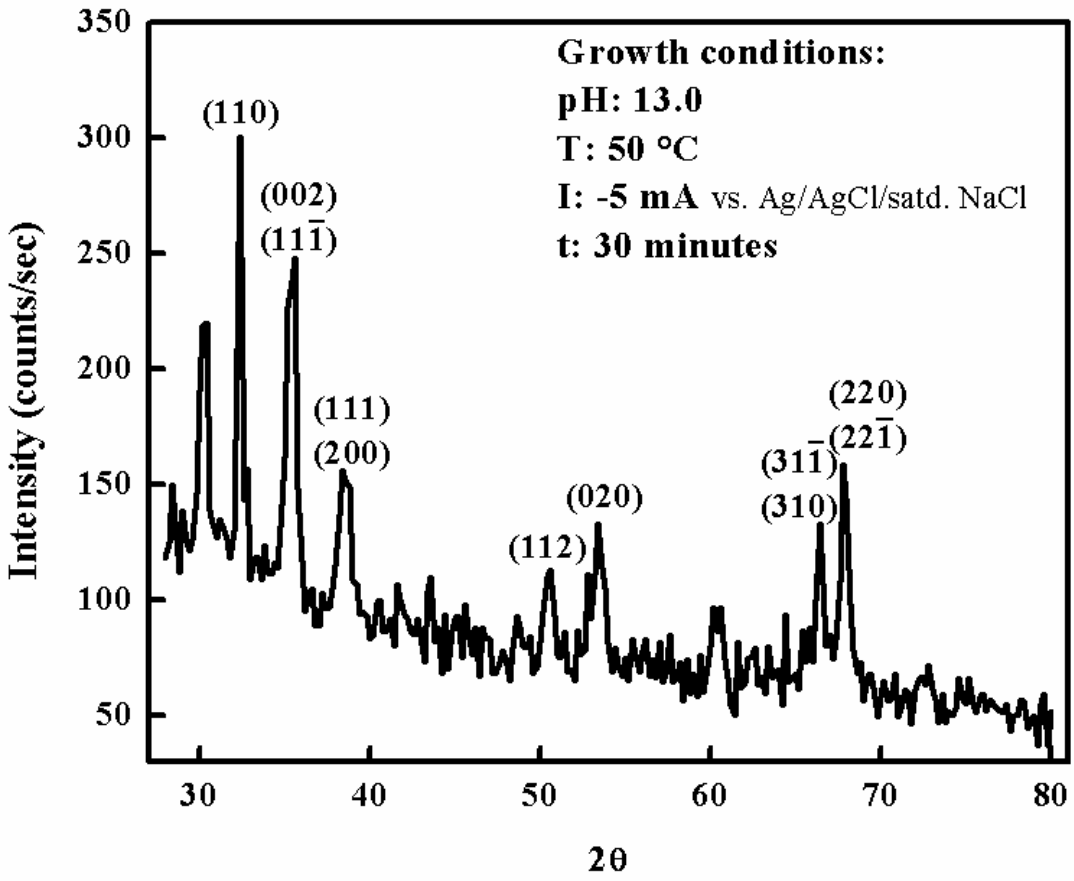

Fig. 6.4 XRD pattern of as-deposited cupric oxide film

As shown, compared with cuprous oxide, even cupric oxide films deposited at high bath pH have a poor crystal quality and show no preferred crystal orientation, which may result from the much more complicated crystal structure.

6.5 SEM characterization

The effect of bath temperature on the crystallinity of as-deposited CuO is investigated. Samples are deposited at different temperatures from 20 °C to 60 °C with a step of 10 °C. SEM is used to characterize the crystallinity of as-deposited cupric oxide and results are shown in Fig. 6.5.

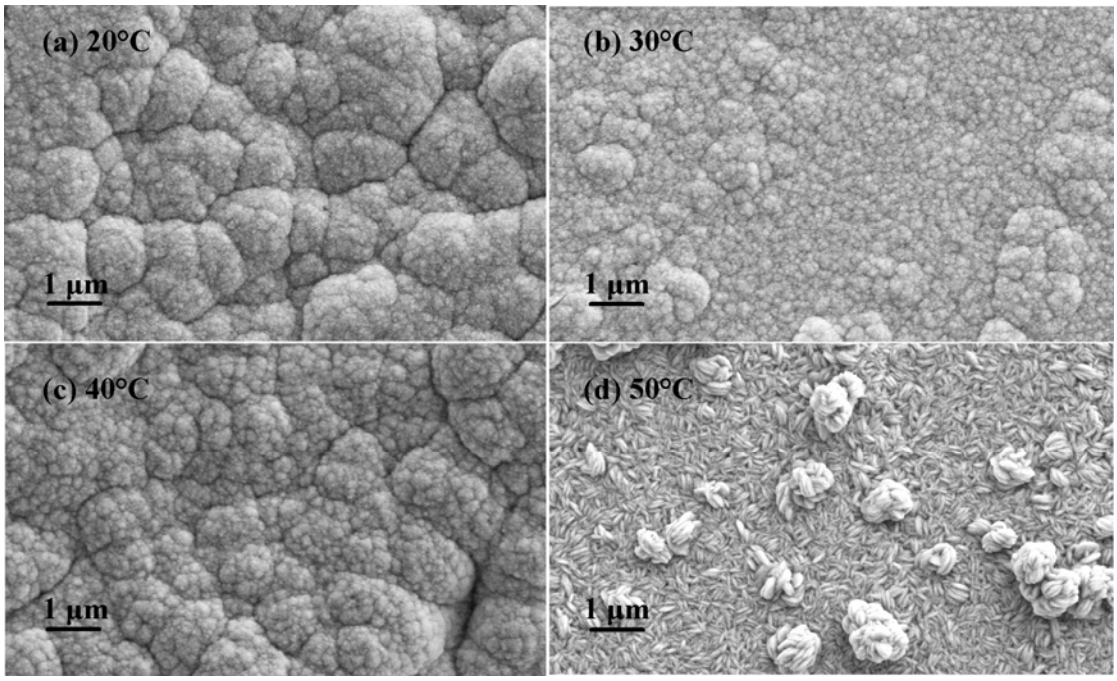

Fig. 6.5 SEM images of electrochemically deposited CuO at (a) 20°C, (b) 30°C, (c) 40°C, and (d) 50°C

As shown, samples deposited below 50 °C show an amorphous-like morphology, while samples deposited above 50°C have a polycrystalline look. As expected, a higher temperature favors crystallization of the CuO film and thus better crystal quality of CuO. With bath temperature above 50°C, there is precipitation in the solution, which affects the deposition of cupric oxide. Therefore, 50°C is determined to be the upper limit in temperature for CuO deposition.

6.6 Electrochemical etching of Cu substrates

In order to investigate the electrochemical etching process, two sets of Cu foils are prepared by electrochemical etching. The first set is ex-situ electrochemically etched in 0.25 M H_2SO_4 at different current densities (i.e. etching rates) for different durations of time. Fig. 6.6 shows the surface roughness by AFM as a function of the amount of

material etched, and the inset is a SEM image of the typical surface morphology of Cu substrate after etching.

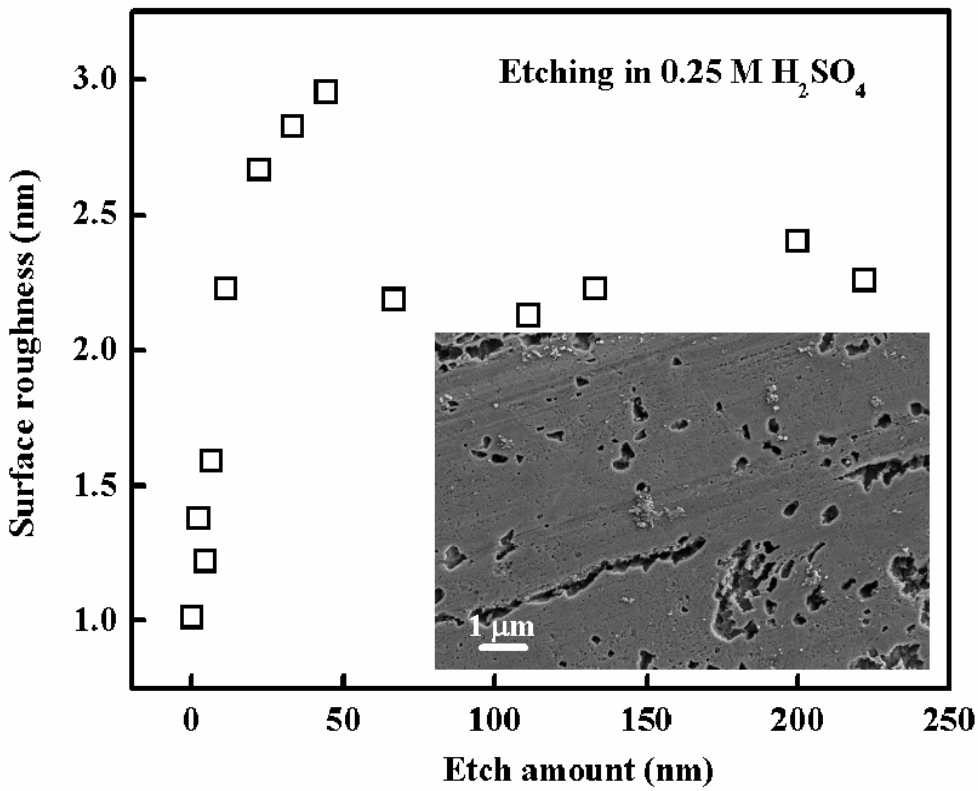

Fig. 6.6 Surface roughness of Cu substrates ex-situ electrochemically etched (ECE) in 0.25 M H_2SO_4

When the etched amount is below 50 nm, surface roughness increases as the etched amount increases. When the etched amount exceeds 50 nm, surface roughness decreases and then stabilizes to about 2.2 nm. From Fig. 6.6, the etching conditions corresponding to the etched amount of 110 nm, which are 50 mA for 30 seconds, are selected for the following deposition experiments.

The second set of substrates undergoes in-situ electrochemical etching in the deposition solution, where the etched substrate is never exposed to air. In-situ etching of

the Cu substrate is more complicated. When an anodic current is applied, there are two competing reactions as follows:

$$Cu - 2e^- \rightarrow Cu^{2+} \quad \text{(6-4)}$$

$$[Cu^{2+} \cdot T] \rightarrow T^{n+} + Ne^- + Cu^{2+} \quad \text{(6-5 (a))}$$

$$Cu^{2+} + 2OH^- \rightarrow Cu(OH)_2 \leftrightarrow CuO\downarrow + H_2O \quad \text{(6-5 (b))}$$

where $[Cu^{2+}\cdot T]$ refers to a Cu(II)-tartrate complex and T^{n+} represents an oxidized tartaric ion. The reaction indicated by equation (6-4) leads to etching of the substrate. The second reaction consists of two steps. The first step indicated by equation (6-5 (a)) leads to oxidation of tartaric ions and breaking of the Cu(II)-tartrate complex. The second step indicated by equation (6-5 (b)) leads to the precipitation of Cu^{2+} ions and the deposition of CuO. For a given Cu(II) concentration, it is found that there exists a critical current density (J_c) between etching and deposition. When the applied current is below J_c, etching takes place. When the applied current is above J_c, deposition occurs. Fig. 6.7 shows the experimentally-determined conditions for etching and deposition. It can be seen that J_c depends on the Cu(II) concentration in the solution. As the Cu(II) concentration decreases, J_c increases.

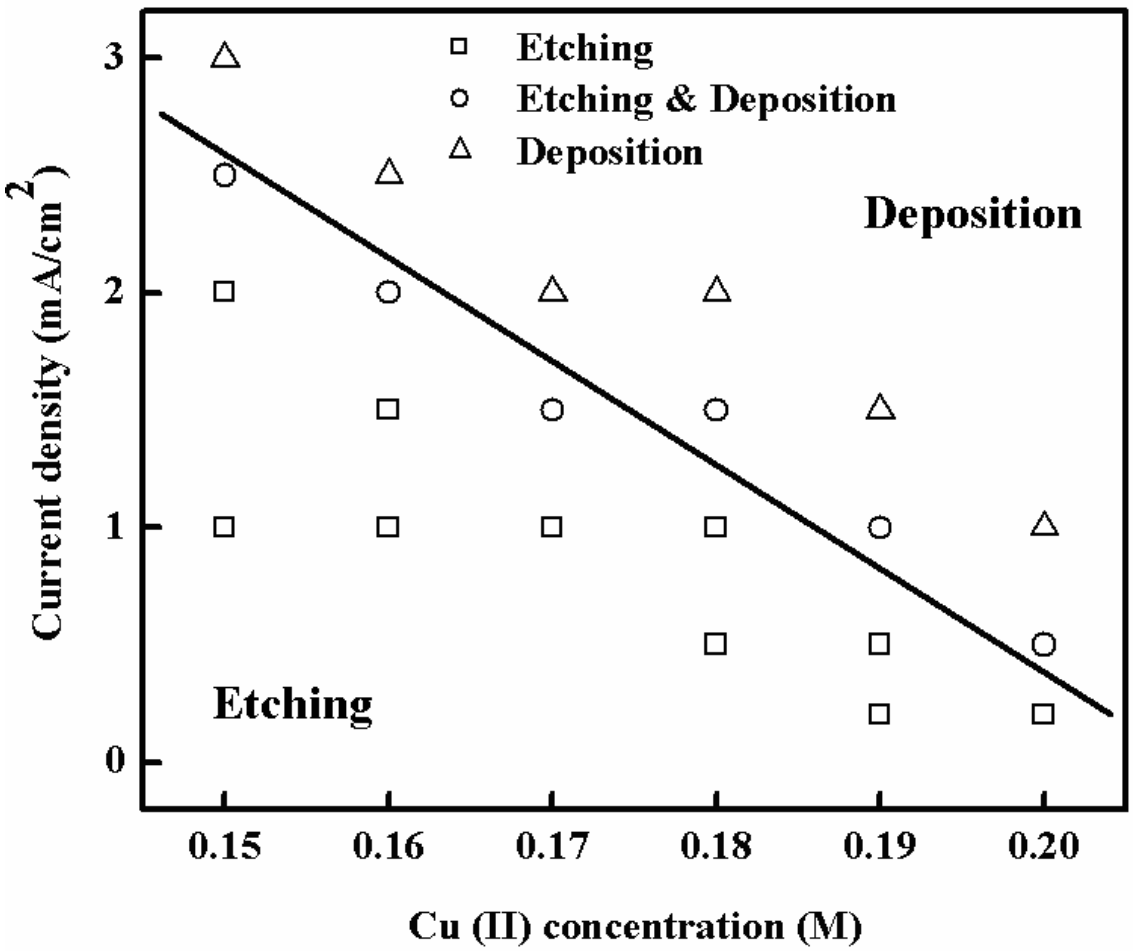

Fig. 6.7 Conditions for in-situ electrochemical etching of Cu substrates in the deposition solution

The surface roughness of in-situ electrochemically etched Cu substrates in the deposition solution with different Cu(II) concentrations is measured with AFM. Fig. 6.8 shows the surface roughness for samples in-situ etched in a deposition solution with 0.18 M Cu(II). The surface is 2–3 times rougher than samples ex-situ electrochemically etched in H_2SO_4. In addition, there is no obvious plateau in surface roughness over etched amount, as is the case for ex-situ etched samples.

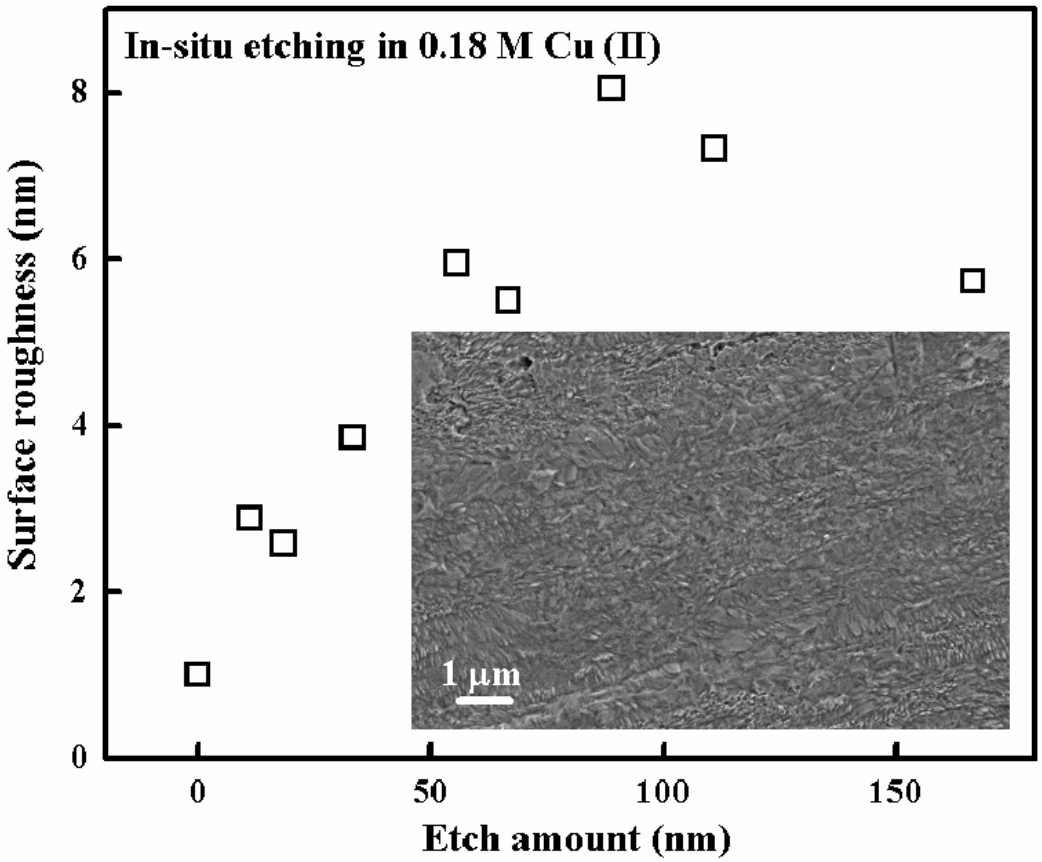

Fig. 6.8 Surface roughness of Cu substrates in-situ electrochemically etched (ECE) in 0.18 M Cu(II)

6.7 I-V characterization

6.7.1 Sample preparation

The samples used for electrical characterization are deposited at 50°C. Before deposition, Cu substrates are etched with four different methods as follows: i) no etching; ii) chemically etched in 1.5 M HNO_3 for 3 minutes; iii) electrochemically etched in 0.25 M H_2SO_4 at a constant current of -50 mA vs. Ag/AgCl/saturated NaCl for 30 seconds; and iv) electrochemically etched in deposition solution at a constant current of -5 mA vs. Ag/AgCl/saturated NaCl for 5 minutes. After deposition, different

metals (Al, Cu, and Ni) are deposited on CuO to form Schottky diodes, of which the detailed process is shown in Fig. 4.12.

6.7.2 I-V characterization

As a metal in contact with a semiconductor, a Schottky barrier is formed. Theoretically, the Schottky barrier height is only determined by the work function of the metal (Φ_M) and the electron affinity of the n-type semiconductor (χ_s).[82] For a p-type semiconductor, the higher the work function of the metal, the easier it is to form an ohmic contact.

Both Cu/CuO and Ni/CuO diodes show ohmic characteristics as shown in Fig. 6.9. Both Cu ((Φ_M=4.7 eV) and Ni (Φ_M=5.1 eV) have a high work function,[82] which explains why they form ohmic contact with the p-type cupric oxide. In Fig. 6.10, the resistivity of the CuO films, extracted from the Cu/CuO and Ni/CuO diodes, is shown. The resistivity varies to some extent but is always in the same order of magnitude.

I-V characteristics of Al/CuO diodes are shown in Fig. 6.11. The four samples with different etching treatments all show Schottky behavior characteristic of a metal/p-type semiconductor junction. However, there is a large variation in current among different samples.

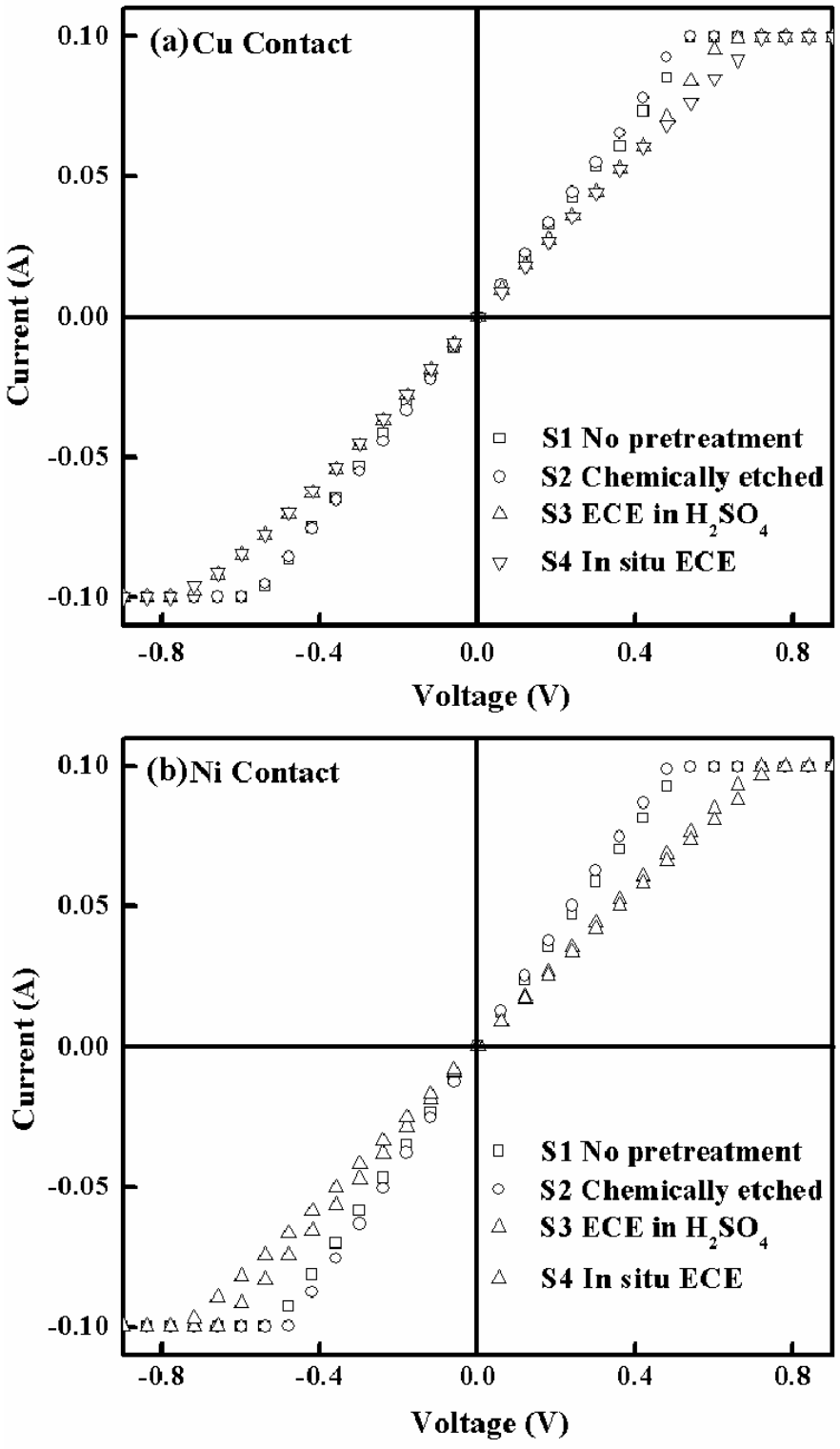

Fig. 6.9 I-V characteristics of (a) Cu/CuO diodes and (b) the Ni/CuO diodes with different substrate etching treatments

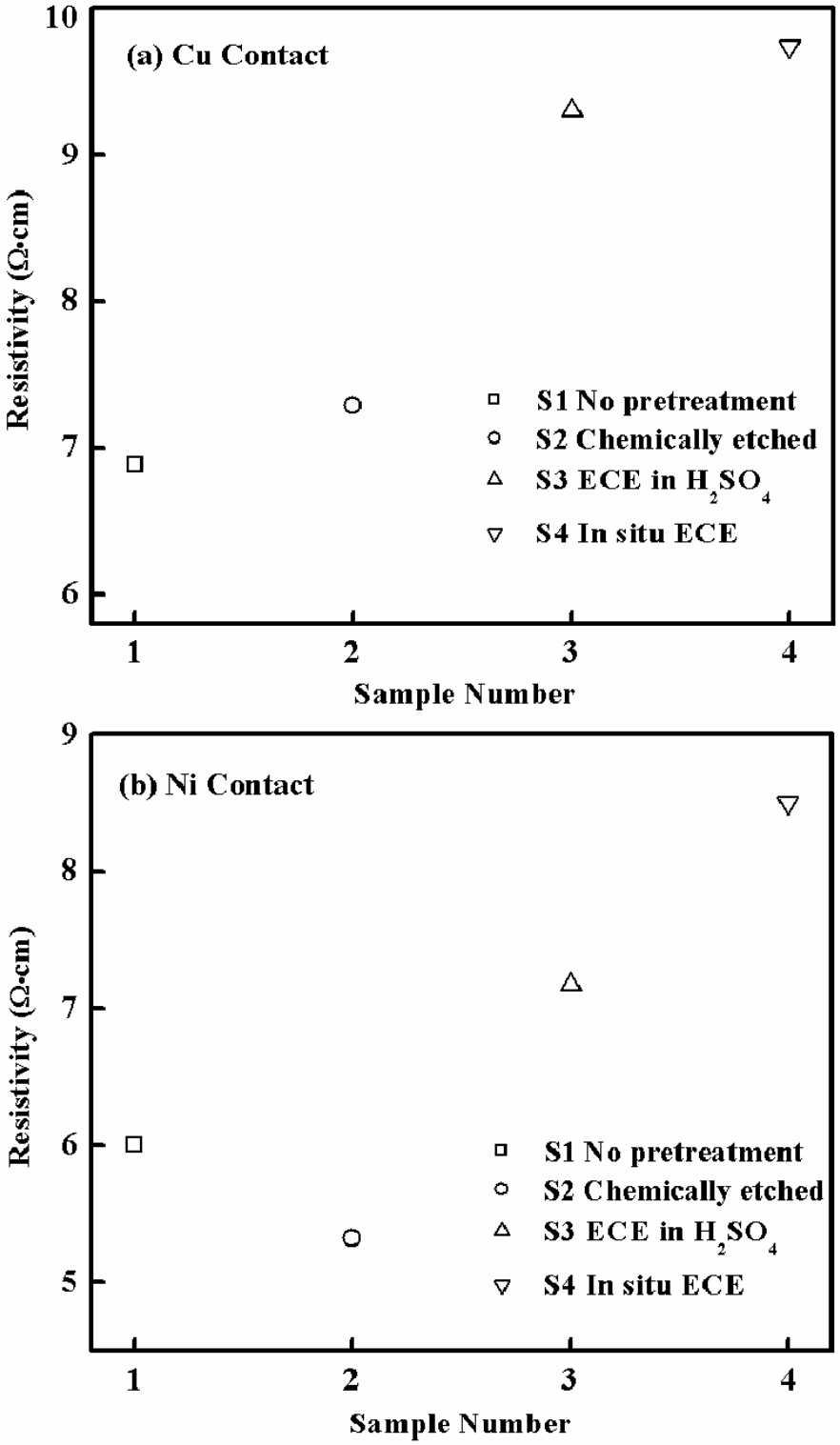

Fig. 6.10 Resistivity of CuO films extracted from (a) Cu/CuO and (b) Ni/CuO diodes with different substrate etching treatments

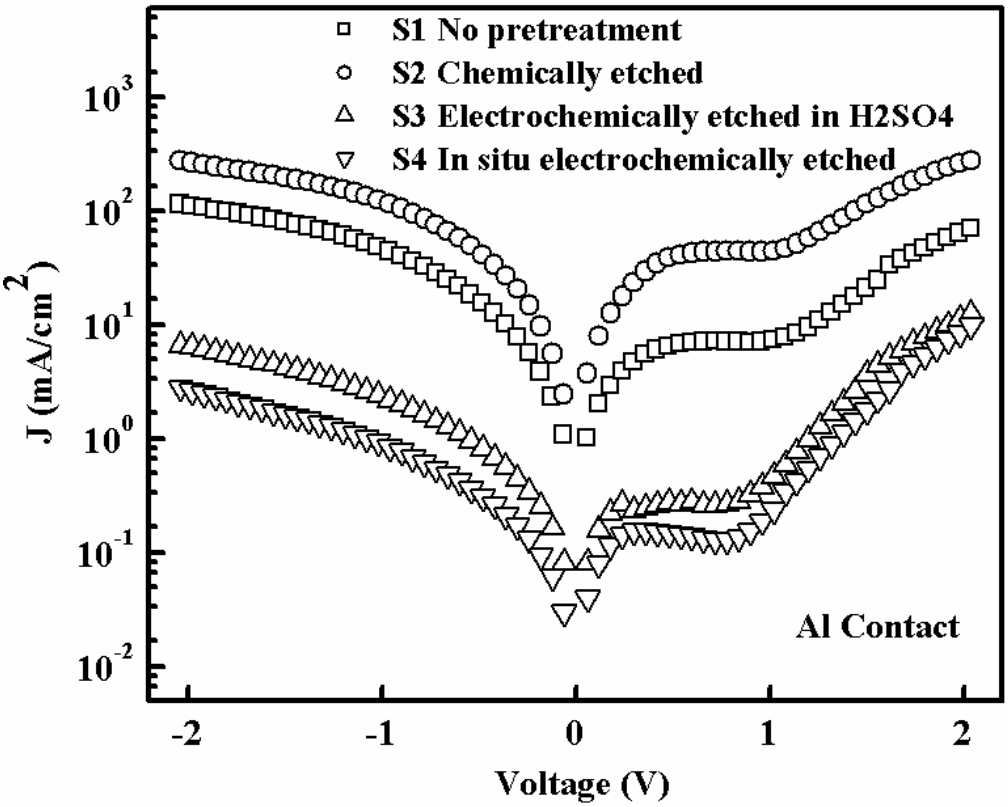

Fig. 6.11 I-V characteristics of Al/CuO diodes with different substrate etching treatments

This variation could come from different starting surface conditions caused by different surface etching methods, or from different CuO film thickness. As these films have similar thickness (about 2.2 μm), the large variation in current is likely caused by different surface etching methods. Lower current density indicates higher resistivity, which is desirable if the CuO film is to be doped n-type. Therefore, it may be concluded that CuO deposited on electrochemically etched Cu substrates has favorable electrical properties. This conclusion is further supported by the result in Fig. 6.12, which shows the ratio of the forward current and the reverse current (i.e. rectification ratio) at V = ±0.8 V for the four Al/CuO diodes. Films deposited on electrochemically etched substrates have the highest rectification ratios, which suggest better Schottky diodes.

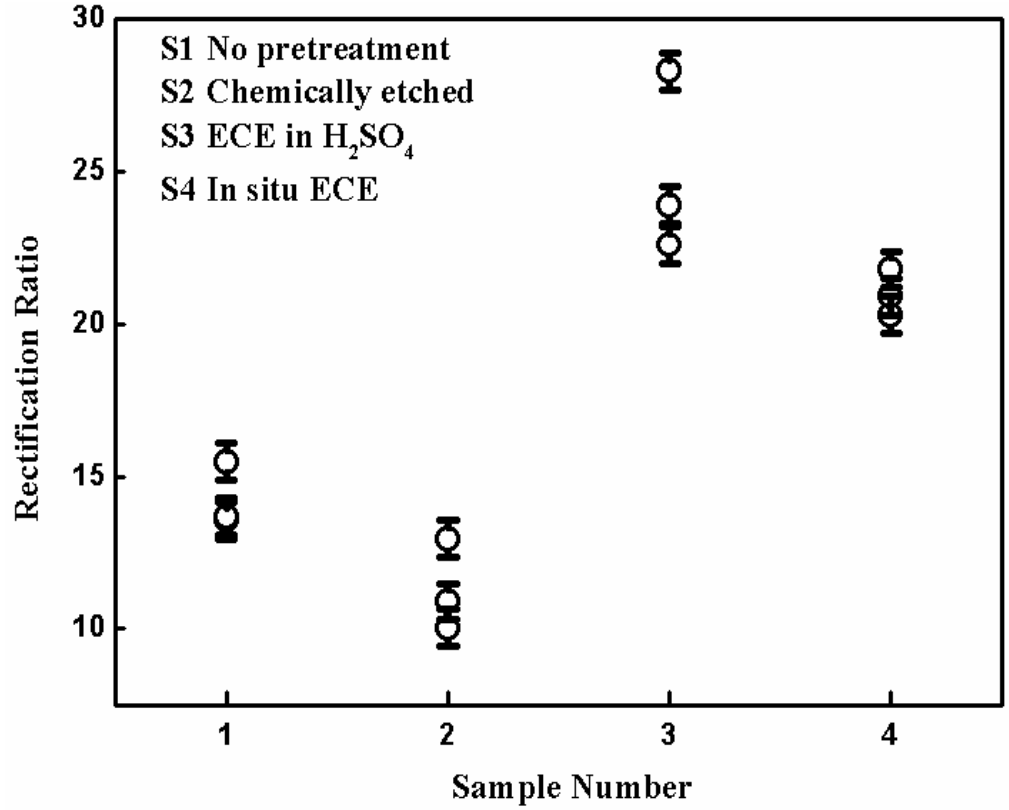

Fig. 6.12 Rectification ratio of Al/CuO diodes at ±0.8 V with different substrate etching treatments

6.8 Summary

Electrochemical etching is proven to be an effective method for Cu substrate cleaning in cupric oxide deposition. In particular, in-situ electrochemical etching is developed, which prevents the cleaned substrate from exposure to air. There exists a critical current density for in-situ electrochemical etching to occur on Cu substrates. Increasing the Cu(II) concentration in the deposition solution reduces the critical current density. I-V characterization shows that CuO deposited on electrochemically etched Cu substrates has favorable electrical properties and better rectification behavior. Transmittance measurements show that electrochemically deposited CuO has an indirect

band-gap of 1.32 eV. SEM reveals that higher deposition temperature improves the crystallinity of as-deposited CuO and at 50°C, polycrystalline CuO is obtained.

Based on the results of chapter 5 and 6, it's found that cuprous oxide is a more promising material for photovoltaic applications. Compared with cupric oxide, electrodeposited cuprous oxide has much better crystallinity, bigger grains, better control over crystal quality and a direct band gap. Therefore, in next chapter we'll only focus on the fabrication of p-n homo-junction in cuprous oxide.

CHAPTER 7

FABRICATION OF P-N HOMOJUNCTION IN CUPROUS OXIDE

As a promising material for photovoltaic applications, cuprous oxide has been extensively studied since the 1970s. Cuprous oxide is well known as a p-type semiconductor due to copper vacancies.[10-17] Lots of efforts have been dedicated to fabricate cuprous oxide based photovoltaic devices, such as Schottky diodes, MIS (metal insulator semiconductor) and hetero-junction solar cell.[17, 18, 20-22, 45-50] Up to now, the best efficiency achieved is 2%. The common conclusion of most of these studies is that the only way to increase the efficiency of cuprous oxide based solar cells is to make a p-n homo-junction of cuprous oxide.

To our knowledge, only few studies reported n-type photoelectrochemical behavior of electrodeposited cuprous oxide. The reason for conduction type change was ascribed to different native point defects, i.e., copper vacancies (p-type) were replaced by oxygen vacancies (n-type).[23, 51, 52] However, no explanation was given on how the native point defects were controlled by deposition conditions, which will be addressed here based on our results.

As discussed in chapter 5, bath pH controls the crystal orientation by controlling the amount of oxygen incorporated into the film. On the other hand, copper vacancies in cuprous oxide are the reason for the p-type conduction. Copper vacancies suggest that

there is stoichiometrically more oxygen than copper in the film. If we can reduce the amount of oxygen incorporated into the film, we should be able to reduce copper vacancies and increase oxygen vacancies. In this way, electrochemically-deposited cuprous oxide may become n-type. Control of oxygen incorporation should be achievable by controlling bath pH. Based on this theory, a series of experiments are designed and both p-type and n-type cuprous oxide films are achieved reproducibly. Furthermore, a p-n homo-junction of electrodeposited cuprous oxide is fabricated by a two-step electrodeposition process. To our knowledge, this is the first p-n homo-junction of cuprous oxide fabricated by any method so far.

7.1 Preparation of n-type cuprous oxide

7.1.1 Sample preparation

Copper sheets (1 cm × 4 cm) with purity of 99.9% are used as the working electrode and a platinum foil is used as the counter electrode. Before deposition, copper sheets and platinum foil are degreased in ultrasonicated acetone, etched in diluted HNO_3 and finally rinsed in de-ionized water.

For n-type cuprous oxide deposition, solution used contains 0.4 M copper sulfate and 3 M lactic acid.[35-39] Bath pH is set between 6.5 and 7.5 by controlled addition of 4 M NaOH. Applied potential is kept at -0.20 ~ -0.3 V (vs. Ag/AgCl/saturated NaCl). Bath temperature is kept at 60 ºC with a Precision 280 water bath. Deposition time for each sample is 60 minutes.

7.1.2 Cyclic voltammetry

Before any deposition, cyclic voltammetry is performed for n-type cuprous oxide deposition. As shown, for n-type cuprous oxide deposition, the applied potential should be kept below -0.3 V to avoid deposition of metallic copper. The corresponding current is much lower than that of p-type cuprous oxide deposition, which results in a much lower deposition rate of n-type cuprous oxide. Therefore the deposition time for n-type cuprous oxide is much longer.

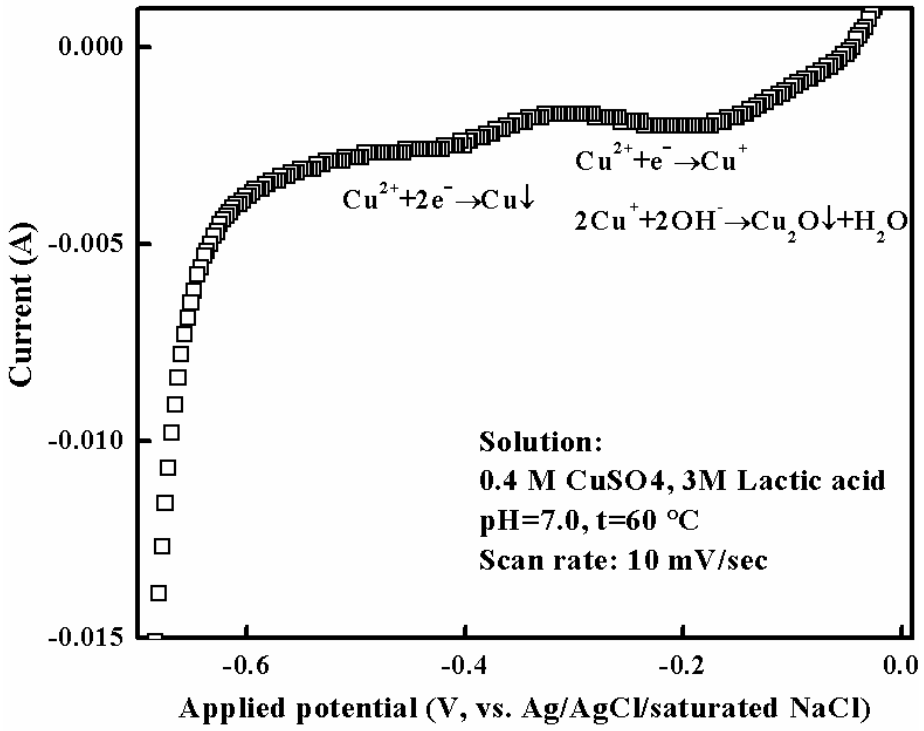

Fig. 7.1 Cyclic voltammetry for solution containing 0.4M $CuSO_4$ and 3M lactic acid (pH=7.0, T=60 ºC)

7.1.3 XRD characterization

An XRD pattern of cuprous oxide deposited at pH of 7.5 is shown in Fig. 7.2 with an XRD pattern of a sample deposited at pH of 10.0 as a comparison. Both XRD

patterns show that as-deposited films are (111) orientated cuprous oxide, while cuprous oxide deposited at pH of 10.0 has much better crytallinity than that of cuprous oxide deposited at pH of 7.5..

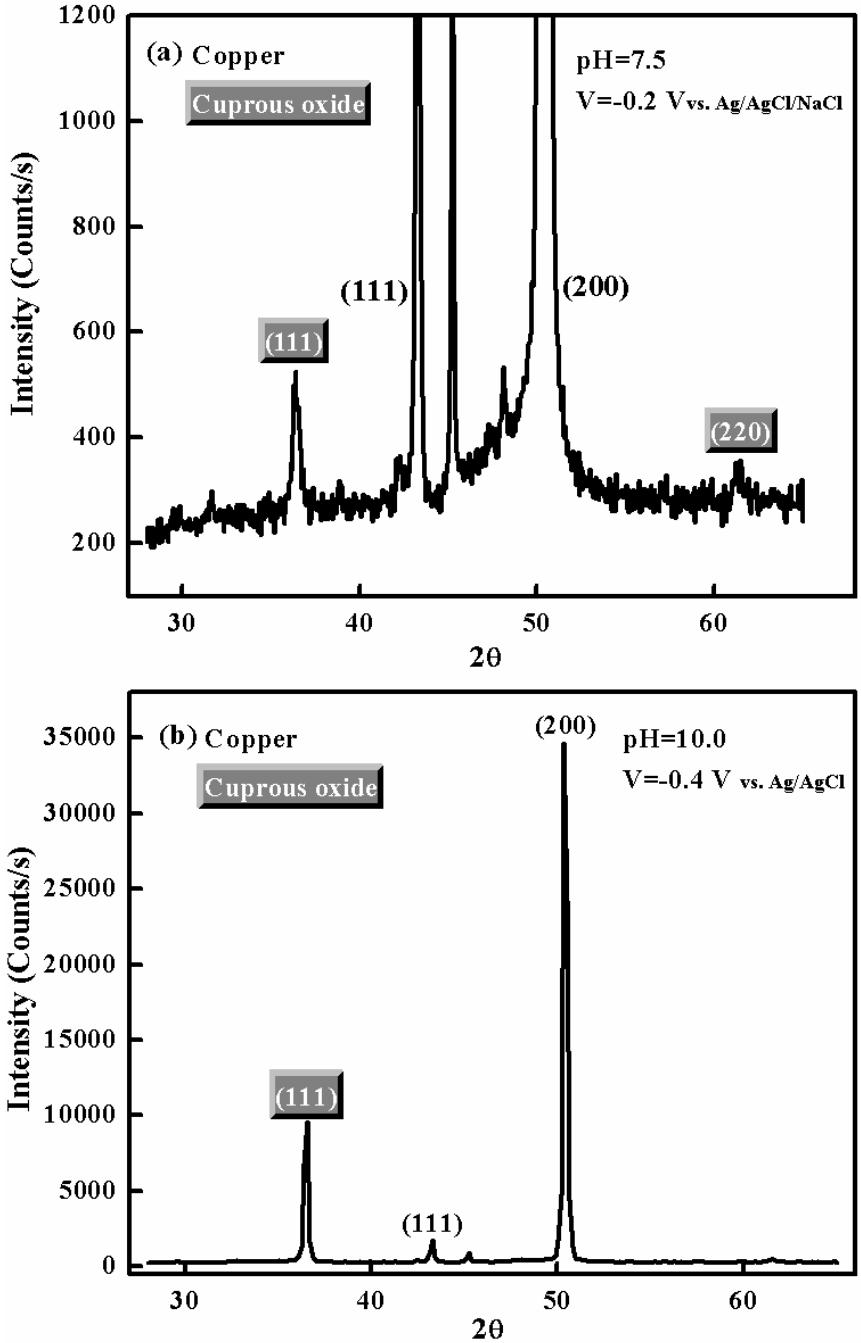

Fig. 7.2 XRD patterns of cuprous oxide deposited at pH: (a) 7.5 and (b) 10.0

7.1.4 SEM characterization

SEM is used to characterize surface morphology of as-deposited cuprous oxide. Samples used are deposited at bath pH of 6.8, 7.25, 7.5 and 11.0, respectively.

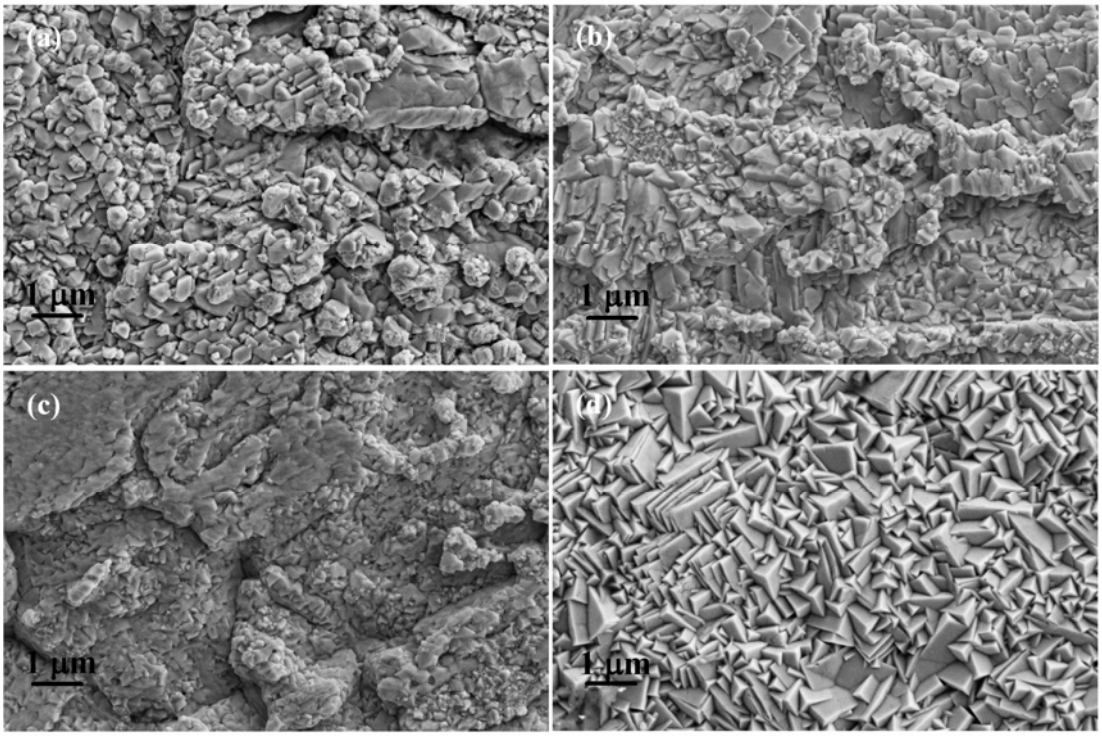

Fig. 7.3 SEM images of cuprous oxide deposited at bath pH: (a) 6.8, (b) 7.25, (c) 7.5 and (d) 11.0

As shown, for cuprous oxide films deposited at lower pH (6.8, 7.25, and 7.5), the grain shape is much less regular and grain size is smaller compared with sample deposited at bath pH of 11.0. The reason for this may be ascribed to the much lower growth rate at lower pH.

7.1.5 Characterization of conduction type

In order to characterize the conduction type of as-deposited cuprous oxide, capacitance-voltage and photocurrent measurements are performed.

7.1.5.1 Capacitance-voltage measurement

Cuprous oxide samples deposited at different bath pH values are selected for capacitance-voltage (C-V) measurements, which are performed in a three-electrode cell. Cuprous oxide is set as the working electrode, and the reference electrode is Ag/AgCl/saturated KCl. The solution used is non-aqueous solution of 0.1 M tetrabutylammonium hexafluorophosphate in acetonitrile.[88] The Mott-Schottky plots ($1/C^2$ vs. V) are presented in Fig. 7.4 and 7.5.

As shown, the Mott-Schottky plots of cuprous oxide deposited at pH lower than 7.5 have a positive slope, which indicates n-type semiconductor behavior. From the slope (S) and the intercept (V_0) with the voltage axis, the carrier concentration and flat band potential (V_{fb}) are calculated according to equations (7-1) and (7-2), respectively.

$$N_D = \frac{2}{e\varepsilon\varepsilon_0 A^2 S} \tag{7-1}$$

$$V_{fb} = V_0 - \frac{KT}{e} \tag{7-2}$$

For the three samples, calculated N_D and V_{fb} are shown in Table 7.1.

Table 7.1 Calculated N_D and V_{fb} of as-deposited n-type cuprous oxide

	pH=6.8	pH=7.25	pH=7.5
N_D ($\times 10^{15}$ cm^{-3})	7.38	2.32	0.2
V_{fb} (V)	0.086	0.079	0.071

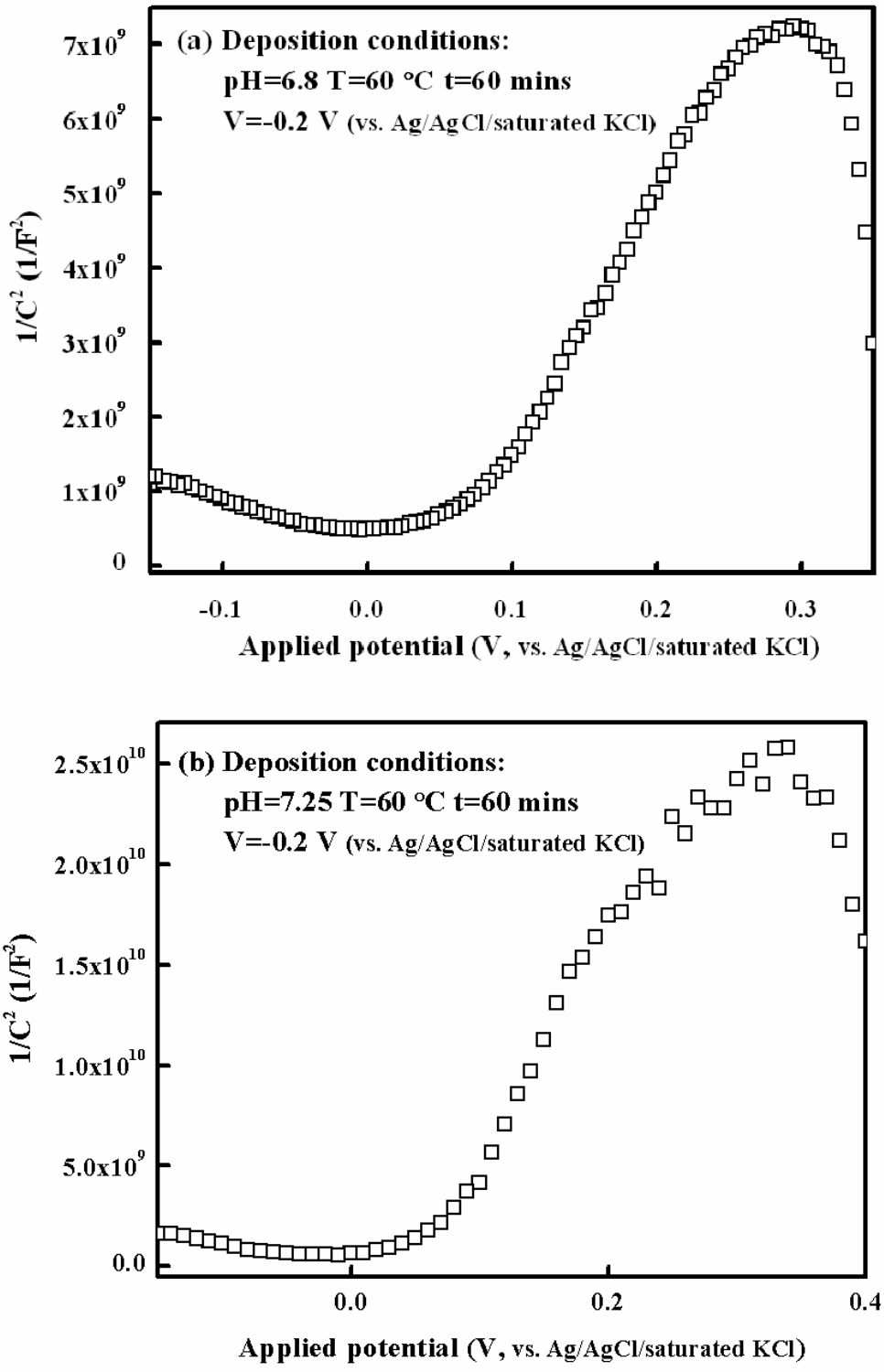

Fig. 7.4 Mott-Schottky plots of cuprous oxide deposited at bath pH: (a) 6.8, (b) 7.25

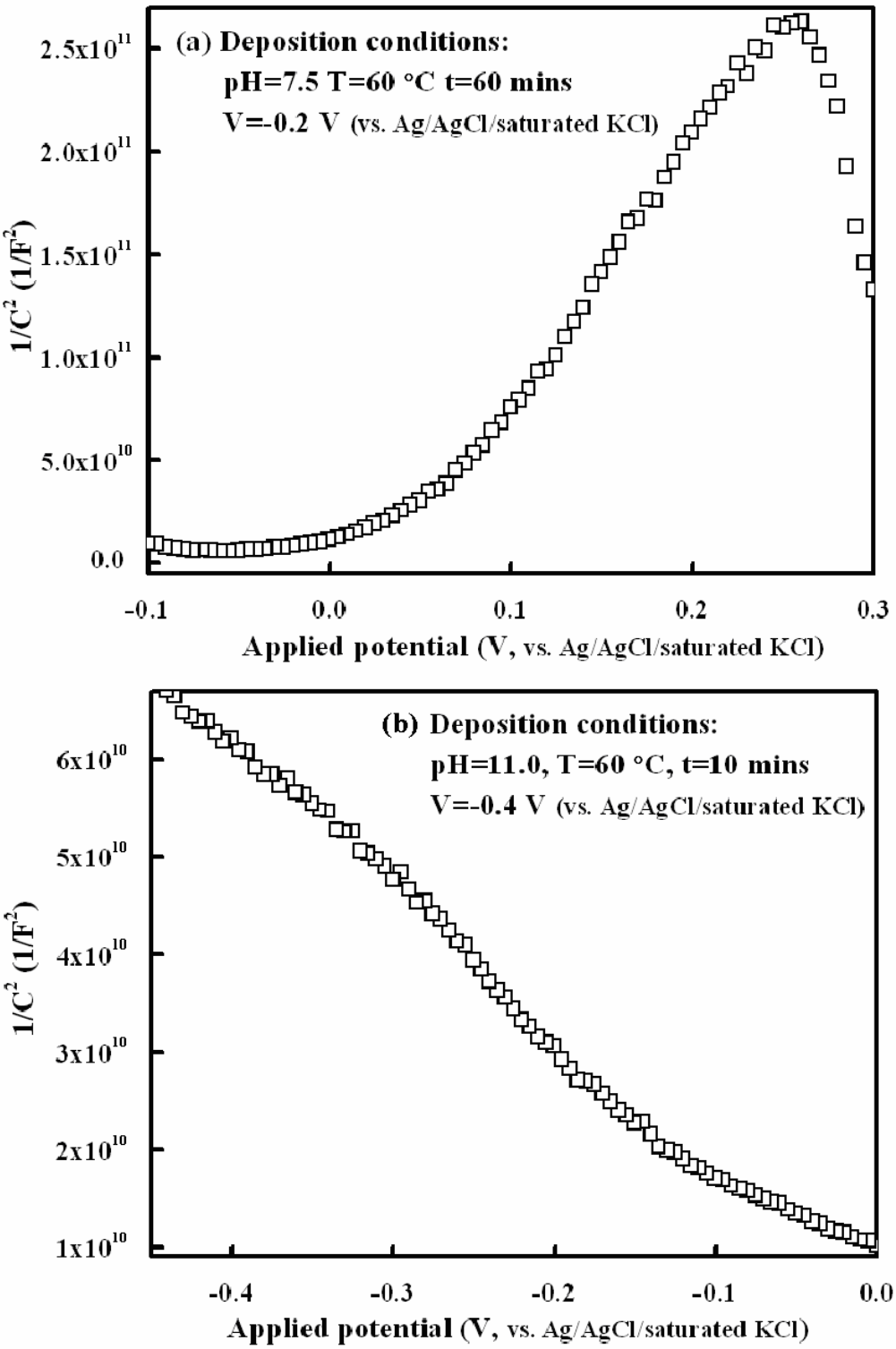

Fig. 7.5 Mott-Schottky plots of cuprous oxide deposited at bath pH: (a) 7.5, (c) 11.0

7.1.5.2 Photocurrent measurement

Besides capacitance-voltage measurement, photocurrent measurement is another method performed to confirm the conduction type of as-deposited cuprous oxide. Photocurrent characterization is carried out in a custom-built system (Fig. 4.8), which includes a light source, an illumination switch, a three-electrode cell and a control system. A 100W tungsten/halogen lamp is used to provide broad spectrum light. The illumination switch is actually a manually controlled light chopper with 5 seconds interval. In the three-electrode cell, the working electrode is as-deposited cuprous oxide film facing the light source, the counter electrode is a platinum foil and the reference electrode is Ag/AgCl/saturated KCl. The cell solution is 0.5 M sodium sulfate (Na_2SO_4) with 0.1 M sodium formate (HCOONa). A PAR 264A polarographic analyzer/stripping voltammeter is used to control the applied potential and scan rate.

For an n-type semiconductor electrode under depletion condition, as light is shed on the surface, electron-hole pairs generated in the depletion region will be separated by the built-in electric field. Electrons move into the semiconductor, while holes move into the solution, which generates an anodic current. For a p-type semiconductor, the generated electrons and holes in depletion region move into reverse directions, which generate a cathodic current. Therefore, from the direction of the photocurrent, the conduction type of a semiconductor electrode can be identified.

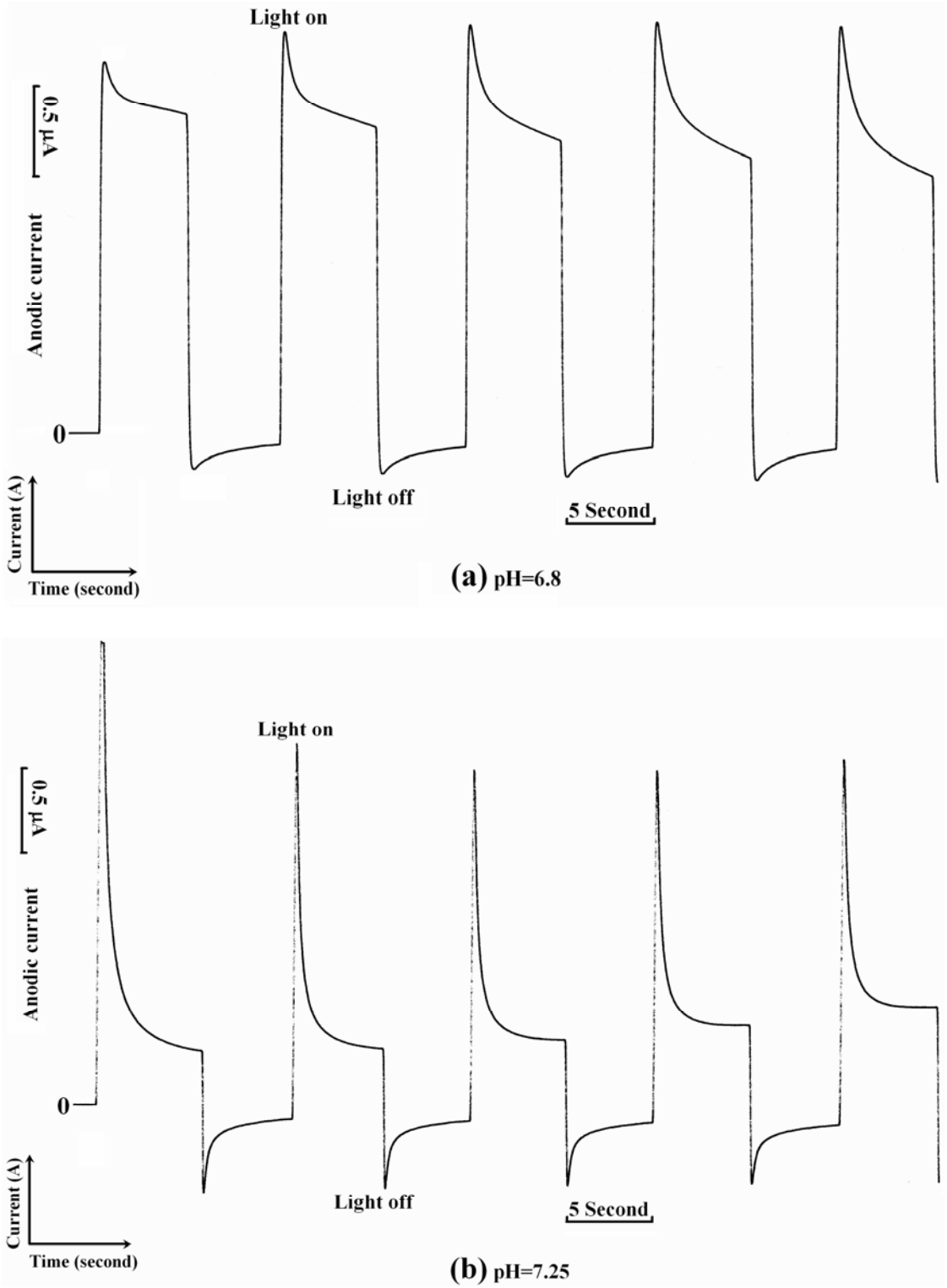

Fig. 7.6 Photocurrent of cuprous oxide films deposited at bath pH: (a) 6.8 and (b) 7.25

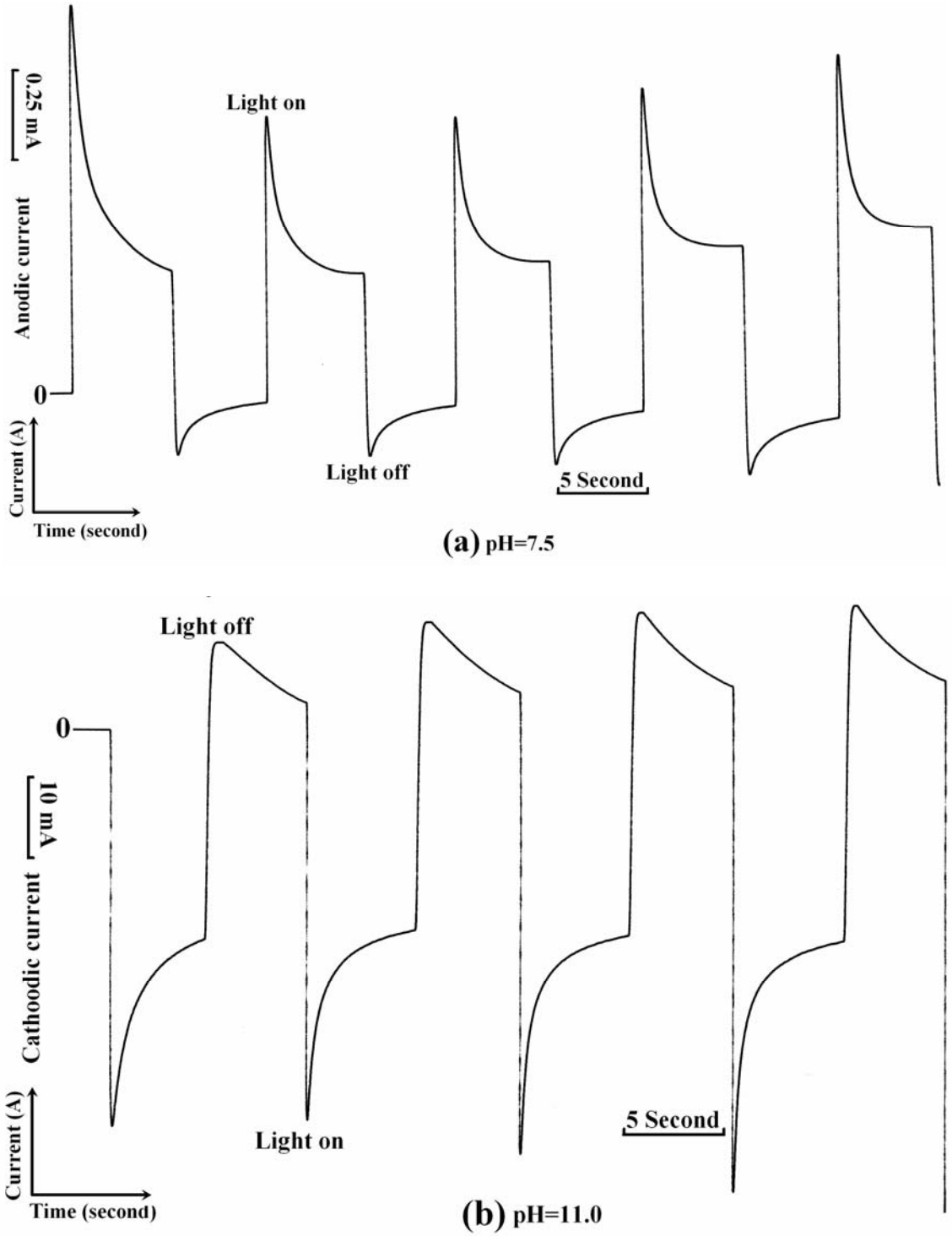

Fig. 7.7 Photocurrent of cuprous oxide films deposited at bath pH: (a) 7.5 and (b) 11.0

As shown in Fig. 7.6 and 7.7, cuprous oxides deposited at pH lower than 7.5 generate an anodic photocurrent, which indicates n-type semiconductor behavior. Cuprous oxide deposited at pH of 11.0 has a cathodic photocurrent indicating p-type semiconductor behavior.

The photocurrent and C-V characterization show consistent results that bath pH does control the conduction type of cuprous oxide. As expected, at different bath pH, the atomic ratio of Cu^{+}/O^{2-} in cuprous oxide film varies, which results in the change of native point defects and thus conduction type.

7.2 Fabrication of p-n homo-junction in cuprous oxide

7.2.1 Sample preparation

A two-step deposition process is performed to fabricate p-n homo-junction of cuprous oxide. The first step is to deposit p-type cuprous oxide. Copper substrate is immersed into a solution with bath pH of 11.0. Cuprous oxide film is deposited at a potential of -0.40 V (vs. Ag/AgCl/saturated NaCl) for 10 minutes at 60 ºC. Right after the p-type cuprous oxide deposition, the substrate with p-type cuprous oxide is put into a solution with bath pH of 6.5 to 7.5. The applied potential is varied between -0.2 V to -0.3 V. Bath temperature is kept at 60 ºC and deposition time is 60 minutes.

7.2.2 SEM characterization

Three sets of samples are prepared for surface morphology characterization. Each set includes three samples: n-type deposition, p-type deposition and p-n junction deposition. SEM images of these three sets of samples are shown in following figures.

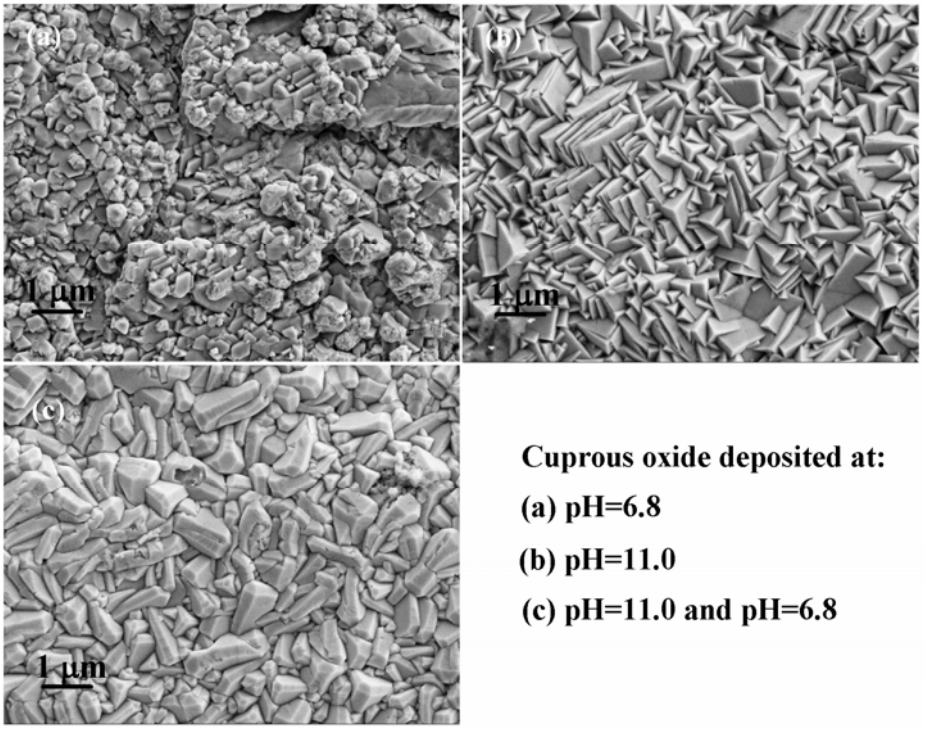

Fig. 7.8 SEM images of cuprous oxide deposited at: (a) pH=6.8, (b) pH=11.0 and (c) pH=11.0 and pH=6.8

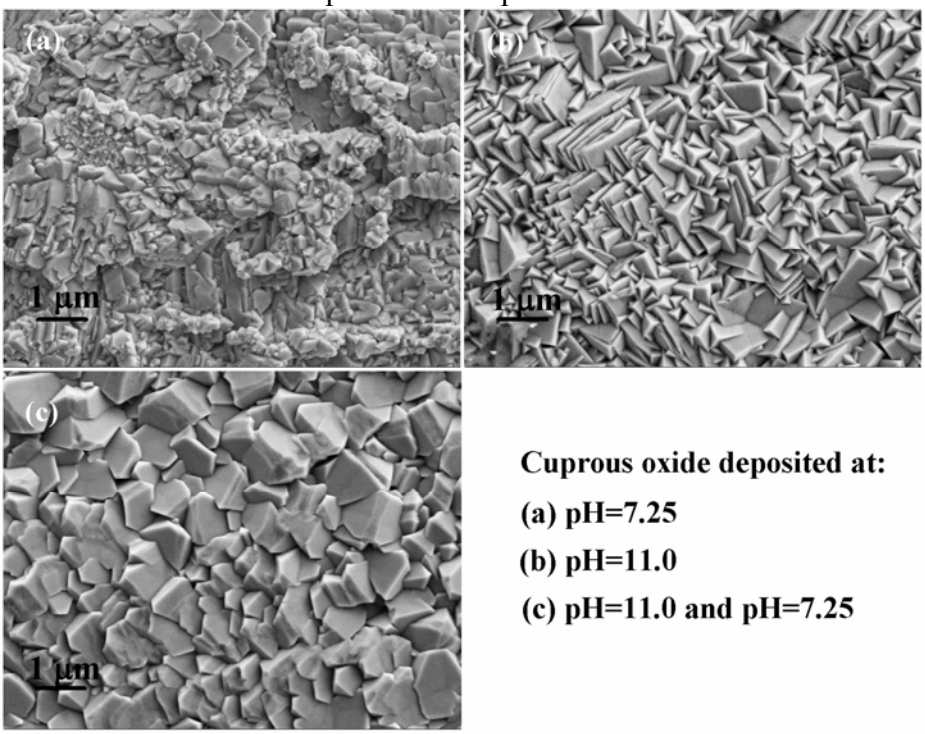

Fig. 7.9 SEM images of cuprous oxide deposited at: (a) pH=7.25, (b) pH=11.0 and (c) pH=11.0 and pH=7.25

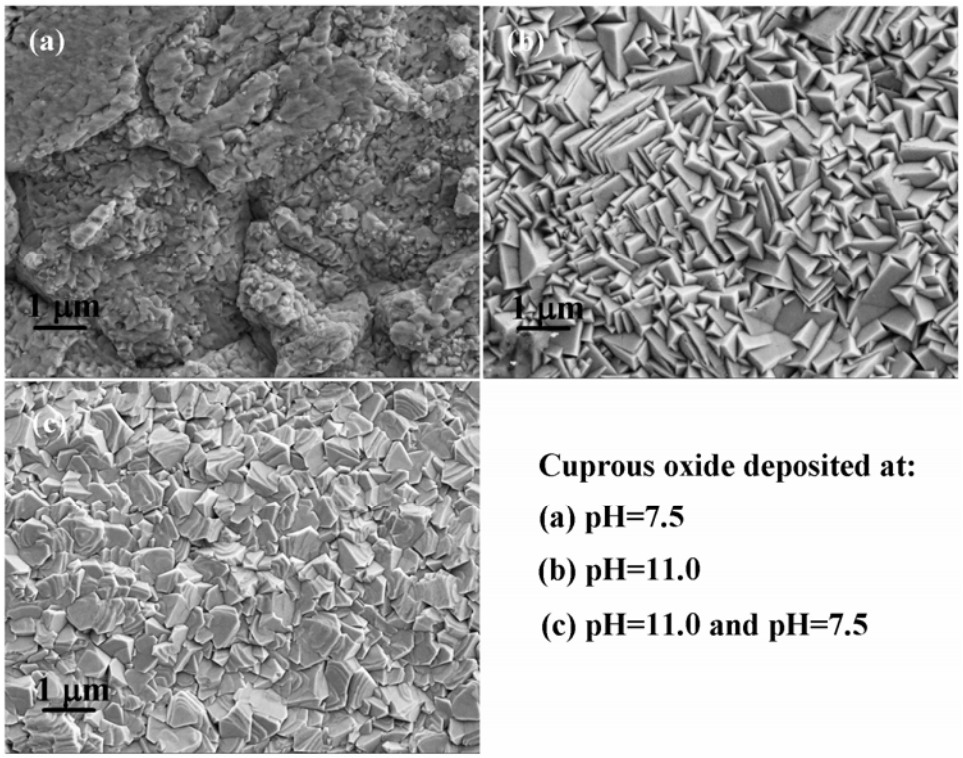

Fig. 7.10 SEM images of cuprous oxide deposited at: (a) pH=7.5, (b) pH=11.0 and (c) pH=11.0 and pH=7.5

As shown, the surface morphology of p-n junction samples shows significant difference from that of n-type or p-type samples. Both n-type and p-type cuprous oxides are directly deposited on copper substrates. While for p-n junction samples, the n-type film is deposited on p-type cuprous oxide. The difference in surface morphology may be ascribed to the different starting surface for deposition.

7.2.3 Photocurrent characterization

Four samples, deposited at pH of 6.8 and 11.0, 7.25 and 11.0, 7.5 and 11.0, and 11.0, respectively, are used for photocurrent characterization to confirm the conduction type of the top layer deposited at lower bath pH (6.8, 7.25 and 7.5).

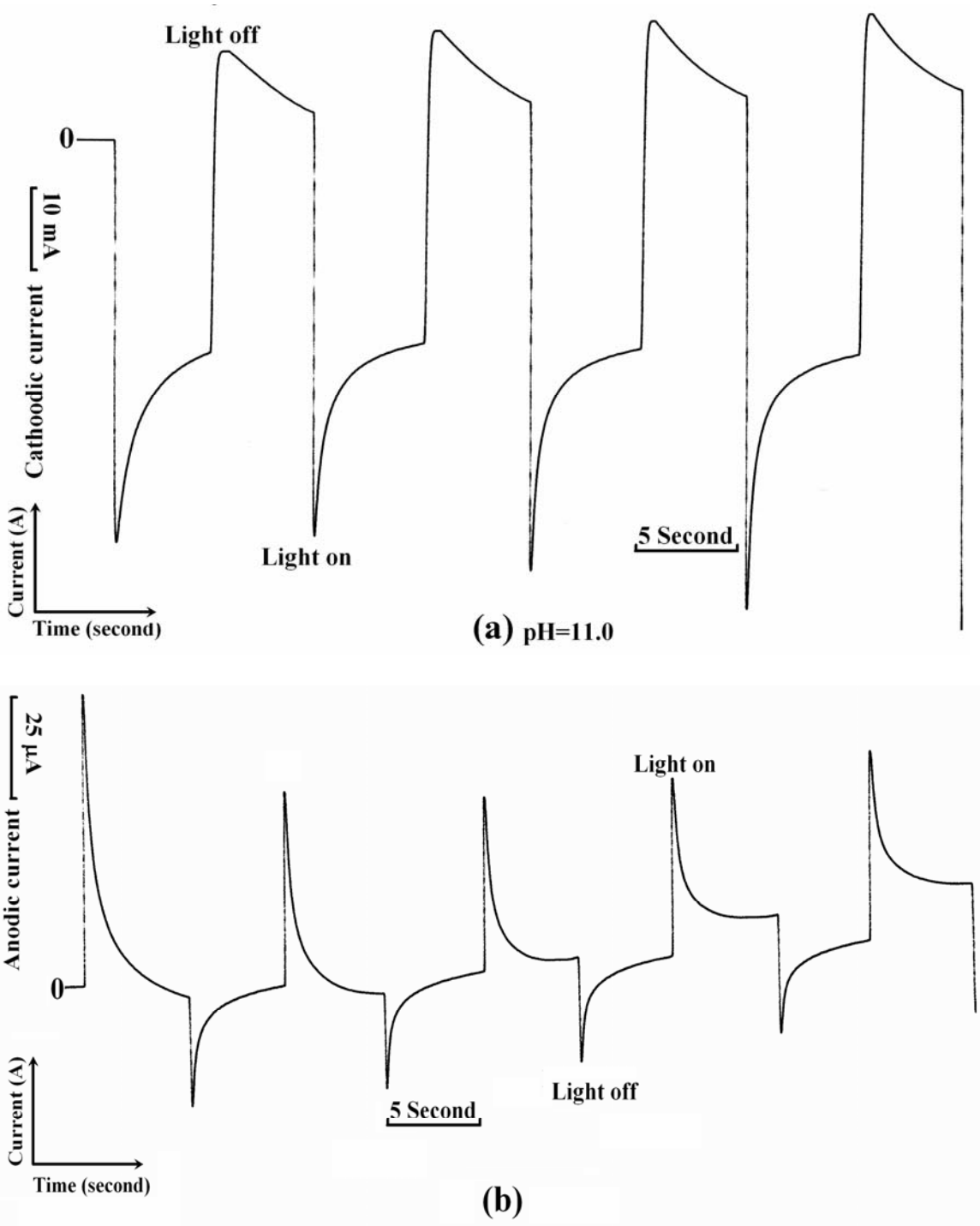

Fig. 7.11 Photocurrent of cuprous oxide films deposited at bath pH: (a) 11.0, (b) 7.5 and 11.0

As shown, cuprous oxide deposited at pH of 11.0 shows a p-type semiconductor behavior. After a deposition of another layer at lower pH (6.8, 7.25 and 7.5), photocurrent indicates an n-type semiconductor behavior, which confirms a successful deposition of n-type cuprous oxide on p-type cuprous oxide and the formation of a p-n homo-junction.

7.2.4 I-V Characterization

7.2.4.1 Sample preparation

p-n homo-junctions of cuprous oxide prepared by a two-step deposition process are used for I-V characterization. The top metal contact is aluminum deposited through a shadow mask with a dot area of $3.6\times10^{-4}cm^2$. As shown in Fig. 7.12, there are three junctions formed in this structure: (1) Schottky junction between n-type cuprous oxide and top Al contact, (2) p-n junction between n-type and p-type cuprous oxide and (3) Schottky junction between p-type cuprous oxide and Cu substrate.

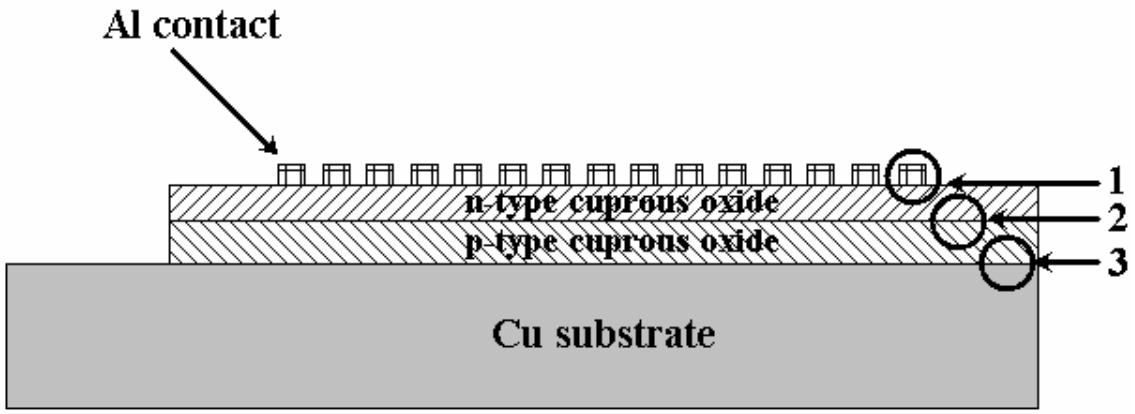

Fig. 7.12 Junctions formed for a p-n junction sample prepared for I-V characterization: (1) Schottky junction between n-type cuprous oxide and top Al contact, (2) p-n junction between n-type and p-type cuprous oxide and (3) Schottky junction between p-type cuprous oxide and Cu substrate

As long as the two Schottky junctions are ohmic contacts, the measured I-V data is only determined by the p-n homo-junction. This is the reason another two sets of samples are prepared to study whether the Schottky junctions (1) and (3) in Fig. 7.12 are ohmic contacts. These two sets of samples are p-type cuprous oxide on Cu substrate with top Cu contact and n-type cuprous oxide on Cu substrate with top Al contact, respectively.

7.2.4.2 I-V characterization

As a metal is in contact with a semiconductor, a Schottky barrier is formed. Theoretically, the Schottky barrier height is only determined by the work function of the metal (Φ_M) and the electron affinity of the n-type semiconductor (χ_s).[82] For a p-type semiconductor, the higher the work function of the metal, the easier it is to form an ohmic contact. While for an n-type semiconductor, the lower the work function of the metal, the easier it is to form an ohmic contact. Copper (Φ_M=4.7 eV) is used as top metal contact for p-type cuprous oxide, while aluminum (Φ_M=4.2 eV) is used as top metal contact for n-type cuprous oxide. I-V data of these two Schottky junctions are shown in Fig. 7.13 and Fig. 7.14, respectively.

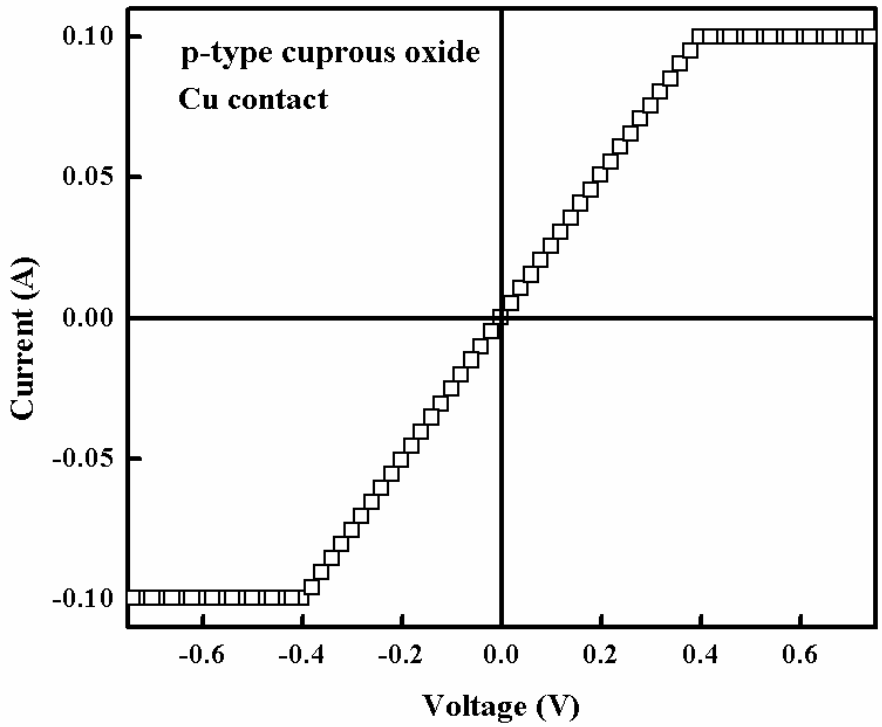

Fig. 7.13 I-V characteristics of Cu/p-Cu_2O Schottky junctions

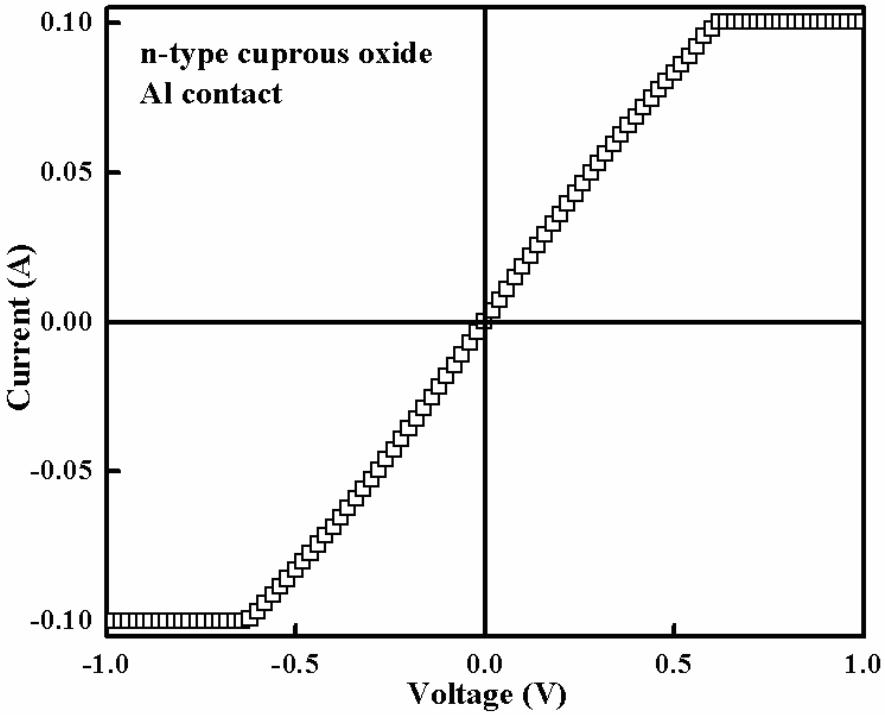

Fig. 7.14 I-V characteristics of Al/n-Cu_2O Schottky junctions

As shown, both Schottky junctions (Cu/p-Cu_2O and Al/n-Cu_2O) show ohmic behavior. Therefore, I-V characteristics of the structure shown in Fig. 7.12 will be determined by the p-n homo-junction of cuprous oxide only.

As shown in Fig. 7. 15, the I-V data shows a typical rectification effect of a p-n junction.

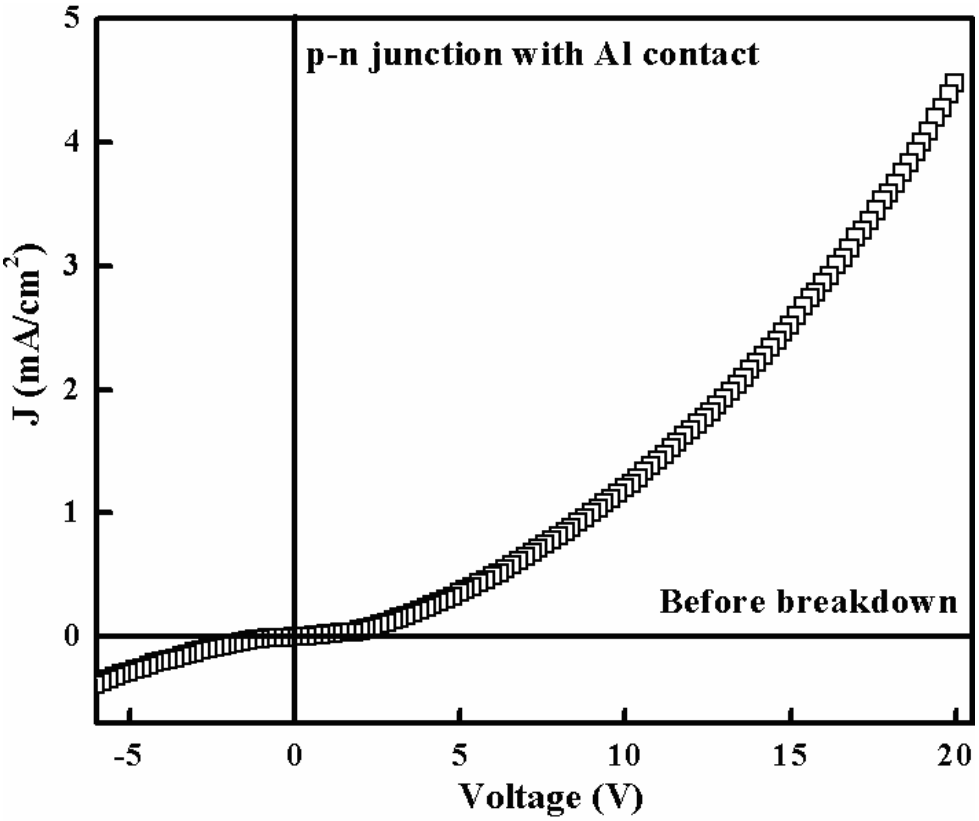

Fig. 7.15 I-V characteristics of p-n homo-junction of Cu_2O

For a p-n junction at equilibrium (V_A=0, Fig. 7.16 (a)), the Fermi level of both p-type and n-type cuprous oxide should be equal. As a result, a depletion region (space charge region) is formed, which works as a barrier for carrier movements (electrons to p-type and holes to n-type). Under forward bias (V_A>0, Fig. 7.16 (b)), the barrier height of the p-n junction is decreased by qV_A and the forward current increases exponentially

with applied potential. When the p-n junction is reversely biased (V_A<0, Fig. 7.16(c)), barrier height is increased to $q(V_{bi}+|V_A|)$, which makes it more difficultly for carriers to pass through the junction. Therefore the reverse current is very small.

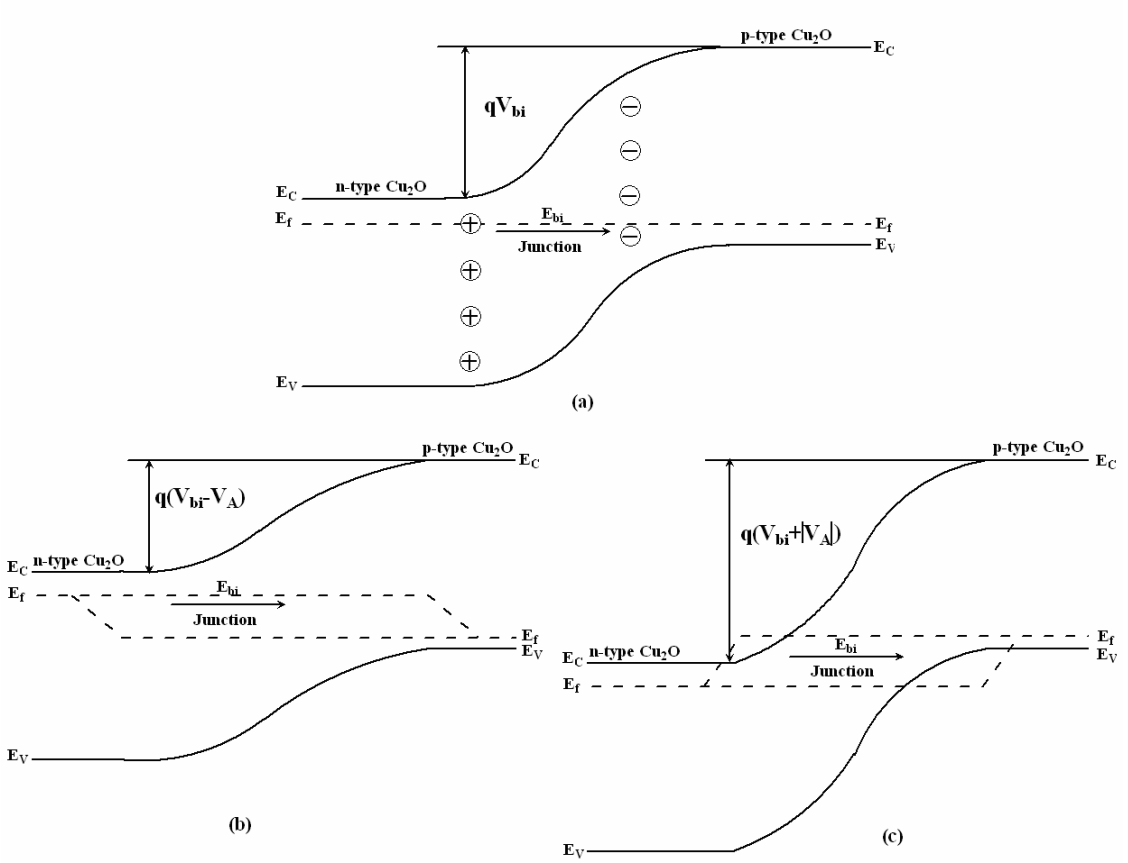

Fig. 7.16 Band structure of p-n junction: (a) at equilibrium, (b) forward bias and (c) reverse bias

However, as the reverse potential passes a certain limit (the breakdown voltage), breakdown happens and the p-n junction no longer shows rectification and turns into an ohmic contact (Fig. 7.17).

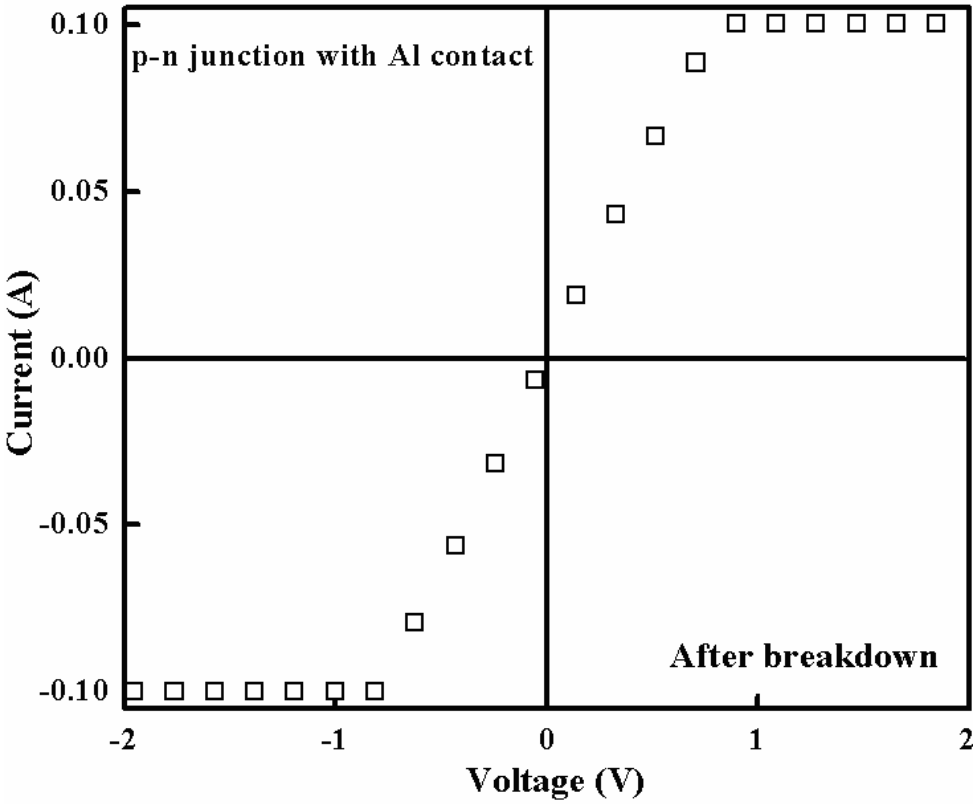

Fig. 7.17 I-V characteristics of p-n homo-junction of Cu_2O after breakdown

7.3 Summary

Based on the theory that bath pH can control the composition and native point defects in electrodeposited cuprous oxide, both p-type and n-type cuprous oxides are successfully deposited at different bath pH values. For sample deposited at pH value below 7.5, cuprous oxide is an n-type semiconductor, while at bath pH values higher than 9.0, cuprous oxide is a p-type semiconductor. Furthermore, a two-step deposition process is used to deposit both p-type and n-type cuprous oxide in sequence to form a p-n homo-junction. I-V data shows a typical rectification behavior of a p-n junction for the prepared samples, which suggests that a p-n homo-junction of cuprous oxide is achieved.

This is the first systematic report on control conduction types of cuprous oxide and fabrication of p-n homo-junction in cuprous oxide. This invention is of great importance because it enables fabrication of solar cell with a reasonable efficiency (~10%) at a very low cost, which may be a break through for the development of solar cell.

CHAPTER 8

CONCLUSIONS AND FUTURE WORK

8.1 Conclusions

Copper oxides, including cuprous oxide and cupric oxide, are prepared by electrochemical deposition. The structural, optical and electrical properties of as-deposited copper oxides are evaluated.

The effect of deposition conditions, especially the deposition pH, on structural, optical and electrical properties of cuprous oxide is well studied. Cuprous oxide deposited at pH above 9.0 is a p-type semiconductor with a direct band gap of 2.06 eV and band gap doesn't change with deposition conditions. Cuprous oxide films deposited at bath pH from 7.0 to 12.0 have three preferred orientations: (100), (110) and (111). Surface morphology and grain size change with film orientation. To explain the pH effect on structural properties of cuprous oxide, a new model is proposed as follows: bath pH controls the orientation of cuprous oxide film by affecting the growth rate of crystallographic planes with different Cu^{+}/O^{2-} ratios. Flat band potential (V_{fb}) is found to shift with crystal orientation. To our knowledge, this is the first report on how bath pH has a profound effect on the electrical properties of cuprous oxide.

Properties of electrodeposited cupric oxide differ a lot from those of cuprous oxide. Cupric oxide has an indirect band gap of 1.32 eV. As-deposited cupric oxide film

doesn't have any preferred orientation and the crystallinity is poor. Electrochemical etching processes, in particular, an in situ electrochemical etching process, are developed for the deposition of cupric oxide. In situ electrochemical etching prevents exposure of the cleaned surface to air or other contaminations before deposition. This is the first report on in situ electrochemical etching for cupric oxide deposition. Electrochemical etching process is proven to be an effective cleaning process. Cupric oxide deposited on electrochemically etched copper substrates has favorable electrical properties.

Comparing cuprous oxide with cupric oxide, it's concluded that cuprous oxide is more suitable for photovoltaic application because it has much better crystallinity, bigger grains, better control over crystal quality and a direct band gap. It is proposed that to achieve n-type cuprous oxide, bath pH plays a significant role since it controls the amount of oxygen incorporated into the film. Bath pH thus controls the native point defects in cuprous oxide. It's found that cuprous oxides deposited at bath pH below 7.5 are n-type semiconductors, while cuprous oxides deposited at bath pH above 9.0 are p-type semiconductors. A well controlled two-step deposition process is developed to fabricate p-n homo-junctions in cuprous oxide. Photocurrent and current-voltage measurements demonstrate a successful fabrication of p-n homo-junctions in cuprous oxide.

The significance of this work is that it paves the way for doping both n-type and p-type cuprous oxide. Cuprous oxide solar cell can thus achieve a much higher

conversion efficiency and because of the inherent nature of the fabrication method the cost will be much lower.

8.2 Future work

8.2.1 Reducing the band gap of cuprous oxide

As known, the ideal band gap for a photovoltaic material is 1.4~1.7 eV, while the band gap of cuprous oxide is 2.06 eV. In order to get a higher efficiency for the solar cells based on cuprous oxide, a concept of mixed-valence copper oxide is proposed.[107] The fundamental idea is to control the band gap of copper oxide CuO_x by controlling the value of x.

8.2.2 Doping of cuprous oxide

Electrical properties of a semiconductor such as carrier concentration, carrier mobility are critical factors for the performance of solar cells. Both p-type and n-type cuprous oxides are achieved and the next step is to control the electrical properties of cuprous oxide. Key issues for doping are the selection of dopants and preparation of solutions for both p- and n-type cuprous oxides. Dopants should be stable in the deposition solution and simultaneously deposited with cuprous oxides.

8.2.3 Fabrication of solar cell based on cuprous oxide

The final goal of this project is to fabricate solar cells based on cuprous oxide and achieve a reasonable conversion efficiency at a very low cost. The proposed structure of solar cells based on copper oxides is shown in Fig. 8.1. The p-n homo-junction of copper oxides can be achieved by well-controlled deposition processes in sequence.

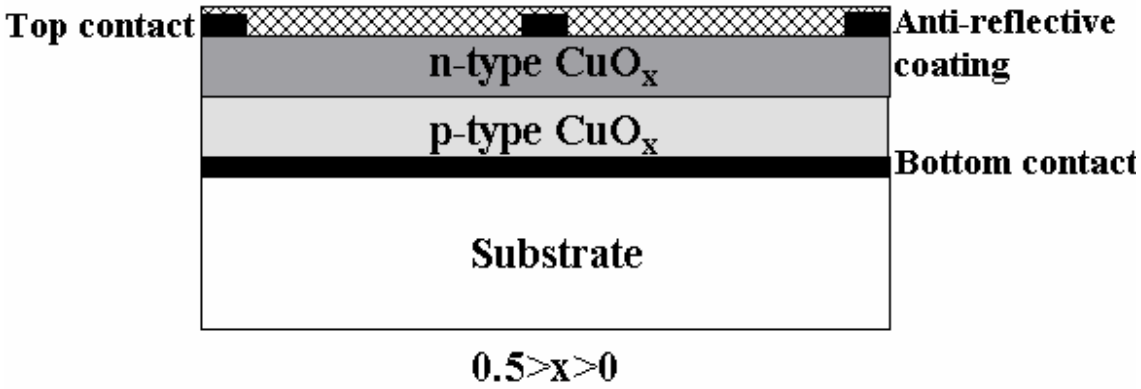

Fig. 8.1 Proposed solar cell structure based on copper oxides (CuO_x)

REFERENCES

1. IEA (International Energy Agency) 2005 Report: Key World Energy Statistics, 1-82, IEA Press, 2005.
2. IEA (International Energy Agency) 2003 Report: Renewables in Global Energy Supply, 1-12, IEA Press, 2003.
3. Nathan S. Lewis, ECS 208th meeting, Los Angeles, California, USA, Oct. 16-21, 2005.
4. M. I. Hoffert, K. Caldeira, A. K. Jain, E. F. Haites, L. D. Danny Harvey, S. D. Potter, M. E. Schlesinger, S. H. Schneider, R. G. Watts, T. M. L. Wigley and D. J. Wuebbles, Nature, **395**, 881 (1998).
5. Tomas Markvart, Solar Electricity, 2nd edition, Chichester, England (2000).
6. A. E. Becquerel, Comt. Rend. Acad. Sci., **9**, 561 (1839).
7. A. Goetzberger, et al., Mater. Sci. and Eng., R, **40**, 1-46 (2003).
8. Paul Maycock, PV News, March, 2005.
9. R. W. G. Wychoff, Crystal Structure, **Volume 1**, Wiley, New York (1965).
10. R. S. Toth, R. Kilkson, and D. Trivich, *J. Appl. Phys.*, **31**, 1117 (1960).
11. R. S. Toth, R. Kilkson, and D. Trivich, *Phys. Rev.*, **122**, 482 (1961).
12. H. L. McKinzie and M. O'Keeffe, Phys. Lett., **24A**, 137-139 (1967).
13. A. P. Young and C. M. Schwartz, J. Phys. Chem. Solids, **30**, 249-252 (1969).
14. M. O'Keeffe and W. J. Moore, J. Chem. Phys., **35**, 1324-1328 (1961).

15. R. Kuzel and F. L. Weichman, J. Appl. Phys., **41**, 271-279 (1970).
16. J. Maluenda, R. Farhi and G. Petot-Ervas, J. Phys. Chem. Solids, **42**, 911-921 (1981).
17. A. E. Rakhshani, Solid-State Electron., **29**, 7-17 (1986).
18. F. L. Weichman, Phys. Rev., **117**, 998-1002 (1960).
19. F. L. Weichman and J. M. Reyes, Can. J. Phys., **58**, 325-333 (1980).
20. L. C. Olsen, F. W. Addis and W. Miller, Sol. Cells, **7**, 247-279 (1982-1983).
21. A. Roos and B. Karlsson, Sol. Energy Mater., **7**, 467-480 (1983).
22. A. A. Berezin and F. L. Weichman, Solid State Commun., **37**, 157-160 (1981).
23. W. Siripala, L. D. R. D. Perera, K. T. L. De Silva, J. K. D. S. Jayanetti, I. M. Dharmadasa, Sol. Energy Mater. Sol. Cells, **44**, 251-260 (1996).
24. M. T. S. Nair, L. Guerrero, O. L. Arenas and P. K. Nair, Appl. Surf. Sci., **150**, 143-151 (1999).
25. T. Mahalingam, J. S. P. Chitra, S. Rajendran, M. Jayachandran and M. J. Chockalingam, J. Cryst. Growth, **216**, 304-310 (2000).
26. B. balamurugan and B. R. Mehta, Thin Solid Films, **396**, 90-96 (2001).
27. V. Georgieva and M. Ristov, Sol. Energy Mater. Sol. Cells, **73**, 67-73 (2002).
28. G. P. Pollack and D. Trivich, J. Appl. Phys., **46**, 163-172 (1975).
29. T. Ito, H. Yamaguchi, K. Okabe and T. Masumi, J. Mater. Sci., **33**, 3555-3566 (1998).
30. D. Trivich and G. P. Pollack, J. Electrochem. Soc., **117**, 344 (1970).
31. D. Tench and L. F. Warren, *J. Electrochem. Soc.*, **130**, 869-872 (1983).

32. H. S. Potdar, N. Pavaskar, A. Mitra, and A. P. B. Sinha, Sol. Energy Mater., **4**, 291-299 (1981).

33. V. F. Drobny and D. L. Pulfrey, Thin Solid Films, **61**, 89-98 (1979).

34. G. Beensh-Marchwicka, L. Krol-Stepniewska, and M. Slaby, Thin Solid Films, **88**, 33-39 (1982).

35. A. E. Rakhshani, A. A. Al-Jassar, and J. Varghese, Thin Solid Films, **148**, 191-201 (1987).

36. A. E. Rakhshani and J. Varghese, Thin Solid Films, **157**, 87-96 (1988).

37. A. E. Rakhshani and J. Varchese, J. Mater. Sci., **23**, 3847-3853 (1988).

38. Y. Zhou and J. A. Switzer, Scripta Mater., **38**, 1731-1738 (1998).

39. T. D. Golden, M. G. Shumsky, Y. Zhou, R. A. VanderWerf, R. A. Van Leeuwen and J. A. Switzer, Chem. Mater., **8**, 2499-2504 (1996).

40. Y. Zhou and J. A. Switzer, Mat. Res. Innovat., **2**, 22-27 (1998).

41. R. P. Wijesundera, M. Hidaka, K. Koga, M. Sakai and W. Siripala, Thin Solid Films, **500**, 241-246 (2006).

42. A. O. Musa, T. Akomolafe and M. J. Carter, Sol. Energy Mater. Sol. Cells, **51**, 305-316 (1998).

43. L. O. Grondahl, Rev. Mod. Phys., **5**, 141-167 (1933).

44. B. Lange, Photoelements and Their Applications, Reinhold, New York (1939).

45. M. Balkanski, Y. Petroff and D. Trivich, Solid State Commun., **5**, 85-88 (1967).

46. J. A. Assimos and D. Trivich, J. Appl. Phys., **44**, 1687-1693 (1973).

47. L. Papadimitriou, N. A. Economou and D. Trivich, Sol. Cells, **3**, 73-80 (1981).

48. J. Herion, E. A. Niekisch and G. Scharl, Sol. Energy Mater., **4**, 101-112 (1980).

49. W. M. Sears and E. Fortin, Sol. Energy Mater., **10**, 93-103 (1984).

50. B. P. Rai, Solar Cells, **25**, 265-272 (1988).

51. W. Siripala and J. R. P. Jayakody, Sol. Energy Mater., **14**, 23-27 (1986).

52. R. Garuthara and W. Siripala, J. Lumin., **121**, 173-178 (2006).

53. S. Åsbrink and L.-J. Norrby, Acta Crystallogr., **B 26**, 8-15 (1970).

54. W. Y. Ching and Y. Xu, Phys. Rev., **40**, 7684-7695 (1989).

55. W. DeSisto, B. T. Collins, R. Kershaw, K. Dwight and A. Wold, Mat. Res. Bull., **24**, 1005-1010 (1989).

56. F. P. Koffyberg and F. A. Benko, J. Appl. Phys., **53**, 1173-1177 (1982).

57. K. Baek and H. L. Tuller, Solid State Ionics, **75**, 179-186 (1995).

58. K. Nakaoka and K. Ogura, J. Electrochem. Soc., **149**, C79-C585 (2002).

59. K. Santra, C. K. Sarkar, M. K. Mukherjee, and B. Ghosh, Thin Solid Films, **213**, 226-229 (1992).

60. A. Y. Oral, E. Mensur, M. H. Aslan, and E. Basaran, Mater. Chem. Phys., **83**, 140-144 (2004).

61. Y. S. Chaudhary, A. Agrawal, R. Shrivastav, V. R. Satsangi, and S. Dass, Inter. J. Hydrogen Energy, **28**, 131-134 (2004).

62. S. C. Ray, Sol. Energy Mater. Sol. Cells, **68**, 307-312 (2001).

63. H. Lin, C. Wang, H. C. Shih, J. Chen, and C. Hsieh, J. Appl. Phys., **95**, 5889 (2004).

64. H. Ki, J. Woo, and H. Dong, Thin Solid Films, **372**, 250-256 (2000).

65. C. G. Cruzan and H. A. Miley, J. Appl. Phys., **11**, 631-634 (1940).

66. M. G. Hapase, M. K. Gharpurey, and A. B. Biswas, Surf. Sci., **9**, 87-99 (1968).

67. Y. K. Jeong and G. M. Choi, J. Phys. Chem. Solids, **57**, 81-84 (1996).

68. S. Jung and H. Yanagida, Sens. Actuators, **B 37**, 55-60 (1996).

69. G. Turky, M. Soliman Selim and G. A. El-Shobaky, Solid State Ionics, **140**, 395-403 (2001).

70. D. P. Bhattacharyya and P. N. Mukherjee, J. Appl. Chem. Biotechnol., **22**, 889-898 (1972).

71. X. G. Zheng, M. Suzuki and C. N. Xu, Mat. Res. Bull., **33**, 605-610 (1998).

72. J. Medina-Valtierra, J. Ramirez-Orbiz, V. M. Arroyo-Rojas, P. Bosch and J. A. de los Reyes, Thin Solid Films, **405**, 23-28 (2002).

73. P. Poizot, C. Hung, M. P. Nikiforov, E. W. Bohannan, and J. A. Switzer, Electrochem. Solid-State Lett., **6**, C21 (2003).

74. K. Ogura, K. Nakaoka, M. Nakayama, and S. Tanaka, J. Electroanal. Chem., **511**, 122-127 (2001).

75. H. M. Kothari, E. A. Kulp, S. Boonsalee, M. P. Nikiforov, E. W. Bohannan, P. Poizot, S. Nakanishi and J. A. Switzer, Chem. Mater., **16**, 4232-4244 (2004).

76. A. J. Bard and L. R. Faulkner, Electrochemical Methods–Fundamentals and Applications, 2nd edition, John Wiley & Sons, New York (2000).

77. G. A. Mabbott, J. Chem. Educ., **60**, 697-702 (1983).

78. P. T. Kissinger and W. R. Heineman, J. Chem. Educ., **60**, 702-706 (1983).

79. http://www.chembio.uoguelph.ca/educmat/chm729/afm/firstpag.htm.

80. A. J. Bard, Science, **207**, 139-144 (1980).

81. N. S. Lewis, Ann. Rev. Mater. Sci., **14**, 95-117 (1984).

82. S. M. Sze, Physics of Semiconductor Devices, 2nd edition, John Wiley & Sons, New York (1981).

83. J. Katayama, K. Ito, M. Matsuoka and J. Tamaki, J. Appl. Electrochem., **34**, 687-692 (2004).

84. W. Siripala, A. Ivanovskaya, T.F. Jaramillo, S-H. Baeck and E.W. McFarland, Sol. Energy Mater. Sol. Cells, **77**, 229-237 (2003).

85. P.E. de Jongh, D. Vanmaekelbergh and J.J. Kelly, Chem. Mater., **11**, 3512-3517 (1999).

86. J. Oh, Y. Tak and J. Lee, Electrochem. Solid-State Lett., **8**, C81 (2005).

87. J. D. H. Donnay and D. harker, Am Mineralogist, **22**, 446 (1937).

88. G. Nagasubramanian, A.S. Gioda and A. J. Bard, J. Electrochem. Soc., **128**, 2158-2164 (1981).

89. E.C. Heltemes, Phys. Rev., **141**, 803-805 (1966).

90. K. Mizuno, M. Izaki, K. Murase, T. Shinagawa, M. Chigane, M. Inaba, A. Tasaka and Y. Awakura, J. Electrochem. Soc., **152**, C179-C182 (2005).

91. P. Singh, R. Singh, R. Gale, K. Rajeshwar and J. Dubow, J. Appl. Phys., **51**, 6286-6291 (1980).

92. P.J. Boddy and W.H. Brattain, J. Electrochem. Soc., **110**, 570 (1963).

93. S.R. Morrison, The Chemical Physics of Surfaces, Plenum Press, New York and London (1977).

94. K. Nakaoka, J. Ueyama and K. Ogura, J. Elerctrochem. Soc., **151**, C661-C665 (2004).

95. R. K. Pandey, S. A. Sahu and S. Chandra, Handbood of Semiconductor Electrodeposition, Marcel Dekker, New York (1996).

96. C. M. Reddy, R. S. Gaston, C. M. Weikart and H. K. Yasuda, Prog. Org. Coat., **33**, 225-231 (1998).

97. J. Alexis, D. Adrian, T. Masri and J. A. Petit, Surf. Eng., **20**, 121-127 (2004).

98. J. Quintana and P. J. Sebastian, Sol. Energy Mater. Sol. Cells, **33**, 465-474 (1994).

99. E. C. Felder, S. Nakahara and R. Weil, Thin Solid Films, **84**, 197-203 (1981).

100. E. Cano, J. L. Polo, A. La Iglesia and J. M. Bastidas, Corros. Sci., **47**, 977-987 (2005).

101. B. W. Gregory, M. L. Norton and J. L. Stickney, J. Electroanal. Chem., **293**, 85-101 (1990).

102. Y. S. Kim, D. Jung and S. Min, Thin Solid Films, **349**, 36-42 (1999).

103. I. Gündiler and L. E. Murr, J. Vac. Sci. Technol., **12**, 762-765 (1975).

104. S. Menezes, W. V. McLevige, E. R. Blazejewski, W. E. Tennant, and J. P. Ziegler, J. Vac. Sci. Technol., **B 9**, 1974 (1991).

105. J. K. Barton, A. A. Vertegel, E. W. Bohannan, and J. A. Switzer, Chem. Mater., **13**, 952 (2001).

106. Q. X. Liu, S. Zein El Abedin, and F. Endres, Surf. Coat. Technol., Article in press, 2006.

107. M. Tao, 4th World conference of Photovoltaic Energy Conversion, IEEE, Hawaii, U. S., 2006.

BIOGRAPHICAL INFORMATION

Longcheng Wang earned a Bachelor of Science degree majored in Materials Science and Engineering from Zhejiang University, Hangzhou, P. R. China in 1998 and later a Master of Engineering degree majored in Materials Science and Engineering from Zhejiang University, Hangzhou, P. R. China in 2002. He registered as a graduate student in Materials Science and Engineering at the University of Texas at Arlington in 2002 and earned a Doctor of Philosophy degree in Materials science and Engineering at the University of Texas at Arlington in December 2006.